Effect of Dissolved-Hydrogen on SCC Behavior of Solution-Annealed 316L and 310S SS in Hot Water

Yen-Jui HUANG

Effect of Dissolved-Hydrogen on SCC Behavior of Solution-Annealed 316L and 310S SS in Hot Water

Yen-Jui HUANG

Graduate School of Energy Science
Kyoto University

2018

Contents

List of tables

List of figures

Chapter 1
Introduction

1.1 Nuclear energy

Nuclear energy has supported human society for nearly sixty years. As a base-load energy source, it provides a good supporting for grid stability; and comparably steady fuel-to-power cost gives stable power price. It also plays a critical role in deducting greenhouse gas emission and securing energy supply. To meet the growing electricity demands and environmental protections, it is worthwhile extending in-service nuclear reactors and developing next generation nuclear energy systems.[1,2]

Light water is mostly used among numerous designs for nuclear power systems. It is easily available and abundant; it has a good heat capacity, neutron economics and moderation ability. More than 80% of civil nuclear reactors adopts light water as main working fluid. Reactors are hence named as Light Water Reactor. By design concept difference, there are three sub-groups under this family: the Pressurized Water Reactor (PWR), the Boiling Water Reactor (BWR) and the Supercritical Water Reactor (SCWR).

Up to date, there are 290 PWR units and 76 BWR units operable worldwide. U.S. owns 99, average age is 36; France owns 58, average age is 32; Japan owns 42, average age is 29.[3] The majority of the three nuclear fleets is built during 1960s to 1980s, with a 40-year operating commission. Since 90s, fleets in U.S. has entered inspections for license renewal and service extension. As of 2018, 89 out of 99 units in U.S. have granted a 20-year service extension from U.S. Nuclear Regulatory Commission. Two reactor categories (900 and 1300MWe) in France are in the third 10-year inspection for license renewal under Électricité de France. Japan`s fleet is under inspections and some are waiting approval.

SCWR is one of Generation IV reactor design which is still under development. [4] It can be benefited from existing expertise in PWR, BWRs and fossil fuel plants that use supercritical water cycle. Its thermal efficiency is up to 44%, which is higher than 33-36% of PWR and BWRs. Its succinct, one-through, direct-cycle design gives economical advantage. Being different from PWR and BWR, supercritical water only partially moderates neutron, which gives SCWR certain fast neutron characteristics and higher radiation fluence within core region.

Light water is also applied in the heat transfer system of International Tokamak Experimental Reactor.[5] It is responsible for extracting heat from plasma-facing components (ex: testing blanket modules and diverters) and transfer heat to secondary heat removal systems. The designed pressure and temperature are similar to in-service PWR. As water flow through testing blanket modules, bred tritium in blanket may penetrate into cooling water. With the aid of high fluence, tritium may react with cooling water and form tritiated water with soluble gaseous TH/H_2.

In late 80s, PWR and BWR applied hydrogen injection technique to aid radiolytic decomposition and to mitigate corrosion. The amount of dissolved-hydrogen is a key to hydrogen water chemistry. In SCWR, enhanced radiation may increase dissolved-hydrogen content. In ITER's heat transfer system, tritiated water and soluble gaseous TH/H_2 may behave like dissolved-hydrogen in LWR. In short, dissolved-hydrogen exists in all water-cooled nuclear energy systems. Recent investigations pointed out that the presence of hydrogen may influence behaviors of stress corrosion cracking on structural materials for the nuclear power plants.

1.2 Nuclear in Japan

Japan's shortage of natural resources and energy greatly influenced its politics and history in past century. Its vulnerable energy supply, revealed by two oil shocks, revealed its vulnerability of energy supply and had government decided expanding nuclear capacity. A fast capacity growth from 1970s to 1990s helped Japan to reduce its dependence on energy imports. By 2011, Japan has 42 operable units (20 PWR units and 22 BWR units); average age is 29. This fleet was held after the Great East Japan earthquake and subsequent accident at 2011. As a consequence, Japan's energy import dependence ramped up to 94% at the end of 2013. An awkward number of Japan's energy supply.

The government reevaluated its energy policy and proposed the 4th Strategic Energy Plan (SEP) in 2014.[6] SEP addressed that nuclear energy is a key base-load power source. Further, it addressed safety will be first priority in achieving stable and affordable energy supply and environmental conservation. Following released document, “Long-Term Energy Supply and Demand Outlook,”[2] set nuclear energy at 20-22% of total energy generation in 2030. Now, five out of 42 units (Sendai 1,2; Takahama 3,4; Ikata 3) are in operation; 9 units receive re-starting approval, 12 units are under inspection. [7]

1.3 Degradation issue in nuclear power plant

One of major degradation issues in PWR and BWR is stress corrosion cracking (SCC). It is a synergic interaction of following factors: the susceptible material, the tensile stress and the corrosive environment. Since the first SCC incident reported by Coriou in 1959[8], numerous factors have been recognized to induce SCC. Chloride ions, sensitized stainless steel, residual stress and dissolved-oxygen, etc. have been recognized as damaging factors. Countermeasures such as water purification and using low-carbon grade stainless steels have been applied. Hydrogen injection and subsequent noble metal chemical addition (in BWR) optimized water chemistry. As a result, incidents of SCC decreased in past twenty years.

Recent works indicate that SCC behaviors relates to the amount of dissolved-hydrogen. Brittle fracture was discovered on specimens tested at relatively higher dissolved-hydrogen amount. Features resembles hydrogen-induced cracking in gaseous hydrogen environment. In this field, a number of works pointed out that increasing Ni content can reduce susceptibility to hydrogen-induced cracking. It is worth investigating the resistance to hydrogen-dissolved high temperature water of current used 316L stainless steel. Furthermore, it is worth searching for next candidate materials.

References

[1] U.S. Energy Information Administration, International Energy Outlook 2016, 2016. doi:www.eia.gov/forecasts/ieo/pdf/0484(2016).pdf.

[2] Long-Term Energy Supply and Demand Outlook, (n.d.). http://www.meti.go.jp/press/2015/07/20150716004/20150716004.html.

[3] NPPs worldwide, (n.d.). http://www.world-nuclear.org/information-library/facts-and-figures/world-nuclear-power-reactors-and-uranium-requireme.aspx.

[4] Schematic of SCWR design, (n.d.). https://www.gen-4.org/gif/jcms/c_42151/supercritical-water-cooled-reactor-scwr.

[5] TCWS of ITER, (n.d.). https://www.iter.org/newsline/singleprint/-/2019.

[6] 4th Strategic Energy Plan, (n.d.). http://www.enecho.meti.go.jp/category/others/basic_plan/.

[7] NPP restart, (n.d.). http://www.fepc.or.jp/theme/re-operation/.

[8] H. Coriou, L. Grall, Y. Le Gall, S. Vettier, Corrosion sous contrainte de I’Inconel dans L’eau a haute temperature, in: Proc. 3eme Colloq. Metall. Sur La Corros., North Holland Publishing Co., Amsterdam, 1959: pp. 161–9.

Chapter 2

Literature review and research objectives

2.1 Types of light water reactors

Followings are general feature designs of light water reactors. Fission reaction occurs within uranium oxide fuel pellets; pellets are enclosed in fuel rods; rods are grouped by hundreds in bundles called fuel assemblies. Control rods and sensors are also located in assemblies. Hundreds of assemblies are put in core plates. This space is called nuclear core and enclosed in reactor pressure vessel. Fission energy heats up water as water flows through core. Water then brings heat out of core and deliver heat energy to secondary systems which transform heat into mechanical energy that produce electricity. (Whether in steam form (in BWR), or to secondary loop (in PWR) or directly drive turbine generator (in SCWR))

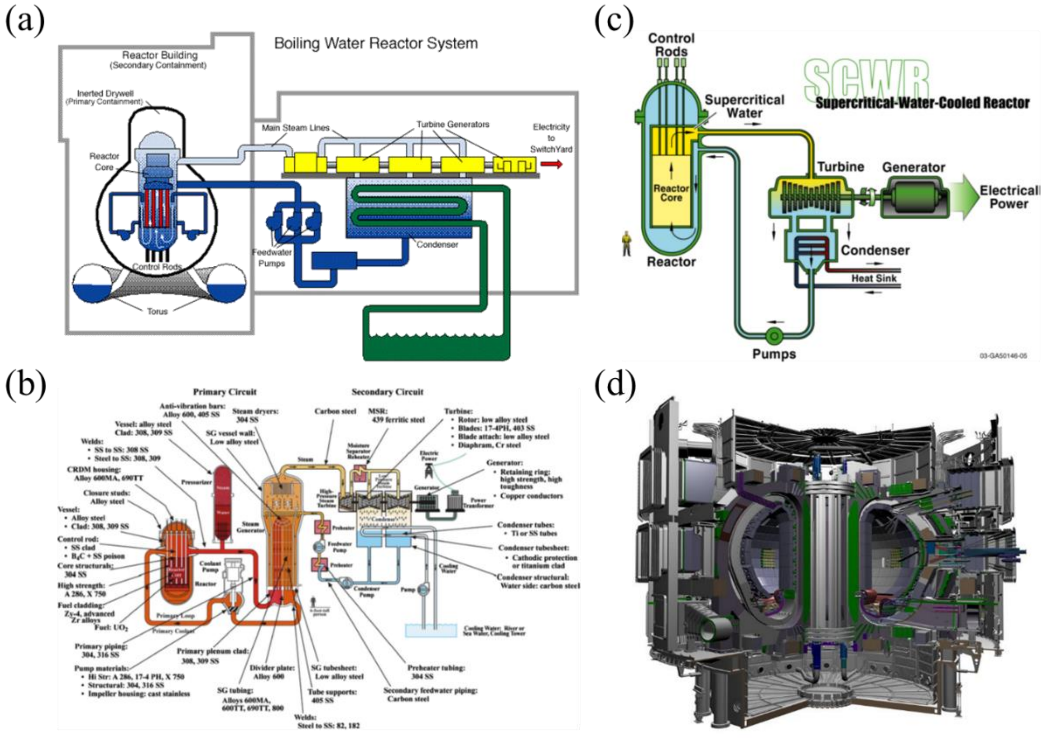

Fig. 2.1 Schematic of (a) BWR (b) PWR (c) SCWR and (d) ITER

In Boiling Water Reactor (BWR), liquid water transforms into steam and steam directly drives generator. Typical BWR circuit design is depicted in Fig. 2.1(a)[1]. In Pressurized Water Reactor (PWR), liquid water in primary loop doesn't go through phase transformation, but deliver heat into secondary loop via heat exchanger. Steam is generated in secondary loop then drives generator. Typical PWR design and structural materials is depicted in Fig. 2.1 (b)[2]. Supercritical Water Reactor (SCWR) is a direct-cycle design, as shown in Fig. 2.1 (c) [3]. It adopts supercritical water which eliminates phase transformation.

Cooling water also functions as moderator, it decelerates fast neutron into thermal neutron. Moderating effect becomes better in denser water because more collision between neutron and water can occur. Once temperature increases, density decreases; the extent of neutrons slowing down also decreases, hence the number of thermal neutrons and the reactivity of core decreases. As a result, less heat is produced and temperature will eventually drop to normal range, re-stabilizing the reaction rate. This feature is called negative temperature coefficient of reactivity. The intrinsic passive safety is critical in light water reactors.

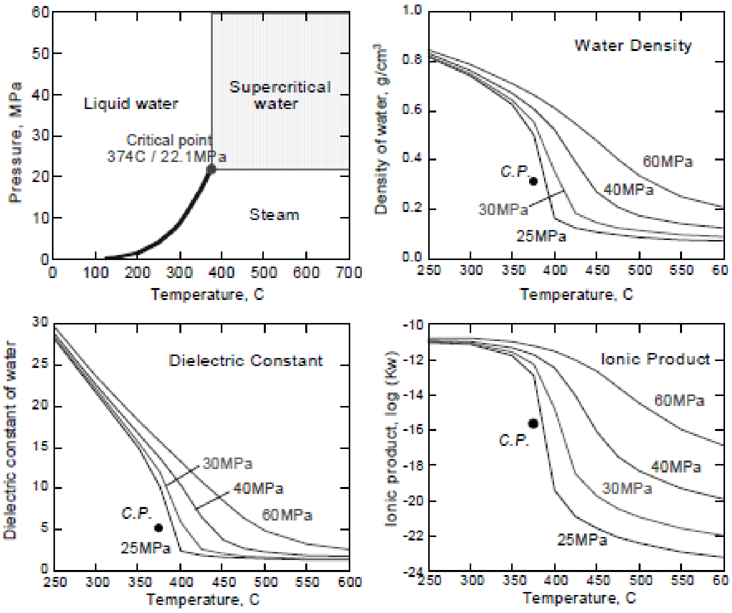

Fig. 2.2 Physical properties of supercritical water[4]

Supercritical water acts different from ordinary water. Above supercritical point (373.94^{o}C, 22.06 MPa), water density drops, gas miscibility increases and solubility to inorganics becomes negligible, as shown in Fig. 2.2. Water and steam become indistinguishable. This allows components like pressurizers, steam generators (in PWR), steam separators, dryers and recirculation pumps (in BWR) being omitted. Supercritical water also has good heat transfer. It allows a huge enthalpy increase which yields high thermal efficiency (~44%) comparing to 33~36% of in-service PWR and BWR. A succinct design lowers constructing cost, higher thermal efficiency provides more electricity, which provides SCWR an economic advantage. Supercritical water also possesses negative temperature coefficient. Yet, its density is lower than ordinary water which only partly moderates neutron. This makes SCWR exhibits certain characteristics of a fast neutron reactor. According to design concept differences, BWR and PWR are Generation II design while SCWR is Generation IV design.

Fusion reactor adopts deuterium-tritium (D-T) reaction, which releases 17.6 MeV per collision. Deuterium is abundant in seawater. Tritium can be bred from Li-6 by neutron bombardment with neutrons of any energy. Both two fuels are regarded as inexhaustible. Conceptually, it is necessary of a container to support extremely high temperature for fusion reaction. Tokamak is one of magnetic-confining design and being considered one of leading candidate. Two different shape of design are developed: the Stellarator (e.g. Wendelstein 7-X, German) and the D-shape like (e.g. International Thermonuclear Experimental Reactor (ITER), France (Fig. 2.1 (d)[5])).

Tokamak magnetically confines gaseous fuels, heats up and turns fuel into hot plasma. Neutrons generated from D-T reaction are absorbed by tritium breeding materials (e.g. lithium compound) that contained in blankets. Blankets absorbs kinetic energy of the neutrons and hence heated up. Heat energy is gathered by coolant flowing through embedded flowing channel. Coolant then transfer heat energy into electricity.

Light water is chosen as coolant for the double-loop heat transfer system of ITER. This system is also known as Tokamak Cooling Water System. Light water is responsible for extracting heat from plasma-facing components (ex: testing blanket modules (TBM) and diverters) and transfer heat to secondary heat removal systems. The designed pressure and temperature of primary loop are similar to in-service PWR. Other proposals use supercritical water. As water flow through TBMs, bred tritium in blanket may penetrate into cooling water. With the aid of high fluence, tritium reacts with cooling water and form tritiated water with soluble gaseous TH/H_2. These tritiated water and gases are extracted by a recovery equipment.

2.2 Austenitic stainless steels

The 300-series austenitic stainless steel is most widely applied as structural components among all types of stainless steel. They can be seen in petrochemical, automotive, aerospace and nuclear industries. This family tree and developments are shown in Fig. 2.3[6] This Iron-based ternary alloy (Fe-Cr-Ni) typically has low carbon content (<0.08%), 16-26 wt% Cr and 3.5-22 wt% Ni. It is a face-centered cubic structure. The structure and austenite phase stability can be predicted from Saeffler-DeLong diagram (Fig. 2.4[7]) Low alloyed stainless steel locates closer to lower left corner, such as type 304. Highly alloyed steels are located closer to upper right corner, such as type 310S. The closer to martensitic region, the easier of steel transform into martensite during cold-work or tensile deformation. In other words, the austenite phase of low alloyed steel is metastable.

As for carbon steel, austenite phase only exists above eutectoid temperature. As steel queches, austenite transforms into a mixture of ferrite and cementite, or into martensite by slight lattice distortion. The addition of carbon, Ni or Mn can lower eutectoid temperature, allowing austenite exists in wider temperature range, even at room temperature. The minimum requirement of Ni content for austenite phase presence at room temperature is roughly at 8%. On the other hand, the addition of Cr and Mo raises eutectoid temperature. Hence, carbon, Ni and Mn are categorized as austenite stabilizer; Cr and Mo are austenite de-stabilizer or ferrite stabilizer.

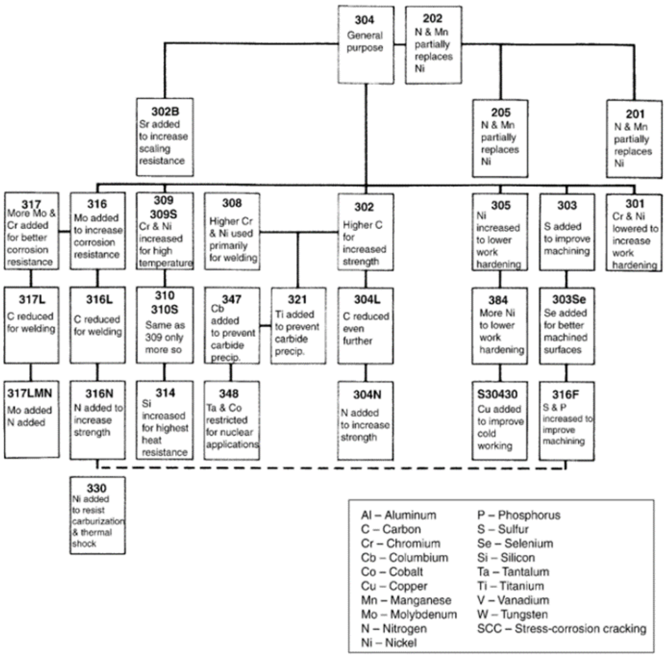

Fig. 2.3 The composition and property linkages in family [8]

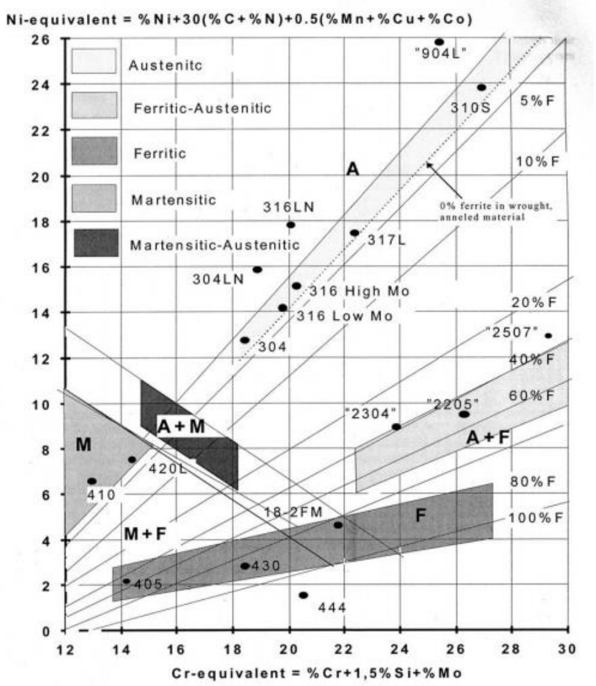

Fig. 2.4 Schaeffler-Delong diagram that predicts phase structure for different alloys and chemical compositions in stainless steels [7]

2.2.1 Effect of alloying elements

Followings briefly describes the effects of alloy elements:

Carbon (C) increases the strength and hardness by solid solution strengthening. It is essential to the formation of cementite and other carbides. In ferritic grades carbon reduces both toughness and corrosion resistance. In martensitic grades carbon increases hardness and strength, but decreases toughness. It is kept at low levels in austenitic grades, because it might form chromium carbide which decreases corrosion resistance.

Chromium (Cr) is responsible for the corrosion resistance. A minimum of 12% is required to form continuous, self-reforming, passive layer of chromia on steel surface. It increases oxidation resistance at high temperatures.

Molybdenum (Mo) improves resistance to pitting and crevice corrosion especially in chlorides and sulphur containing environments. It slightly increases mechanical strength. However, it enhances the risk of secondary phase formation in austenitic steels.

Nickel (Ni) also increases strength, ductility and toughness by solid solution strengthening. It also improves the resistance to sulfuric acid attack.

Manganese (Mn) is similar to nickel. It can improve hot ductility. It also increases the solubility of nitrogen. It preferentially reacts with oxygen and sulfur, forming MnO and MnS;

therefore, it functions a deoxidizer and desulfurizer. It is used as a substitute for nickel in 200 series.

Silicon (Si) increases oxidation resistance. It promotes ferritic microstructure and increases strength. It is used as a deoxidizer during steel manufacturing.

2.2.2 Carbide precipitation

In steels, strong carbide formers include Cr, Mo, V, W, Ti and Nb. Carbide precipitates in steel is mainly $M_{23}C_6$, where M represents abovementioned elements. Other carbide forms such as M_7C_3, M_6C and MC also form under different heat treating process or application condition. During steel fabrication, rapid quenching from annealing temperature is applied to prevent Cr diffusion. The relationship between carbide precipitation and carbon content is delineated in Fig. 2.5 [6].

Once steels are kept at elevated temperature ranging from 475 to 815 °C, Cr may diffuse, react with carbon and form chromium carbide. This reaction consumes large amount of Cr in matrix and depletes adjacent Cr in matrix. Phenomenon and Cr concentration profile near Cr-depleted zone are depicted in Fig. 2.6 (a) and (b)[9], respectively. If Cr content is below 12%, continuous passive chromia layer cannot be formed. Steels are hence sensitive to corrodants and may suffer intergranular corrosion or intergranular attack. This degradation in corrosion resistance is named as sensitization.

Some works show that sensitization occurs at low-temperature region (300-425 °C) as well. Cr still remain diffusible within this temperature region. Reaction with carbon is likely to happen. But requires nucleation sites such as pre-existing carbides at grain boundary. Sources of carbides could come from welding, slow-cooling from solution-annealing or precipitation at deforaion-induced martensite. Low-temperature sensitization is likely to occur after long time operation (e.g. over a decade).

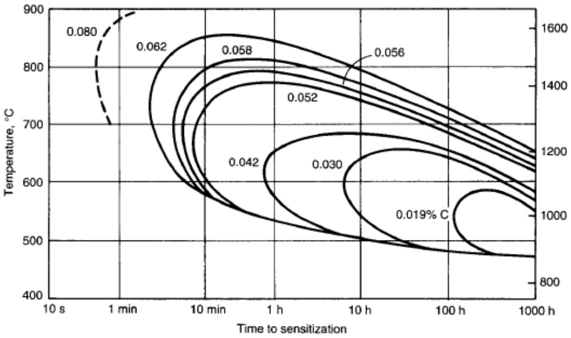

Fig. 2.5 The relationship between carbide precipitation and carbon content [6]

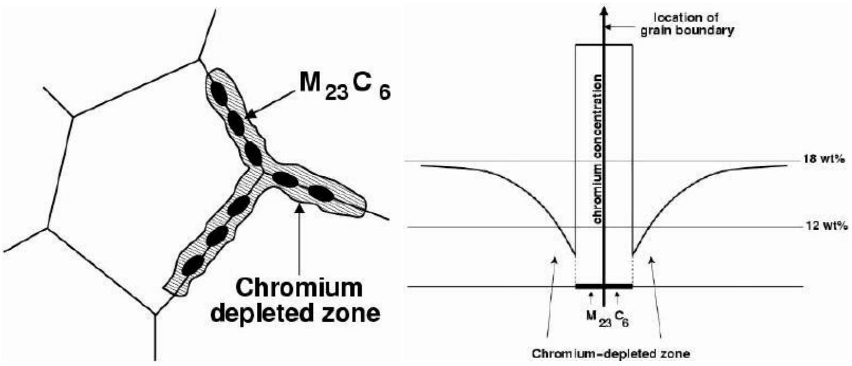

Fig. 2.6 Schematic of (a) Cr-depleted zone and (b) Cr concentration profile as M23C6 precipitates adjacent to grain boundary [9]

2.3 Oxide film structure

At room temperature, stainless steels form a passive oxide film on its surface. This film, with several nm in thickness, prevents further oxidation into steels. At hot water, passive film transforms to a double-layer structure: a dense, Cr-rich spinel inner layer (typical formula is $Fe_xNi_yCr_{3-x-y}O_4$ where x, y varies with testing alloys) and a porous, magnetite outer layer with Fe_3O_4 or Fe_2O_3. Systematic analysis of oxide formation under different water chemistry is conducted by Kim's group, Uchida's group and Yeh's group. Of which results are summarized in Table 2.1. Kim points out that whether under oxygen dissolved or hydrogen dissolved environment, the thickness of inner layer is around 200nm.

Table 2.1 Summary of oxide film structure analysis of SSs from selected research groups

Author	Material	Condition	Outer layer	Inner layer	Thk (mm)
Y.-J. Kim [10]	304	200ppb [O_2],2weeks	α-Fe_2O_3	$FeCr_2O_4$ Cr-rich	~1.2
		200ppb[H_2O_2],2weeks	γ-Fe_2O_3 Ni-rich	$NiFe_2O_4$	~1.325
		150ppb [H_2]	Fe_3O_4(large) $FeCr_2O_4$(small)	$FeCr_2O_4$ Cr-rich	~0.9
	316	200ppb [O_2] + 20ppb [H_2],2weeks	γ-Fe_2O_3(large) α-Fe_2O_3(medium)	$Fe_xCr_{3-x}O_4$	
S. Uchida [11–13]	304	200ppb [O_2],200hr	Fe_3O_4(main)	$FeCr_2O_4$	Outer : ~0.27 Inner : ~0.2
		100ppb [H_2O_2],200hr	α-Fe_2O_3(main)	$NiFe_2O_4$ Fe_3O_4	Outer : ~0.5 Inner : ~0.27
Y. Wada [14,15]	304	[O_2], 170hr	Fe_3O_4(main)+ α-Fe_2O_3	$FeCr_2O_4$	
		1ppm [H_2O_2],30hr	α-Fe_2O_3(main) +Fe_3O_4	$NiFe_2O_4$	

C.-M. Yu[16]	304	300ppb [O_2],240hr	α-Fe_2O_3		
		50ppb [H_2],240hr	Fe_3O_4(large) $NiFe_2O_4$, $FeCr_2O_4$(small)		
Y.-C. Chien[17]	304	300ppb [O_2],240hr	α-Fe_2O_3(main)		
		300ppb [O_2],240hr -> 150ppb [H_2],240hr	Fe_3O_4(main)		
Po-I Wu[18]	304	300ppb [O_2],2weeks	Fe_3O_4(main)+α-Fe_2O_3		Outer : ~0.7 Inner : ~0.5
		300ppb [H_2O_2],240hr	α-Fe_2O_3(main)+Fe_3O_4 +$NiFe_2O_4$		Outer : 0.8~1 Inner : 0.3~0.35
		300ppb [O_2],240hr -> 150ppb [H_2],240hr	Fe_3O_4		Outer : ~0.7 Inner : ~0.2
		300ppb[O_2],2weeks -> 300ppb [H2O2],240hr	γ-Fe2O3	Fe_3O_4 $NiFe_2O_4$	

2.4 Stress Corrosion Cracking

Stress corrosion cracking (SCC) is one of environmental-assisted cracking phenomenon. It is a degradation combines following three factors: the susceptible materials, the tensile stress, and the corrosive environment, as shown in Fig. 2.7 (a). It is regarded as a synergistic interaction of metallurgical, mechanical and electrochemical aspects.

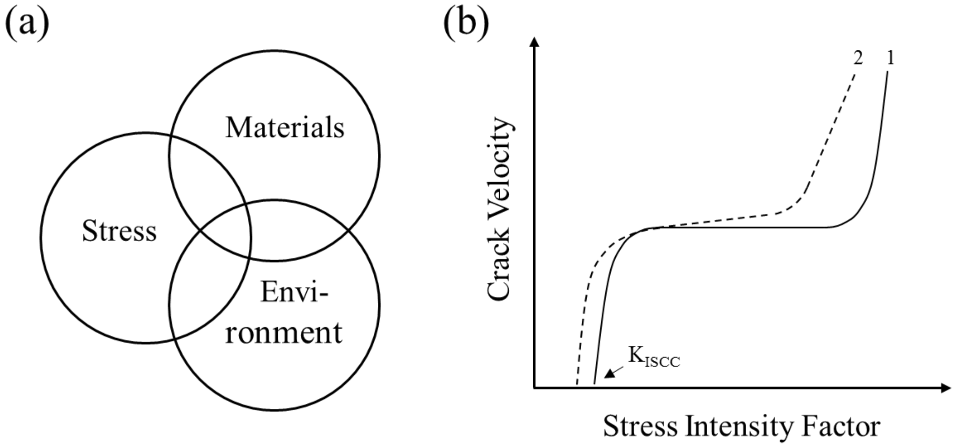

Fig. 2.7 Schematics of (a) SCC factors (b) crack development at different stages.

Crack is perpendicular to stress direction. Cracking can be divided into three stage: incubation, initiation and propagation. Crack initiates as stress intensity surpasses threshold value, K_{ISCC}. The crack growth rate during propagation is nearly constant until crack enters final fracture. The more severe of an environment, the smaller the K_{ISCC} and the faster the velocity will be. This progress is depicted in Fig. 2.7 (b). Fracture could be intergranular or transgranular, or a mixed mode of them. The definition of crack nucleation and initiation varies among researches. Some refer to impurities and/or precipitations at specimen surface. Some suggested that the localized metal ion dissolution at the intersection of slip bands and specimen surface serves as initiation site. Some views pitting as a precursor of cracking.

SCC occurs on almost every internal component of BWR and PWR. Numerous derivative submodes exist due to different water chemistry, fracture characteristics and incident locations. For instance, primary water SCC (PWSCC) describes incidents in primary water of PWR; intergranular SCC (IGSCC) describes intergranular fracture; low potential SCC (LPSCC) represents incidents at lower potentials close to hydrogen equilibrium; and interdendritic SCC (IDSCC) highlights those happens within welding-developed dendritic structure in weld metal

2.4.1 Inducing factors and countermeasures

Followings are major causes and countermeasures of the three factors.

In *material* aspects, classical sensitization and low-temperature sensitization are major causes of intergranular corrosion and intergranular SCC. Mechanism is described in section 2.2. Adding carbide stabilizer such as Ti, Nb and Ta reduces degree of sensitization. Types of stainless steels include 321(Ti added) and 347(Nb, Ta added); types of Ni-based alloys include Alloy 82 and Alloy 52. Reducing carbon content below 0.03% is another solution. Low-carbon grade stainless steels such as 304L and 316L. Increasing Cr to strengthen self-healing passive film is also feasible, such as Alloy 690 (comparing to Alloy 600).

In *tensile stress* aspects, structural load and residual stress are two major causes. Residual stress within materials could come from heat treating, welding process or cold working. Heat treating and welding process (whether similar or dissimilar, one-pass or multi-pass) have material and workpiece experienced uneven thermal cycle from weld pool center to periphery. This results in microstructure distortion and multi-layered new microstructure different from original ones. Affected regions are called heat-affected zone (HAZ). Extensive SCC incidents are reported within HAZ. Cold work produced hardened layer near surface also affects SCC susceptibility.[19–23] A number of works indicated HV270~300 could be a threshold of SCC occurrence. [24,25] Nonetheless, root cause remains opaque.

Solution-annealing heat treatment is an effective way to annihilate residual tensile stress. Shot peening[26], water jet peening[27], laser peening[28] and mechanical stress improvement process[29] are able to decrease the degree of tensile stress state and create compressive stress state on component surface. In welding technique improvement, the consensus is lowering total heat energy input. Change of design reduces required welding processes. Advanced technique such as last pass heat sink welding can create residual stress state in welds. High energy beam welding technique, such as laser beam welding and electron beam welding, has higher energy density that are able to achieve smaller HAZ. Comparing to traditional gas tungsten arc welding and shield metal arc welding, rapid thermal cycle of a welding process prevent welds from thermo-induced microstructural changes, such as sensitization.

In *environment* aspects, one important indicator is the electrochemical corrosion potential (ECP). ECP reflects overall redox reaction on metal at equilibrium state. It can indicate the aggressiveness of water environment. For instance, flow-rate and temperature greatly affects rate constant of a redox reaction on material. Flow-accelerated cracking are prone to occur on elbow piping and often accompanied with wall thinning. Aggressive species such as chloride ions and sulfate ions are known detrimental. Oxidants such as hydrogen peroxide and oxygen in water shapes a corrosive environment and increases ECP on metals. Typically, normal water chemistry contains 200ppb dissolved-oxygen with ECP around +100 $mV_{SHE.}$ To reduce oxidant level, lower corrosion potential, hydrogen was injected into feedwater to modify water chemistry.

In BWR, this technique is known as Hydrogen Water Chemistry (HWC). SCC are suppressed when corrosion potential reaches “protection potential” of $-230mV_{SHE.}$ [30] Changes of ECP after HWC application is shown in Fig. 2.8 [31] The relationship between ECP and crack growth rate is described in Fig. 2.9 [32,33]. Nonetheless, recombination effectiveness relies on gamma-radiation in downcomer, of which the design varies from plant to plant, no standard HWC is applicable. Alternation between normal and hydrogen water chemistry lead to a Co^{60} concentration increase and radiation buildup [34]. Further, its coverage region is limited, leaving steam region unprotected [31,32] Increasing H_2 injection amount to expand coverage causes N^{16} increase in main steam lines. Noble metal chemical addition (NMCA) is later introduced to improve the efficiency of recombination process and to expand coverage region. Pt compounds are able to adhere to wetted area, including components in steam phase. Online NMCA is also developed which allows addition during full-power operation. Benefits in reducing corrosion potential and exchange current density is illustrated in Fig. 2.10.

In PWR, primary water contains 1000ppm B as H_3BO_3 for reactivity control and 2 ppm

Li as LiOH for pH control (at the start of a cycle). It contains hydrogen around 30 cc. STP/kg H_2O thus operates at lower corrosion potential. Water environment is less aggressive. Boron and Lithium concentration shift pH value and following Fe/Fe ion equilibrium boundary and corrosion resistance. Yet, high strength materials, such as Alloy 600, still suffers PWSCC at this normal operating condition.

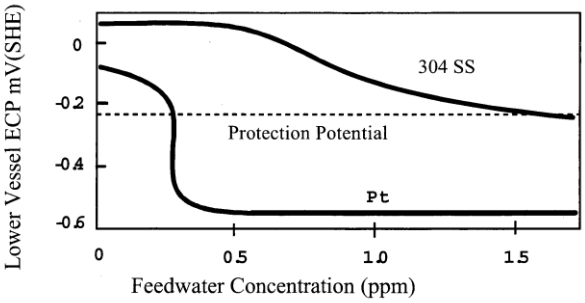

Fig. 2.8 Changes of ECP on 304 stainless steel as a function of hydrogen concentration[31]

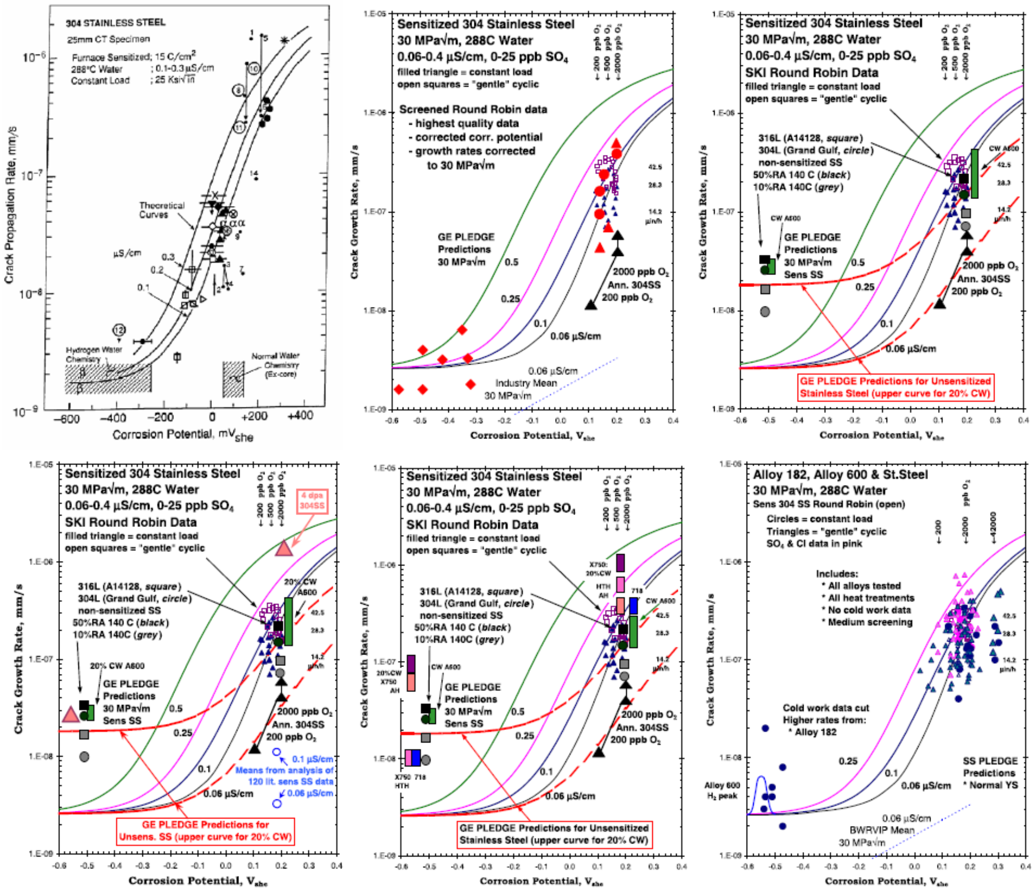

Fig. 2.9 The relationship between ECP and crack growth rate

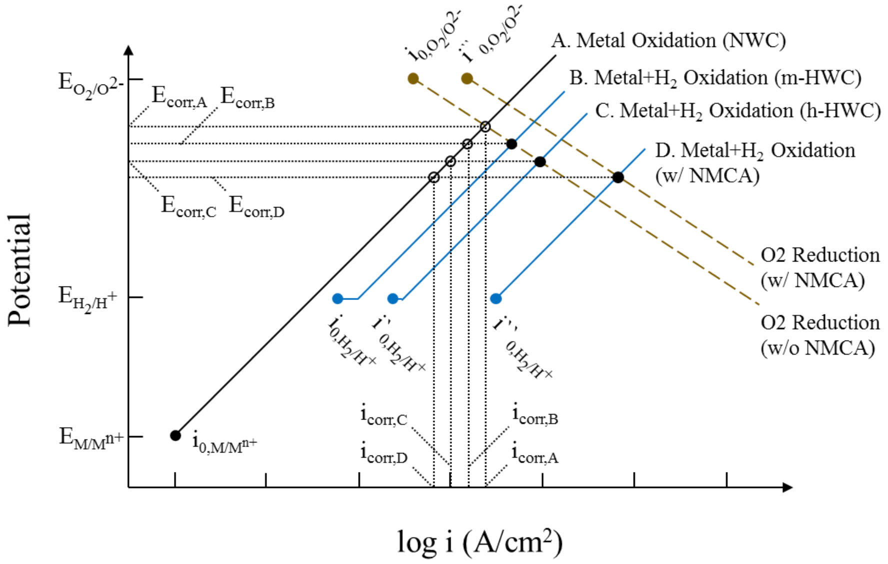

Fig. 2.10 Schematic of corrosion potential-current density diagram showing benefits of EPMA application on ECP decrement

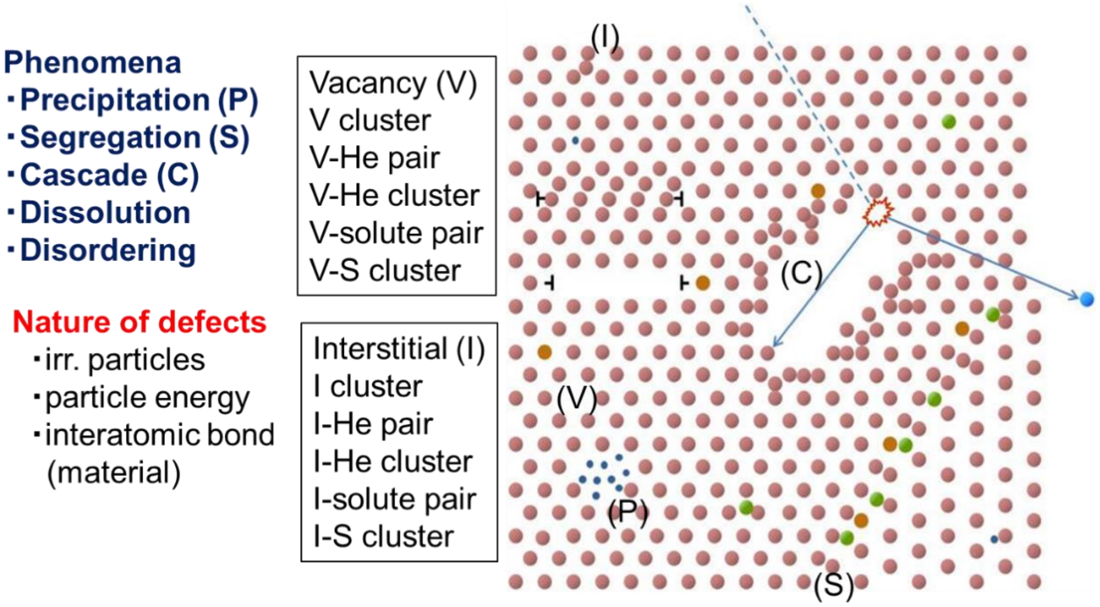

Fig. 2.11 Schematic of microstructure in irradiated stainless steel [35]

Irradiation is a unique factor among inducing factors. Radiation interacts with cooling water; radiolysis increases hydrogen peroxide and oxygen concentration. Neutron radiation displaces atoms, creating vacancy and self-interstitial atom pair. Most of defects are unstable and annihilates by recombination. Remaining defects reforms into stable forms such as dislocation loops, void and cavities and precipitates at dislocations, grain boundaries or precipitate/matrix interfaces. Fig. 2.11 [35] is a schematic that shows typical microstructures of irradiated material. Defects interact with elements such as Cr, Mo, and Ni. Unbalancing element content within metal matrix. For instance, Cr has higher diffusivity and higher exchange frequency with voids. Voids deplete Cr adjacent to grain boundaries and form a Cr-depleted zone. This phenomenon is called radiation-induced segregation. Typically, susceptibility to IGSCC of stainless steel is proportional to neutron fluence.

2.4.1.1 Inhibitive protective coating

The concept of inhibitive protective coating (IPC) technique is lowering mass transportation rate, reaction rate and consequential overall exchange current density on specimen surface by applying a non-directive barrier coating on component surface. Candidate materials include titanium oxide and zirconium oxide. Application method include alloying, plasma-spray[36], sol-gel [37,38]and hydrothermal deposition[16–18,39–41]. Hydrothermal deposition method is suitable for in-service plants. By injecting Zr-included chemical compound suspension into feedwater, compound adsorbs onto oxide films and forms an inhibitive barrier.

2.4.2 Mechanisms

So far, several models are applicable to certain metal-environment systems. Models and mechanisms remain separate and consensus. SCC is considered being controlled by electrochemical process at crack-tip. Electrochemical reaction involves anode and cathode reaction:

Anode: $M^{-}> M^{n+} + ne^{-}$

Cathode: $O_2 + 2H_2O + 4e^{-} \text{->} 4OH^{-}$ or $2H^{+} + 2e^{-} \text{->} H_2$

Anode reaction is dominant by metal dissolution process. Several models are stemmed from this concept. In cathode reaction, which reaction takes place depends on the local electrochemical pH, potential, oxygen, hydrogen and ion concentrations at the crack-tip. Some works conjecture that hydrogen generated at crack-tip affects crack behavior.

2.4.2.1 Metal dissolution

Pre-existing active path model describes that metal dissolution at a pre-existed initiation site or crack-tip triggers crack advance. As a metal is under tensile stress state condition in a corrosive environment, the passive film may brake caused by the combination of tensile stress and electrochemical reaction, resultantly exposing fresh crack surface to environment. This creates a localized galvanic pair (unprotected area as anode, passive region as cathode) and provides a starting point for corrosion and followed by creation of clean surface or cracks. Corrosion thereby follows this pre-existed path till component failure. Initiation sites, for instance, include the intersection between surface and slip planes and/or deformation band/texture and between surface and grain boundary and precipitates at grain boundary.

Film rupture (or slip-dissolution) model is a refinement model. In this model, passive film covers surface and crack tip. Crack growth stops and reactivates until sufficient buildup of the crack tip strain to rupture passive film. (Fig. 2.12[42]) Crack advances intermittently, leaving striations (crack-arrest mark) on fractured surface. F. P. Ford and Peter L. Andresen based on the concept of "film rupture-dissolution-repassivation cycle" and developed an empirical formula to predict crack-tip strain rate. In this model, corrosion potential and environments at crack-tip are controlled by external (surface) environment. Potential difference between crack-tip and surface dominates ion transportation. (Fig. 2.13 [42]) Crack growth rate is controlled by crack-tip strain rate. If strain rate is too high, mechanical process dominates crack advance and make it irrelevant with environment. Controversially, if strain rate is too low, general corrosion process will dominate crack advance and stop crack growth. This model is also referred as “Ford–Andresen film rupture model" Recently, however, some critics on the lack of presumptions of electrochemical reaction.

Coupled Environment Fracture Model (CEFM) is proposed by D. D. Macdonald that bases on “electron charge conservation”[43]. This model presumes that crack tip is narrower than crack mouth, and its mass transfer rate is lower than that of crack mouth. Electrochemical reaction occurs at crack-tip and consumes oxygen. Oxygen is replenished by fresh oxygen diffused from surface. Once oxygen consuming rate is higher than replenishing rate, it will achieve a relatively low ECP while surface remains relatively high ECP state. This potential difference forms a potential gradient, driving metal ions from crack-tip to surface. Meanwhile, electrons migrate to surface and recombine with metal ions or being consumed by other reduction process. Electron charges are therefore conserved.

Film rupture model and Coupled Environment Fracture Model well describe behavior of intergranular SCC, but rules out the transgranular SCC.

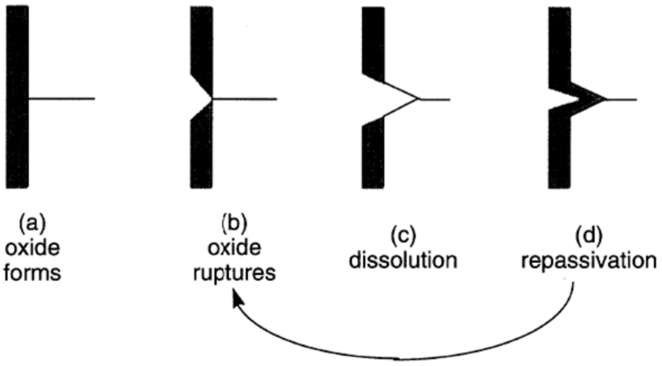

Fig. 2.12 Schematic of film rupture model [42]

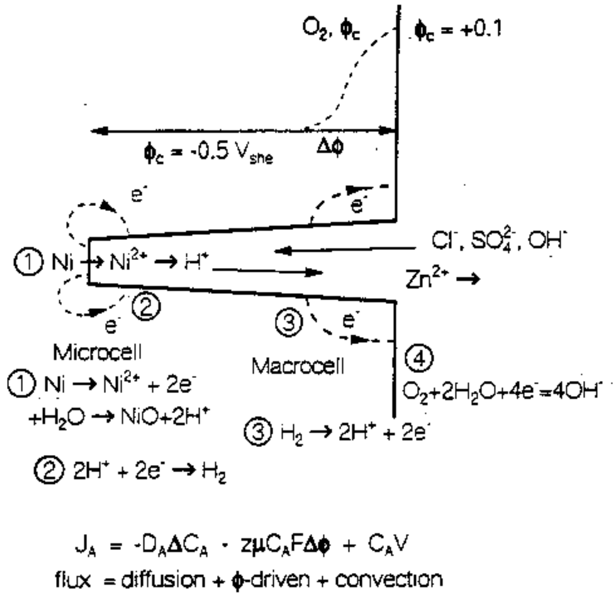

Fig. 2.13 Electrochemical reaction at crack-tip and surface of slip-dissolution model [42]

2.4.2.2 Hydrogen embrittlement

Hydrogen could be introduced during fabrication (internal) or by exposure to hydrogen-containing environment (external). In water or other aqueous solutions, hydrogen was generated by cathodic reaction, whether by nature or by artificially applied potential. For the occurrence of hydrogen-induced cracking, hydrogen must be transported to and being trapped at a certain potential degradation site. Fig. 2.14 [44] illustrate this trapping concept. The critical hydrogen concentration to cause hydrogen-induced cracking and hydrogen diffusion rate, which may determine the incubation period for concentration buildup, are important steps as well. Alloying elements such as carbon influence diffusion rate; types of defects affect trap binding energies and trapping capacity.

Several mechanisms have been proposed for hydrogen-induced cracking. One is

Hydrogen-enhanced decohesion (HEDE), proposed by R. A. Oriani [44] and his colleagues. Another is hydrogen-enhanced localized plasticity (HELP), proposed by H. K. Birnbaum, P. Sofronis and co-workers.[45] Still, another mechanism such as high gas pressure in internal voids and formation of brittle hydride and hydride-induced embrittlement. Considering water environments and materials used in practical light water reactors, HEDE and HELP are two viable mechanisms in explanation.

The HEDE mechanism proposed that localized hydrogen weakens metal-metal bonding strength at or near crack-tip by decreasing electron-charge density between metal-metal atoms. The HELP mechanism based on experiments carried out over a range of strain rates and temperatures. Hydrogen in a solid-solution decreases the repulsive stress field between dislocations and the barriers to dislocation motion. This results in an increased amount of deformation in a localized region and a reduced macroscopic ductility.

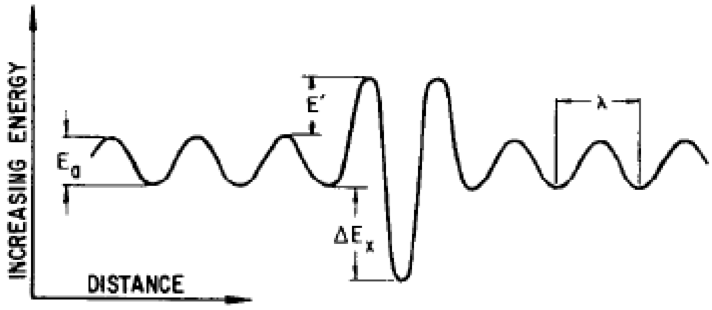

Fig. 2.14 Model of hydrogen tapping site [44]

2.5 SCC in hydrogen-dissolved water environments

As discussed in section 2.3, SCC occurs on numerous types of stainless steels, Ni-based alloys and weld metals used in components or welding process at oxygenated or deaerated boiling water environment and primary water environment in pressurized water. Extensive incidents have been reported. Aside design and material changes, improvements of stress-relief treatments and welding techniques, water chemistry optimization are commonly used techniques. Current in-service BWR and PWR injects hydrogen into feedwater to mitigate corrosion and to reduce radiolysis.

Early PWRs in the U.S. were operated with water with dissolved-hydrogen around 25-50 cc. STP/kg H_2O so as to provide enough margin against radiolysis. Researchers from Électricité de France S.A. found that 10 cc/kg would be enough if dissolved-oxygen was in good control. In searching adequate dissolved-hydrogen margin, several research teams found that PWSCC crack growth rate (CGR) of Alloy 600 reached a maximum when corrosion potential close to the Ni/NiO thermodynamic equilibrium. Some captions and collected works, as shown in Fig. 2.15 [46], Fig. 2.16, [47], Fig. 2.17 and Fig. 2.18, provide glance on these research results. Fukumura tested cold-worked (CW) Alloy 600 and found CGR peaked at DH=0.5 ppm, 290°C. (Fig. 2.16(e) [48]) Yamada tested CW TT690 alloy and reported CGR peaked at 30 cc/kg, 360°C. (Fig. 2.16(f) [49]) The crack initiation and growth time of Alloy 600 was examined by Molander and his co-workers, as presented in Fig. 2.16 (c) and (d) [50], respectively. Results showed that as hydrogen content increased, crack initiation time decreased.

Effects of hydrogen on Ni-based weld metal was also examined. Works from Pacific Northwest National Laboratory (PNNL) and S. M. Bruemmer (Fig. 2.17 (e)[51]) showed a maximum CGR on Alloy182 and Alloy 82 respectively. Bruemmer compared his works and PNNL`s works. He suggested that alloy compositions and testing temperatures shifted the peak of CGR. Temperature effect was further examined by Andresen. Fig. 2.17(c) [52] and Fig. 2.17(d) [53] showed effect of dissolved-hydrogen and effect of temperature on PWSCC CGR for Alloy 182. Fig. 2.17(d) profiled results of changing from 25 cc/kg to other content. Reducing from 25 cc/kg to 4 cc/kg or below seemed detrimental to materials. On the other hand, increasing from 25 cc/kg to 45 cc/kg or higher seemed beneficial. Fig. 2.17(a) [54] is prediction results at different temperatures of Alloy 82.

A number of works studied CGR behavior for cold-worked type 316(L) stainless steel. However, variance exists among these works. Choi tested as-received 316L and found that CGR at 50 cc/kg was higher than at 25 cc/kg. The CGR of warm-rolled 316L was higher than as-received one, as shown in Fig. 2.18 (d) [55] G. Furutani reported that IGSCC percentage of CW 316 increased as dissolved-hydrogen increased, as shown in Fig. 2.18 (a) [56] On the other hand, Meng found a monotonic decrease on 28% CW 316NG steel, as shown in Fig. 2.18 (b) [20]. Zhong tested heavy and moderate CW 316 steel at 325°C. He reported a minimum strain at 15 cc/kg, as shown in Fig. 2.18 (c) [57] Fukumura examined non-sensitized 316 SS and found a minimum CGR at 30 cc/kg, 310°C, as shown in Fig. 2.18 (e) [58].

Investigations extended into BWR operating conditions. However, available data was limited. Andresen's model predicted CGR of Ni-based alloys. Results suggested a small peak in crack growth rate at Ni/NiO boundary, as marked in star symbol in Fig. 2.17 (f) [54]. Corresponding hydrogen level was shown in Fig. 2.17 (b) [54], which is close to moderated HWC (200-400ppb). Nono found a brittle fracture on solution-annealed 316L at DH=0.4 ppm, 288°C. [59] Abovementioned researches are summarized in Table 2.2.

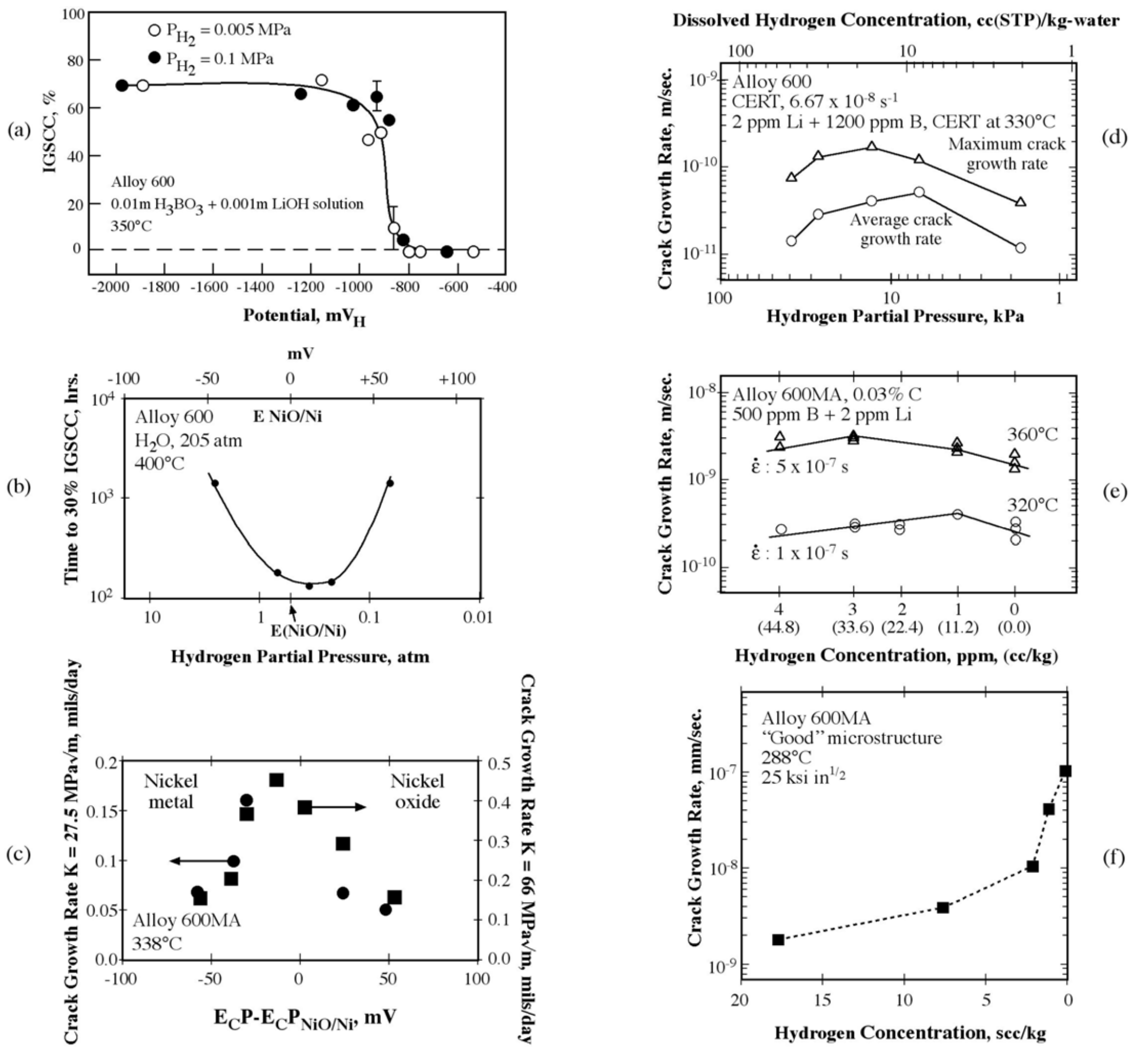

Fig. 2.15 Caption of PWSCC CGR tests for milled-annealed Alloy 600 under hydrogenated primary water environment. Data from (a) Totsuka, (b)Scott and Combrade, (c) Morton, (d) Lee, (e) Totsuka and (f) Andresen and Angeliu [46]

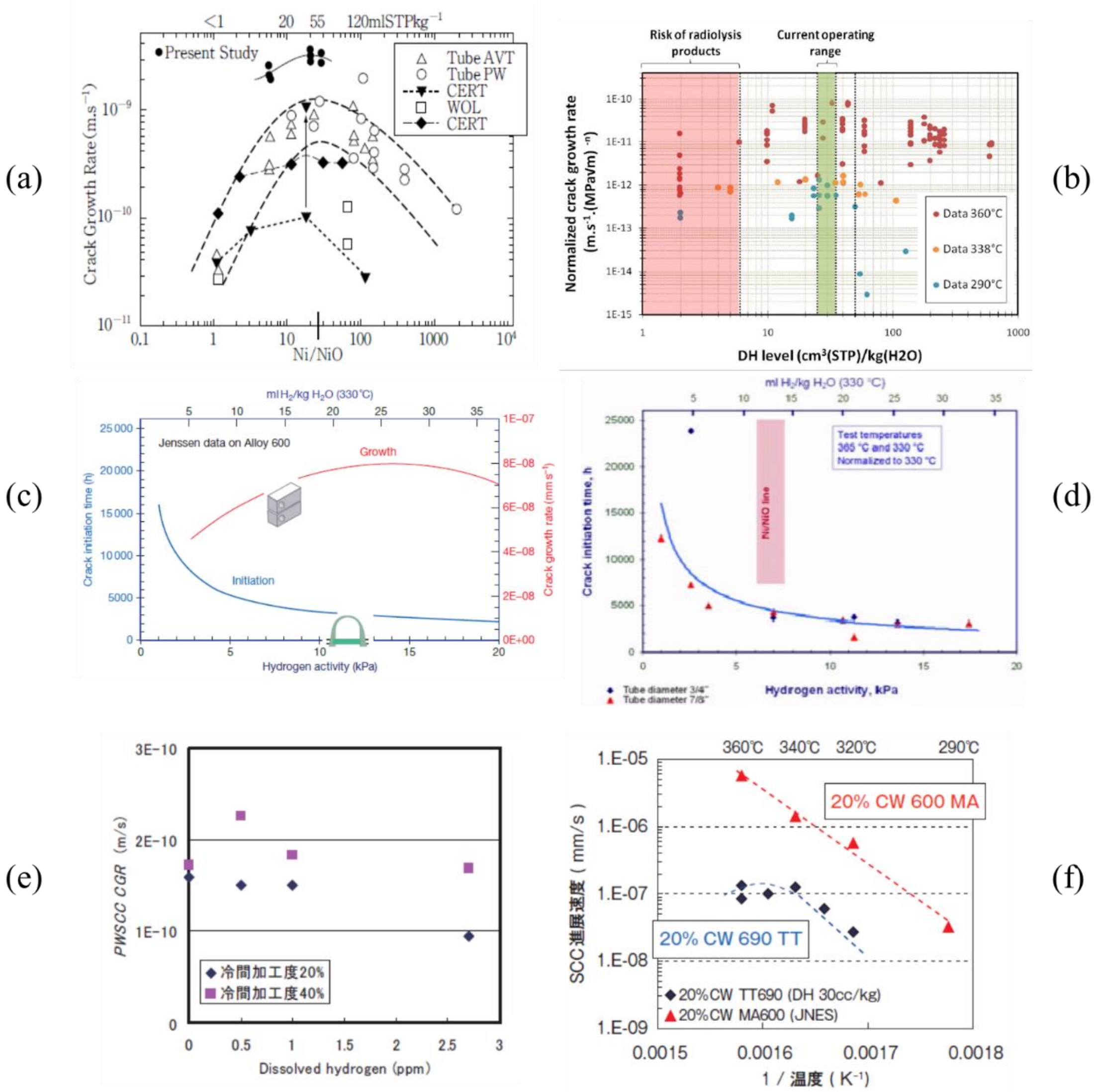

Fig. 2.16 Caption of PWSCC CGR tests for Alloy 600 under hydrogenated primary water environment. Data from (a) Totsuka[47], (b) Labousse (where red are from Soustelle; orange are from Morton and blue are from Caron)[60], (c),(d) Molander[50], (e) Fukumura[48] and (f) Yamada.[49]

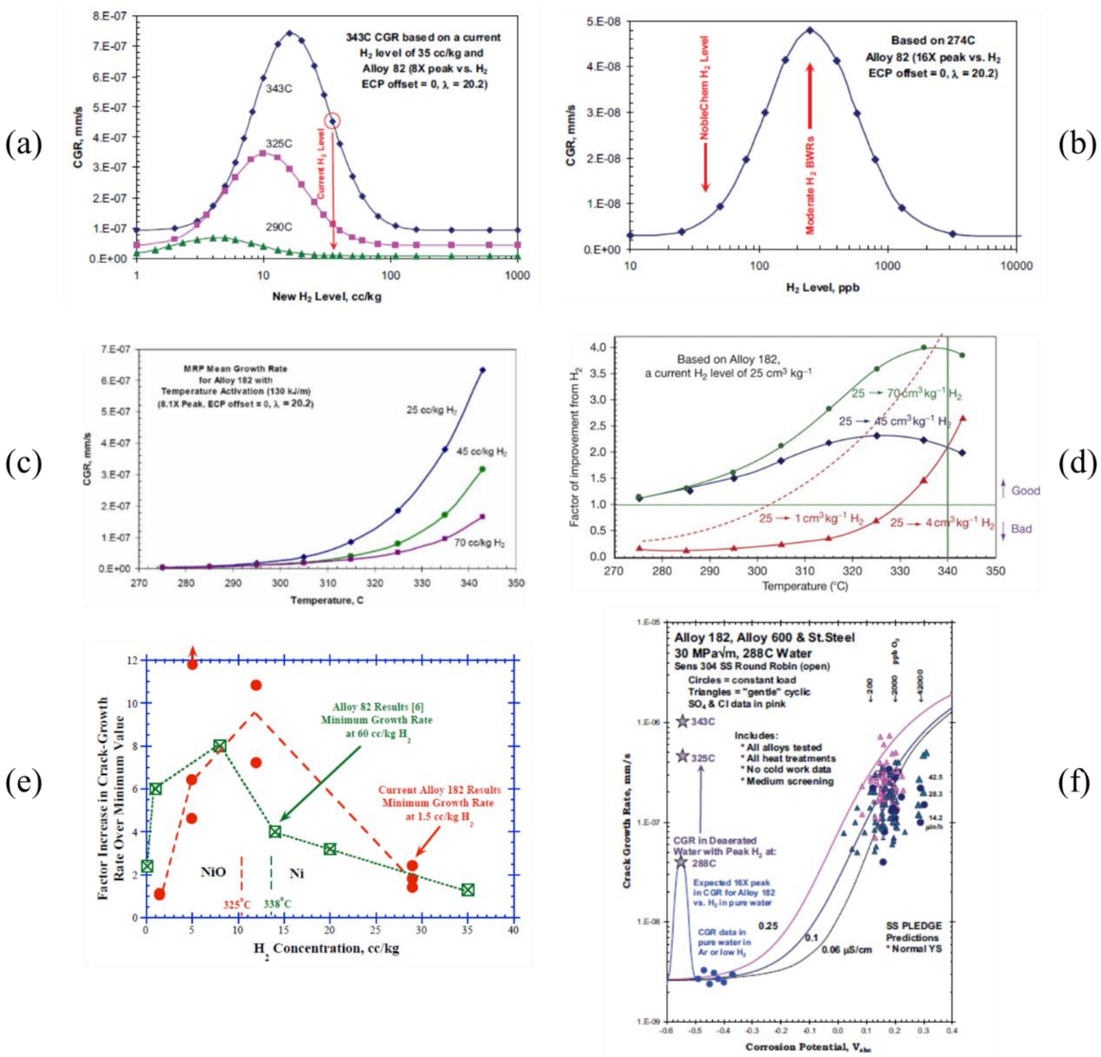

Fig. 2.17 Caption of PWSCC CGR simulations/tests for A182/82 under hydrogenated primary water environment. Data from (a-d,f) Andresen [53,54]and (e) Bruemmer.[51]

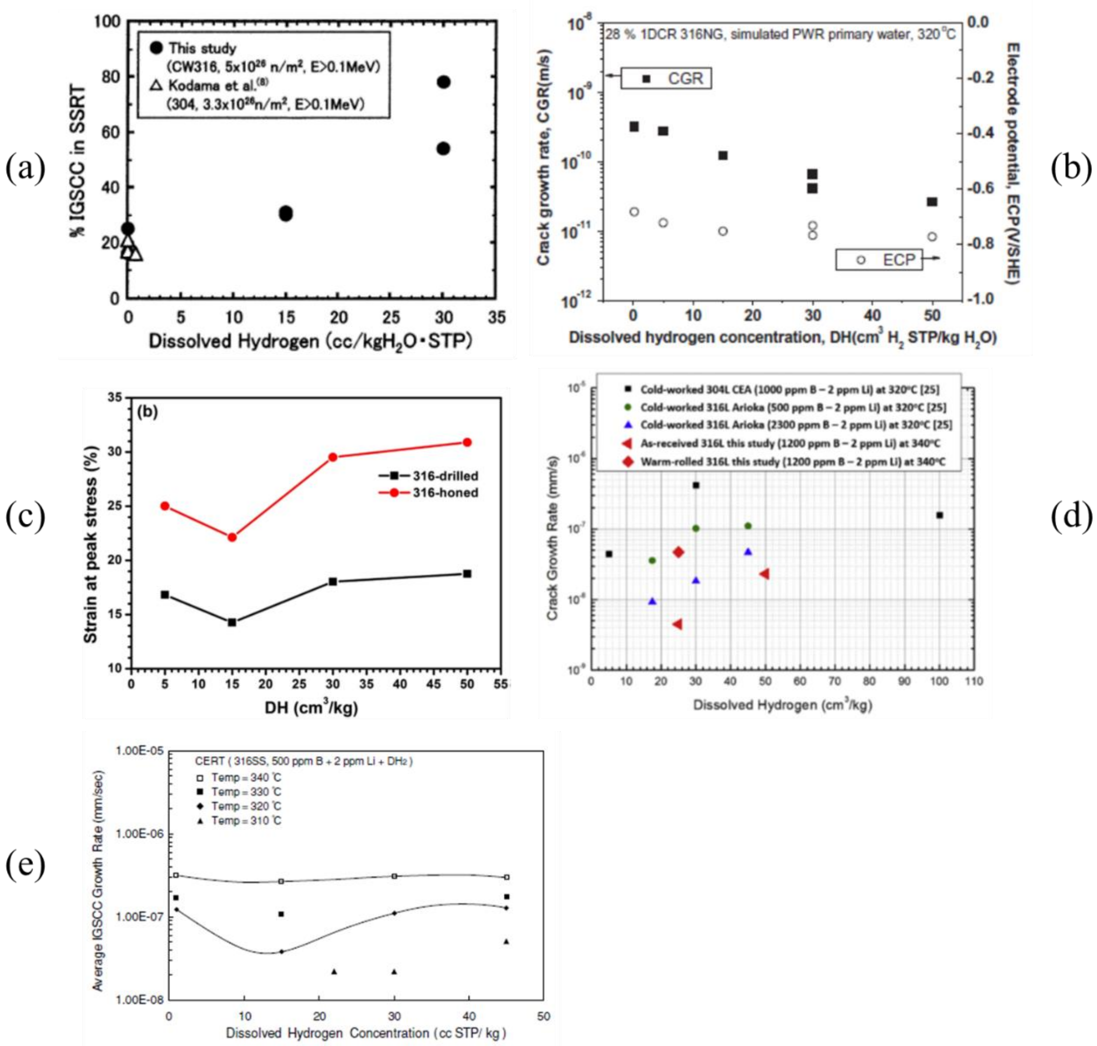

Fig. 2.18 Caption of PWSCC CGR tests for stainless steels under hydrogenated primary water environment. Data from (a) Furutani[56], (b) Meng[20], (c) Zhong[57], (d) Choi[55] and (e) Fukumura[58]

Table 2.2 Summary of researches relates to hydrogenated high temperature water

Author	Materials	Method	Behavior	peak temp.	DH Range	Ref.
Totsuka	A600	CGR	peak (50)	360		[47]
Labousse	MA-A600		peak (40/35/25)	360/338/290		[60]
Molander	A600	CGR	peak (27)			[50]
Fukumura	CW20%-A600	CGR	peak (0.5ppm)	290	0-2.7 (ppm)	[48]
Yamada	CW20%-TT690	CGR	peak (30)	360	0-45	[49]
Andresen	A82	simulation	peak (16/10/5)	343/325/290		[53]
PNNL	A182	CGR	peak (12)	325		[51]
Bruemmer	A82	CGR	peak (8)	338	1-35	[51]
Furutani	CW 316	CGR	increase	320	0-30	[56]
Meng	CW316NG	CGR	decrease	320	0.16-50	[20]
Zhong	CW316	SSRT	minimum (15)	325	5-50	[57]
Choi	AS 316L	CGR	increase	340	25/50	[55]
Fukumura	SA316	SSRT	minimum(30)	310	15-45	[58]

2.5.1 Ni/NiO phase transitions

Recent research works point out that PWSCC CGR highly relates to Ni/NiO phase stability. The stability is thermodynamically determined and hence varies with reaction concentration and temperature. Pourbaix diagram depicts this relationship, as shown in Fig. 2.19(a) [54]. At 300^{o}C, Ni/NiO boundary line is close to H_2/H_2O. Corresponding SCC submode of Alloy 600 is shown in Fig. 2.19 (b). Simulation determined Ni/NiO boundary line within 280 to 360^{o}C is shown in Fig. 2.20 (a) [61]. Andresen further give detailed number of this boundary line, as shown in Fig. 2.20 (b). [54] Furthermore, different corrosion environment at crack-tip and surface lead to different pH value and corrosion potential [46].

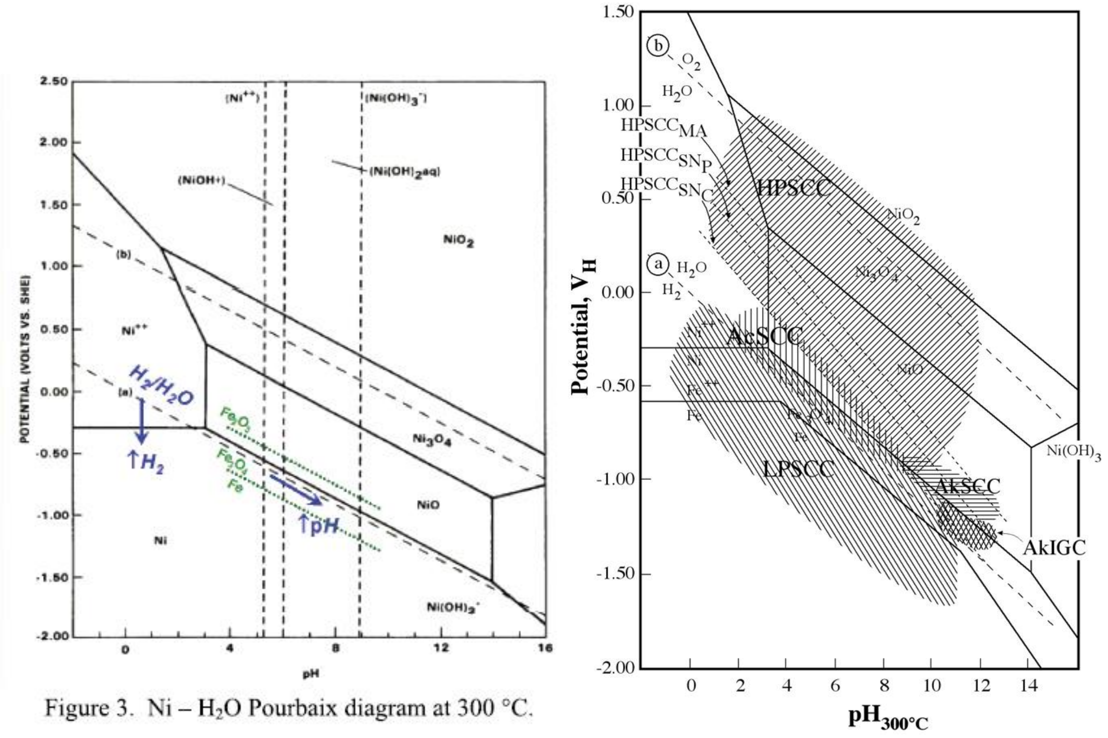

Figure 3. Ni – H2O Pourbaix diagram at 300 °C.

Fig. 2.19 The (a) Ni-H_2O Pourbaix diagram at 300°C and corresponding (b) IGC/SCC submode of Alloy 600. [46,54]

(a)

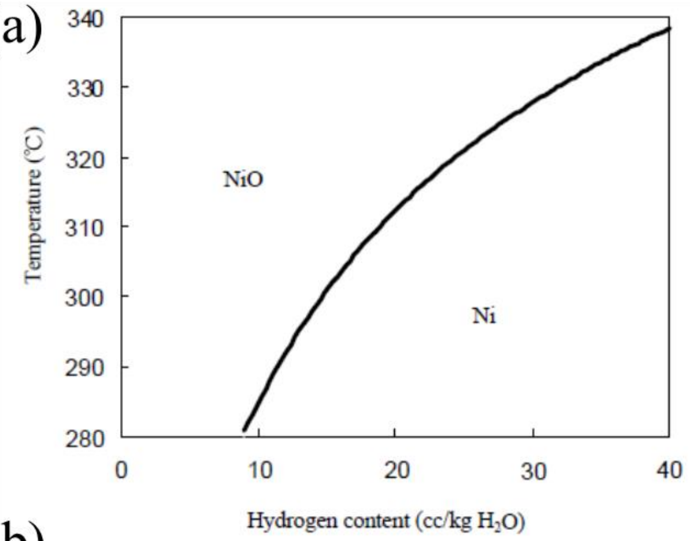

(b)

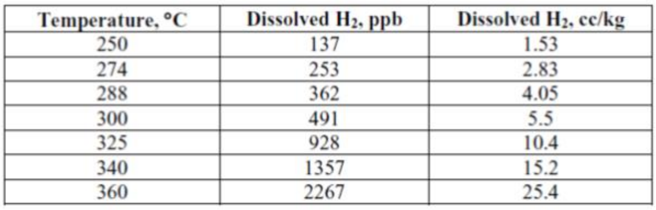

Temperature, °C	Dissolved H_2, ppb	Dissolved H_2, cc/kg
250	137	1.53
274	253	2.83
288	362	4.05
300	491	5.5
325	928	10.4
340	1357	15.2
360	2267	25.4

Fig. 2.20 (a) Relationship between Ni/NiO phase boundary and dissolved-hydrogen near 300°C and (b) corresponding calculated hydrogen content.

2.6 Research objectives

This research aims to investigate the effect of dissolve-hydrogen on solution-annealed SCC of 316L and 310S stainless steel in hot water, pressurized water and supercritical water. Slow strain rate test (SSRT) was adopted and carried out in simulated water-circulating loop. The SCC susceptibility is evaluated by fracture mode change examined by scanning electron microscope after SSRT. Effects of temperature, sensitization heat treatment and amount of dissolved-hydrogen were discussed. To provide information for maintaining structural integrity of in-service plants.

Reference

[1] Schematic of BWR circuit, (n.d.). http://www.nucleartourist.com/images/bwr-cycle.gif.

[2] S.J. Zinkle, G.S. Was, Materials challenges in nuclear energy, Acta Mater. 61 (2013) 735–758. doi:10.1016/j.actamat.2012.11.004.

[3] Schematic of SCWR design, (n.d.). https://www.gen-4.org/gif/jcms/c_42151/supercritical-water-cooled-reactor-scwr.

[4] Y. Watanabe, H. Abe, Y. Daigo, Environmentally assisted cracking of sensitized stainless steel in supercritical water: effects of physical property of water, GENES4/ANP2003, Kyoto, Japan. (2003) Paper 1183.

[5] TCWS of ITER, (n.d.). https://www.iter.org/newsline/singleprint/-/2019.

[6] M. Mcguire, Austenitic Stainless Steels, in: Stainl. Steels Des. Eng., 2008: pp. 69–78. doi:http://dx.doi.org/10.1016/B0-08-043152-6/00081-4.

[7] T. H Licentiate, P. Hedström, Deformation induced martensitic transformation of metastable stainless steel AISI 301, 2005.

[8] Alloy Digest Sourcebook: Stainless Steels, ASM International, 2000. https://www.asminternational.org/home/-/journal_content/56/10192/06940G/PUBLICATION.

[9] Carbide precipitation, (n.d.). http://thomas-sourmail.net/stainless/.

[10] Y.-J. Kim, Analysis of Oxide Film Formed on Type 304 Stainless Steel in 288°C Water Containing Oxygen, Hydrogen, and Hydrogen Peroxide, CORROSION. 55 (1999) 81–88. doi:10.5006/1.3283969.

[11] Y. MURAYAMA, T. SATOH, S. UCHIDA, Y. SATOH, S. NAGATA, T. SATOH, Y. WADA, M. TACHIBANA, Effects of Hydrogen Peroxide on Intergranular Stress Corrosion Cracking of Stainless Steel in High Temperature Water, (V), J. Nucl. Sci. Technol. 39 (2002) 1199–1206. doi:10.1080/18811248.2002.9715311.

[12] T. MIYAZAWA, S. UCHIDA, T. SATOH, Y. MORISHIMA, T. HIROSE, Y. SATOH, K. IINUMA, Y. WADA, H. HOSOKAWA, N. USUI, Effects of Hydrogen Peroxide on Corrosion of Stainless Steel, (IV), J. Nucl. Sci. Technol. 42 (2005) 233–241. doi:10.1080/18811248.2005.9726384.

[13] T. MIYAZAWA, T. TERACHI, S. UCHIDA, T. SATOH, T. TSUKADA, Y. SATOH, Y. WADA, H. HOSOKAWA, Effects of Hydrogen Peroxide on Corrosion of Stainless Steel, (V) Characterization of Oxide Film with Multilateral Surface Analyses, J. Nucl.

Sci. Technol. 43 (2006) 884–895. doi:10.1080/18811248.2006.9711173.

[14] Y. WADA, A. WATANABE, M. TACHIBANA, K. ISHIDA, N. UETAKE, S. UCHIDA, K. AKAMINE, M. SAMBONGI, S. SUZUKI, K. ISHIGURE, Effects Of Hydrogen Peroxide On Intergranular Stress Corrosion Cracking Of Stainless Steel in High Temperature Water, (IV), J. Nucl. Sci. Technol. 38 (2001) 183–192. doi:10.1080/18811248.2001.9715020.

[15] K. ISHIDA, Y. WADA, M. TACHIBANA, H. HOSOKAWA, M. NAKAMURA, Effects of Noble Metal Deposition upon Corrosion Behavior of Structural Materials in Nuclear Power Plants, (I), J. Nucl. Sci. Technol. 42 (2005) 799–808. doi:10.1080/18811248.2004.9726449.

[16] C.-M. Yu, Electrochemical Behavior of Type 304 Stainless Steels Treated with ZnO in Simulated Boiling Water Reactor Environments, 2007.

[17] Y.-C. Chien, Electrochemical Characteristics of Oxygen and Hydrogen on ZrO2 Treated Type 304 Stainless Steels with Different Surface Oxide Structures in Simulated Boiling Water Reactor Environments, 2005.

[18] P.-Y. Wu, The Influence of ZrO2 Treatment on the Electrochemical Behavior of hydrogen peroxide on Type 304 Stainless Steels in High Temperature Water, 2008.

[19] M.B. Toloczko, P.L. Andresen, S.M. Bruemmer, SCC CRACK GROWTH OF COLD-WORKED TYPE 316 SS IN SIMULATED BWR OXIDIZING AND HYDROGEN WATER CHEMISTRY CONDITIONS, in: 13th Int. Conf. Environ. Degrad. Mater. Nucl. Power Syst., Whistler, British Columbia, n.d.: pp. 1–11.

[20] F. Meng, Z. Lu, T. Shoji, J. Wang, E. hou Han, W. Ke, Stress corrosion cracking of uni-directionally cold worked 316NG stainless steel in simulated PWR primary water with various dissolved hydrogen concentrations, Corros. Sci. 53 (2011) 2558–2565. doi:10.1016/j.corsci.2011.04.013.

[21] D.J. Paraventi, W.C. Moshier, THE EFFECT OF COLD WORK AND DISSOLVED HYDROGEN IN THE STRESS CORROSION CRACKING OF ALLOY 82 AND ALLOY 182 WELD METAL, in: Proc. 12th Int. Conf. Environ. Degrad. Mater. Nucl. Power Syst. – Water React. –, 2005.

[22] J. Chen, Z. Lu, Q. Xiao, X. Ru, G. Han, Z. Chen, B. Zhou, T. Shoji, The effects of cold rolling orientation and water chemistry on stress corrosion cracking behavior of 316L stainless steel in simulated PWR water environments, J. Nucl. Mater. 472 (2016) 1–12. doi:10.1016/j.jnucmat.2016.01.018.

[23] S. Lozano-Perez, T. Yamada, T. Terachi, M. Schröder, C.A. English, G.D.W. Smith, C.R.M. Grovenor, B.L. Eyre, Multi-scale characterization of stress corrosion cracking of cold-worked stainless steels and the influence of Cr content, Acta Mater. 57 (2009) 5361–5381. doi:10.1016/j.actamat.2009.07.040.

[24] Y. Katayama, M. Tsubota, Y. Saito, Effect of the plastic strain level quantified by EBSP method on the stress corrosion cracking of L-grade stainless steels, 12th Int. Conf. Environ. Degrad. Mater. Nucl. Power Syst. – Water React. (2005) 31–38.

[25] M.F. Chiang, M.C. Young, J.Y. Huang, Effects of hydrogen water chemistry on corrosion fatigue behavior of cold-worked 304L stainless steel in simulated BWR coolant environments, J. Nucl. Mater. 411 (2011) 83–89. doi:10.1016/j.jnucmat.2011.01.035.

[26] W. Sagawa, T. Aoki, T. Itou, K. Enomoto, E. Hayashi, T. Ishikawa, Stress corrosion cracking countermeasure observed on Ni-based alloy welds of BWR core support structure, Nucl. Eng. Des. 239 (2009) 655–664. doi:https://doi.org/10.1016/j.nucengdes.2008.12.016.

[27] K. HIRANO, K. ENOMOTO, E. HAYASHI, K. KUROSAWA, Effects of Water Jet Peening on Corrosion Resistance and Fatigue Strength of Type 304 Stainless Steel, J. Soc. Mater. Sci. Japan. 45 (1996) 740–745. doi:10.2472/jsms.45.740.

[28] Y. Sano, M. Obata, T. Kubo, N. Mukai, M. Yoda, K. Masaki, Y. Ochi, Retardation of crack initiation and growth in austenitic stainless steels by laser peening without protective coating, Mater. Sci. Eng. A. 417 (2006) 334–340. doi:https://doi.org/10.1016/j.msea.2005.11.017.

[29] L.F. Fredette, Surge Nozzle NDE Specimen Mechanical Stress Improvement Analysis, United States, n.d.

[30] W. Bilanin, D. Cubicciotti, R.L. Jones, A.J. MacHiels, L. Nelson, C.J. Wood, Hydrogen water chemistry for BWRs, Prog. Nucl. Energy. 20 (1987) 43–70. doi:10.1016/0149-1970(87)90011-4.

[31] BWRVIP-62NP , Revision 1 : BWR Vessel and Internals Project Technical Basis for Inspection Relief for BWR Internal Vessel and Internals Project Internal Components with Hydrogen Injection, n.d.

[32] R.. Horn, G.. Gordon, F.. Ford, R.. Cowan, Experience and assessment of stress corrosion cracking in L-grade stainless steel BWR internals, Nucl. Eng. Des. 174 (1997) 313–325. doi:10.1016/S0029-5493(97)00131-3.

[33] P.L. Andresen, M.M. Morra, IGSCC of non-sensitized stainless steels in high temperature water, J. Nucl. Mater. 383 (2008) 97–111. doi:10.1016/j.jnucmat.2008.08.005.

[34] C.C. Lin, F.R. Smith, R.L. Cowan, Effects of hydrogen water chemistry on radiation field buildup in BWRs, Nucl. Eng. Des. 166 (1996) 31–36. doi:10.1016/0029-5493(96)01196-X.

[35] K. Fukuya, H. Nishioka, K. Fujii, Irradiation Behavior of Stainless Steels in Light Water Reactors, Institute of Nuclear Safety System, Inc., 2009. http://ci.nii.ac.jp/ncid/BA89141629.

[36] Y.-J. Kim, P.L. Andresen, Application of Insulated Protective Coatings for Reduction of Corrosion Potential of Type 304 Stainless Steel in High-Temperature Water, CORROSION. 54 (1998) 1012–1017. doi:10.5006/1.3284814.

[37] M. Atik, M.A. Aegerter, Corrosion resistant sol-gel ZrO2 coatings on stainless steel, J. Non. Cryst. Solids. 147–148 (1992) 813–819. doi:https://doi.org/10.1016/S0022-3093(05)80722-7.

[38] M. Atik, C.R. Kha, P. De Limaneto, L.A. Avaca, M.A. Aegerter, J. Zarzycki, Protection of 316L stainless steel by zirconia sol-gel coatings in 15% H2S04 solutions, J. Mater. Sci. Lett. 14 (1995) 178–181.

[39] T.-K. Yeh, Y.-C. Chien, B.-Y. Wang, C.-H. Tsai, Electrochemical characteristics of zirconium oxide treated Type 304 stainless steels of different surface oxide structures in high temperature water, Corros. Sci. 50 (2008) 2327–2337. doi:https://doi.org/10.1016/j.corsci.2008.05.012.

[40] T.-K. Yeh, Y.-J. Huang, M.-Y. Wang, C.-H. Tsai, Hydrothermal treatments of TiO2 on Type 304 stainless steels for corrosion mitigation in high temperature pure water, Nucl. Eng. Des. 254 (2013) 228–236. doi:https://doi.org/10.1016/j.nucengdes.2012.09.012.

[41] T.-K. Yeh, P.-I. Wu, C.-H. Tsai, Corrosion of ZrO2 treated type 304 stainless steels in high temperature pure water with various amounts of hydrogen peroxide, Prog. Nucl. Energy. 57 (2012) 62–70. doi:https://doi.org/10.1016/j.pnucene.2011.12.014.

[42] F.P. Ford, P.L. Andresen, Development and use of a predictive model of crack propagation in 304/316L, A533B/A508 and Inconel 600/182 alloys in 2880C water, The Metallurgical Society Inc, United States, 1988.

[43] D.D. MacDonald, M. Urquidi-MacDonald, A coupled environment model for stress corrosion cracking in sensitized type 304 stainless steel in LWR environments, Corros.

Sci. 32 (1991) 51–81. doi:10.1016/0010-938X(91)90063-U.

[44] R. A. ORIANI, The diffusion and trapping of hydrogen in high purity aluminum, Acta Matallurgica. 18 (1970) 147–157. doi:10.1016/S1359-6454(98)00333-4.

[45] H.K. Birnbaum, P. Sofronis, Hydrogen-enhanced localized plasticity-a mechanism for hydrogen-related fracture, Mater. Sci. Eng. A. 176 (1994) 191–202. doi:10.1016/0921-5093(94)90975-X.

[46] R.W. Staehle, Assessment of Internal Oxidation (IO) as a Mechanism for Submodes of Stress Corrosion Cracking that Occur on the Secondary Side of Steam Generators., Miner. Met. Mater. Soc. Prep. Div. Eng. Technol. Off. Nucl. Regul. Res. U.S. Nucl. Regul. Comm. Washington, DC 20555-0001 NRC Job Code W6588 NUREG/CR-6827 RWS 154. (2004).

[47] N. Totsuka, Y. Nishikawa, N. Nakajima, Influence of Dissolved Hydrogen and Temperature on Primary Water Stress Corrosion Cracking of Mill Annealed Alloy 600, Corros. 2002. (2002) 1–11.

[48] T. Fukumura, N. Totsuka, Effect of Dissolved Hydrogen Concentration on PWSCC Crack Growth Rate of Alloy 600 at 290℃, J. Inst. Nucl. Saf. Syst. 17 (2010) 122–129.

[49] T. Yamada, M. Aoki, T. Miyamoto, K. Arioka, SCC growth behavior of cold worked alloy 690 in high-temperature water－Dependence of test temperature, dissolved hydrogen in water, grain boundary carbide and chemical composition－, J. Inst. Nucl. Saf. Syst. 21 (2014) 133–143.

[50] A.. Molander, A.. Jenssen, K.. Norring, M.. Ko¨ nig, P.-O. Andersson, Comparison of PWSCC initiation and crack growth data for Alloy 600, in: VGB NPC’08 Water Chem. Conf., Berlin, n.d.

[51] S.M. Bruemmer, J.S. Vetrano, M.B. Toloczko, Microstructure and SCC Crack Growth of Nickel-Base Alloy 182 Weld Metal in Simulated PWR Primary Water, in: 13th Int. Conf. Environ. Degrad. Mater. Nucl. Power Syst., Whistler, British Columbia, 2007: pp. 1–11.

[52] P.. Andresen, A.. Ahluwalia, J.. Wilson, J. Hickling, Effects of dissolved H2 and Zn on PWSCC of Ni alloys, in: VGB NPC’08 Water Chem. Conf., Berlin, n.d.

[53] A. P., H. J., A. A., W. J, Effect of H2 on mitigation of PWSCC in nickel alloys, in: Optim. Dissolved Hydrog. Content PWR Prim. Cool., Tohoku University, Sendai, Japan, 2007.

[54] P. Andresen, P. Chou, Effects of Hydrogen on SCC Growth Rate of Ni Alloys in BWR

Water, in: 15th Int. Conf. Environ. Degrad. Mater. Nucl. Power Syst. - Water React., 2011: pp. 2039–2059.

[55] K.J. Choi, S.C. Yoo, H.H. Jin, J. Kwon, M.J. Choi, S.S. Hwang, J.H. Kim, Crack growth behavior of warm-rolled 316L austenitic stainless steel in high-temperature hydrogenated water, J. Nucl. Mater. 476 (2016) 243–254. doi:10.1016/j.jnucmat.2016.04.051.

[56] G. Furutani, N. Nakajima, T. Konishi, M. Kodama, Stress corrosion cracking on irradiated 316 stainless steel, J. Nucl. Mater. 288 (2001) 179–186. doi:10.1016/S0022-3115(00)00704-2.

[57] X. Zhong, S.C. Bali, T. Shoji, Effects of dissolved hydrogen and surface condition on the intergranular stress corrosion cracking initiation and short crack growth behavior of non-sensitized 316 stainless steel in simulated PWR primary water, Corros. Sci. 118 (2017) 143–157. doi:10.1016/j.corsci.2017.02.003.

[58] T. Fukumura, T. Terachi, K. Arioka, Influence of Temperature and Water Chemistry on IGSCC Susceptibility of SUS316 in High-Temperature Water, J. Inst. Nucl. Saf. Syst. 11 (2004) 143–152.

[59] M. Nono, T. Nakajima, M. Iwama, R. Kasada, A. Kimura, SCC behavior of SUS316L in the high temperature pressurized water environment, J. Nucl. Mater. 417 (2011) 878–882. doi:10.1016/j.jnucmat.2010.12.150.

[60] M. Labousse, D. Déforge, F. Gressier, S. Taunier, M.L.C. Edf, OPTIMIZATION OF THE DISSOLVED HYDROGEN LEVEL IN PWR TO MITIGATE STRESS CORROSION CRACKING OF NICKEL ALLOYS . BIBLIOGRAPHIC REVIEW , MODELLING AND RECOMMANDATIONS . Review of experimental results regarding DH effect on initiation and propagation of SCC on, in: Int. Coop. Gr. Environ. Assist. Crack. 2012, 2012.

[61] T. Nakagawa, N. Totsuka, T. Terachi, N. Nakajima, Influence of Dissolved Hydrogen on Oxide Film and PWSCC of Alloy 600 in PWR Primary Water, J. Nucl. Sci. Technol. 8 (2001) 111–117. doi:10.1080/18811248.2003.9715330.

Chapter 3
Experimental methods

3.1 Materials

The materials used in this research are 304, 304L, 316L and 310S stainless steel (SS) plates and bars supplied by Nilaco Corporation. Chemical compositions are shown in Table 3.1. Each plate of the commercial steels were machined into SS-J2 plate type tensile specimens for hot water testing loop. The geometries of the gage section of the specimens was 5mm in length, 1.2mm in width, 0.5mm in thickness. Also the commercial bars were machined into round bar type specimens for supercritical water testing loop. The gage section was 10mm in length and 2mm in diameter. The geometries of plate type and round bar type specimen design were shown in Fig. 3.1 (a) and (b), respectively.

Among numerous corrosion testing method, slow-strain rate test (SSRT) method is chosen for this work. This accelerated corrosion test is suitable to observe crack initiation, which meets objectives of this work. On contrary, compact tension (CT) specimen is designed for measuring stress intensity and crack growth rate. It is suitable for crack propagation.

Before testing, solution-annealing heat treatment was applied to all specimens. Specimens were vacuum sealed in quartz tube at 4 x 10^{-5} torr, then were put in a muffle furnace set at 1050 °C for 1 hour. The quartz tubes were broken in iced water to finish quenching process. A part of specimens further received a sensitization heat treatment so as to simulate situations at elevated application temperature and to simulate post-weld heat treatment. The sensitization treatment was done for 304 and 304L SS at 650 °C for 1 hour, followed by quenching into iced water, while for 316L and 310S SS it was done at 700 °C for 100 hour and followed by quenching into iced water.

Plate type specimens were polished from #1200 to #4000 with SiC sand papers then buff-polished from 3 to 0.25 μm with diamond spray. Round bar type specimen was polished from #1200 to #4000 with SiC sand paper. After polishing, specimen was cleaned in ultrasonic cleaner with demineralized water.

Table 3.1 Chemical compositions of testing materials

wt%	Fe	Cr	Ni	C	Mo	Mn	Si	Co	P	S
304	bal.	18.14	8.06	0.06	-	0.79	0.48	-	0.033	0.008
316L	bal.	17.41	12.13	0.01	2.05	1.06	0.73	-	0.032	0.004
310S	bal.	24.76	19.17	0.02	-	0.8	0.7	0.1	0.022	-

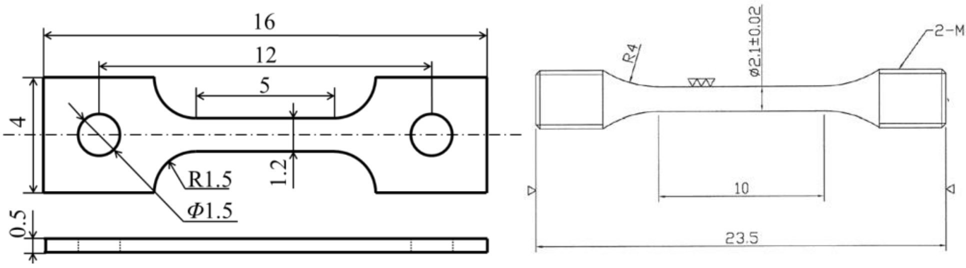

Fig. 3.1 Geometries of testing specimens for (a) hot water loop and (b) pressurized and supercritical water loop

3.2 Slow strain rate testing loops

The hot water loop and supercritical water loop were designed and manufactured by TOSHIN KOGYO Co. ltd. Their schematic view and photograph were shown in Fig. 3.2 and Fig. 3.3, respectively. Both hot water and supercritical water loop include a primary loop and a water chemistry monitoring loop. A high-pressure pump sent high purity water into a heat exchanger, pre-heater then to the autoclave where testing specimen was set. Water was then cooled through the heat exchanger and chilled through the external chiller and finally back to the water reservoir.

High purity nitrogen, oxygen and hydrogen were injected into water reservoir to control dissolved-oxygen and dissolved-hydrogen content. The sensors to measure conductivity, dissolve-oxygen and dissolved-hydrogen are provided by TOA-DKK Co. ltd.. They were installed in water chemistry monitoring loop. The water conductivity was kept below 0.1µS/cm during tests. A servo-motor was connected to drive cross-head under controlling by a computer. The strain rate was set at 5 x 10^{-7}/s. Corresponding cross-head speed of plate type and round bar type specimen was 0.00015 mm/min and 0.0003 mm/min, respectively.

Hot water loop can provide pressure at 7.8±0.2 MPa and temperature at 288±10 °C so as to simulate BWR environment. Supercritical water loop can provide two water environments: pressurized water with pressure at 15.5±0.2 MPa and temperature at 340±10 °C; and supercritical water with pressure at 25±0.3 MPa and temperature 500±10 °C. The former simulates PWR and ITER operating conditions; while the latter simulates SCWR operating conditions.

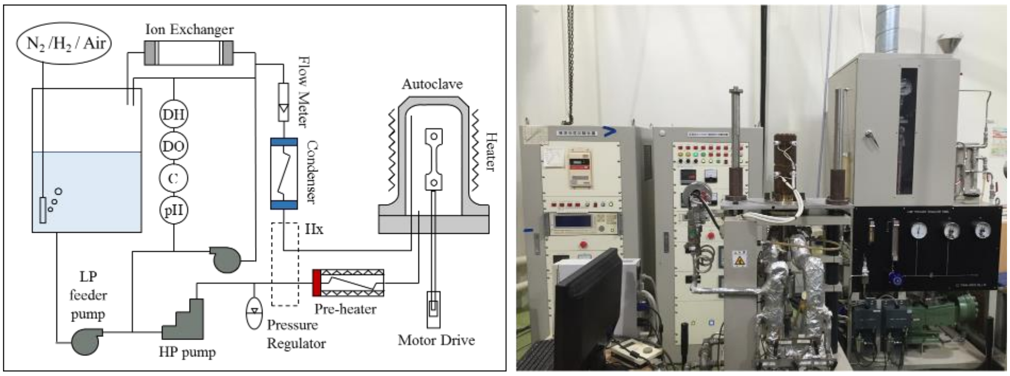

Fig. 3.2 Schematics and photo of hot water circulating loop

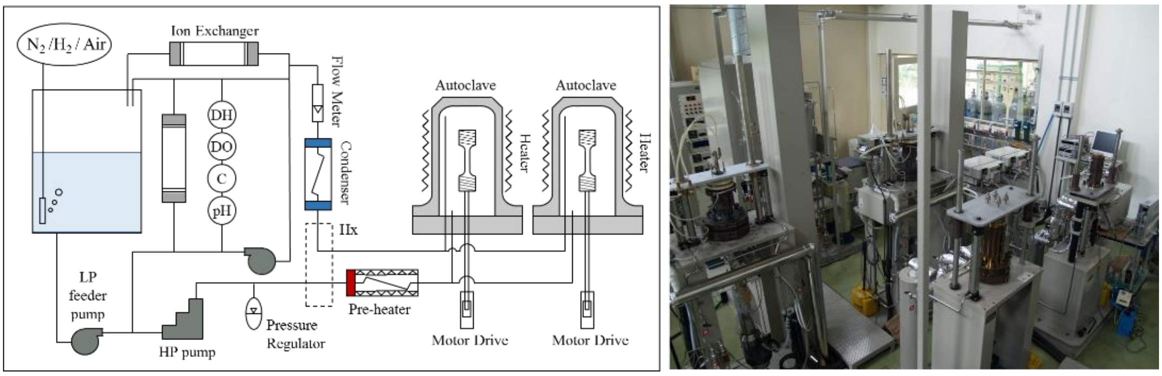

Fig. 3.3 Schematics and photo of pressurized and supercritical water circulating loop

3.3 Material characterization

Microhardness of solution-annealed specimen was measured by Vickers hardness tester (HMV-G G21 FA, Shimadzu, Ltd.). Indent force and time were HV0.1 (0.98N, 100gf) and 10 seconds. Indentation was applied 10 times for average. The averaged hardness of 304, 316L and 310S SS was 167.5, 133.7 and 150.5, respectively.

Grain structure was revealed by etching in a solution mixed 10 g oxalic acid with 100 ml demineralized water. Structure was photographed by optical microscope (BX51M, OLYMPUS) equipped with digital camera. Grain structure of 304, 316L and 310SS were shown in Fig.3.5 (a), (b) and (c), respectively. The averaged grain size was measured by intersection method. Grain diameter of 316L SS was 59 µm; of 310S SS was 26 µm.

After slow strain rate test, fractured surface and side morphology of specimen was characterized by scanning electron microscope (SEM, VE-9800 KEYENCE Japan). Fracture mode of crack initiation was examined by electron backscattering diffraction method with Orientation Imaging Microscopy (OIM) equipped in a field-emission SEM (Ultra-55, Carl Zeiss Co. Ltd.)

The structure of oxide film was characterized by X-ray diffraction (RINT-TTR III, Rigaku Co. Ltd.) with scan speed 1^o/min and angle from 5^o to 100^o. The X-ray source was Co-Kα with 1.79026Å in wavelength. Chemical composition of oxide layer was determined by field-emission electron probe micro-analyzer (FE-EPMA, JXA-8500F JEOL) equipped with wavelength-dispersive X-ray spectrometer (WDS). Compositional depth was profiled by field-emission auger electron spectroscopy (FE-AES, JAMP-9500FV)

Chapter 4

SCC susceptibility of solution-annealed 316L SS in hydrogenated hot water below 288°C

4.1. Introduction

Stress corrosion cracking (SCC) is one of critical environmental-assisted degradation issues in nuclear power plants [1] which may influence reactor operation and subsequent energy economics. Austenitic stainless steel (SS), type 316L, has been one of structural materials for shroud of boiling water reactors (BWR), and sometime suffered SCC during operation [2–5]. In order to overcome this issue, hydrogen was injected into feedwater to recombine with corrodants such as oxygen and hydrogen peroxides [2,5–9]. As a consequence, corrosion current density on stainless steels was decreased. This recombination efficacy and covering region were further extended to a noble metal chemical addition technique [10]. The usage of noble metals also reduces dissolved-hydrogen (DH) requirement from several hundreds of ppb to several tens of ppb. Corrosion potential was also kept at low level as well.

As for the effect of DH in the water on the SCC of stainless steels, Arioka et al. [3] carried out slow strain rate test (SSRT) on solution-annealed 316 SS, and they found a minimum crack growth rate (CGR) at 15 cc/kg at a temperature between 320 and 340 °C. A number of works on cold-worked 316L SS, however, were contrary to Arioka's results, which might be due to the difference in the evaluation method. For example, Zhong et al. [11] reported a maximum at 15 cc/kg at 320 °C. Fukumura [12] and Choi [13] reported that CGR increased from 15 to 45 cc/kg at 320 °C. Fracture mode also varies among researchers. Nono [14] reported transgranular stress corrosion cracking (TGSCC) on solution-annealed 316L SS in a hot water with DH=0.4 ppm at 288 °C. Arioka et al. [3] reported an intergranular crack initiation and transgranular crack propagation in water with 30 cc/kg of hydrogen at 320 °C.

Hydrogen-assisted degradation is well known as hydrogen induced cracking (HIC) or hydrogen embrittlement in gaseous environment. Caskey [15] came up similar results from the tensile tests conducted in 69 MPa D_2 gas, indicating that the susceptibility decreased as Ni content increased between 15 to 25 wt%. Han [16], Chen [17] and Lai [18] attributed the susceptibility differences between austenitic SSs to the preference of martensite formation. Martensite that has a BCT structure is more susceptible to hydrogen embrittlement than austenite that has a FCC structure, resulting in an accelerating crack growth. On the other hand, stabilized austenitic SS can prevent martensite formation hence reduces susceptibility to HIC.

Since hydrogen behavior in materials, such as diffusion, solubility and binding (trapping) behavior as well as corrosion reactions, is remarkably affected by temperature, it is considered that the SCC in hydrogenated water strongly depends on temperature and probably amount of hydrogen. In this work, we investigated the effects of temperature and the amount of DH on the SCC susceptibility of solution-annealed 316L SS and discuss the SCC mechanism in hydrogenated hot water.

4.2 Experimental

4.2.1 Material and specimens preparation

The material used in this study is a commercial 316L SS provided by Nilaco Co. The chemical compositions are listed in Table 4.1. The geometries of a plate type tensile specimen is shown in Fig. 4.1. The gauge length, width and thickness was 5 mm, 1.2 mm and 0.5 mm, respectively. Prior the test, specimens were solution-annealed at 1050 ^{o}C for 1 hour, followed by quenching into iced water. Specimen surfaces were polished by SiC sand papers from #800 to #4000 then grinded up to 0.25 um with diamond powder. Before test, specimen was cleansed in an ultrasonic cleaner.

Table 4.1 Chemical compositions of 316L stainless steel

wt%	Fe	Cr	Ni	Mo	Mn	C	Si	P	S
316L	bal.	17.41	12.13	2.05	1.06	0.01	0.73	0.032	0.004

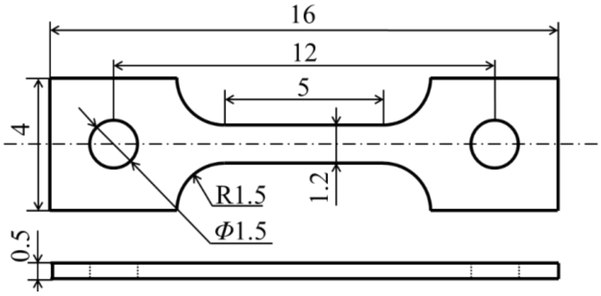

Fig. 4.1Geometries of tensile test specimen for SSRT

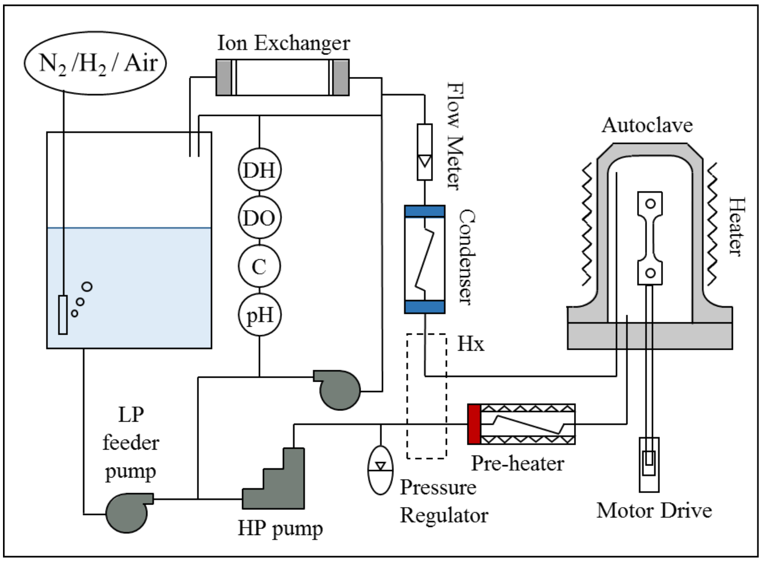

Fig. 4.2 Schematic view of hot water circulating loop

4.2.2 Slow-strain rate test (SSRT)

Fig. 4.2 is the schematic view of testing loop, which consists of a primary loop and a water chemistry monitoring loop. The primary loop was capable of providing pressurized water at room temperature (RT), 150, 220 and 288 °C at a pressure of 7.8 MPa by manipulating a pressure relief valve. A high pressure pump drove water into a pre-heater, two autoclaves, heat-exchanger and ion-exchanger, and back it to a water tank. A condenser dumped residual heat to an external chiller. High purity hydrogen and nitrogen were injected into the water tank to control amount of dissolved-oxygen (DO) and DH. Deaerated water condition (both the dissolved oxygen and hydrogen were lower than 10 ppb) and another three DH contents (0.1 ppm, 0.4 ppm and 1.4 ppm) were chosen to simulate different operating conditions. Additional two DO contents (0.2 ppm and 10 ppm) were conducted for comparison. Strain rate was set at 5 x 10-7/s. After SSRT, fractured surface was examined by scanning electron microscope (SEM). Fracture mode was examined by electron backscattering diffraction (EBSD). The orientation imaging microscopy (OIM) detector was equipped in a field-emission SEM, Ultra-55, produced by Carl Zeiss Co., Ltd. Before analysis, specimen surface was grinded with 0.25μm diamond powder and then by silica colloidal powder. Austenite phase was chosen for Kikuchi pattern recognition.

4.3 Results

4.3.1 Effect of dissolved-hydrogen (DH) and dissolved-oxygen (DO)

Fig. 4.3 is the stress-strain curves of solution-annealed 316L SS tested in hot water with various water chemistry conditions at 288^{o}C, which include dissolved-oxygen (DO) 10, 0.2 ppm; dissolved-hydrogen (DH) 0.1, 0.4, 1.4 ppm and deaerated (both DO and DH were less than 10ppb). After test, mechanical properties were obtained and summarized in Table 4.2 and plotted in Fig. 4.4. Stress-strain behavior was not much affected by DO content. Total elongation of DO=0.2 ppm and DO=10ppm were about 50%. The change in water chemistry, from DO to DH content, resulted in the change in the stress-strain behavior where the total elongation was down to 37.4% in water with DH=1.4ppm.

Fig. 4.5 shows the fractured specimens tested at 288 ^{o}C with various water chemistry. Specimens tested in water with DO content showed a complete ductile behavior, showing dimples in the center region. Almost no crack occurred on the side surface of the specimens, which was in a good agreement with stress-strain behaviors and mechanical properties. On the contrary, brittle fracture appeared on specimens tested in deaerated water and all hydrogen-dissolved water. Transgranular (TG) SCC was found on fractured surface and side surface. Furthermore, intergranular (IG) was also confirmed on the specimens tested in hydrogenated water. An example of close view of the IG crack was shown in Fig. 4.6. Furthermore, the mechanical properties of these specimens were different from specimens in DO content. Total elongation was around 40% or below; reduction in area was smaller and TG area percentage was higher. The percentage was around 30% except for the DH=0.4ppm condition, which was up to 41%. More cracks were found on the side surface, as shown in Fig. 4.5(e).

Table 4.2 Summary of mechanical properties: UTS (Ultimate Tensile Strength), TE (Total Elongation), RA (Reduction in Area), TG% (Area % of transgranular cracking to area of fractured surface) and oxide film thickness of solution-annealed 316L stainless steel after SSRT. “n.m.” is the abbreviation of “not measured.”

Water chemistry (ppm)	Temperature (°C)	UTS (MPa)	TE (%)	RA (%)	TG (%)	thk (nm)
DO 10	288	484.5	52.4	73.9	0.0	4233.6
DO 0.2	288	440.2	50.8	n.m	0.0	1144.1
Deaerated	288	449.9	40.0	49.0	32.2	137.8
DH 0.1	288	394.3	40.5	n.m	32.2	117.6
DH 0.4	25	555.3	74.8	82.4	0.0	6.7
	150	415.5	39.7	82.5	0.0	16.8
	220	440.5	35.5	69.2	0	121.0
	288	468.5	39.9	41.4	41.0	231.8
DH 1.4	25	553.2	87.3	80.8	0.0	1.7
	150	515.4	49.3	72.8	0.0	3.4
	220	496.3	56.4	52.6	22.7	99.1
	288	440.4	37.4	48.3	31.5	193.2

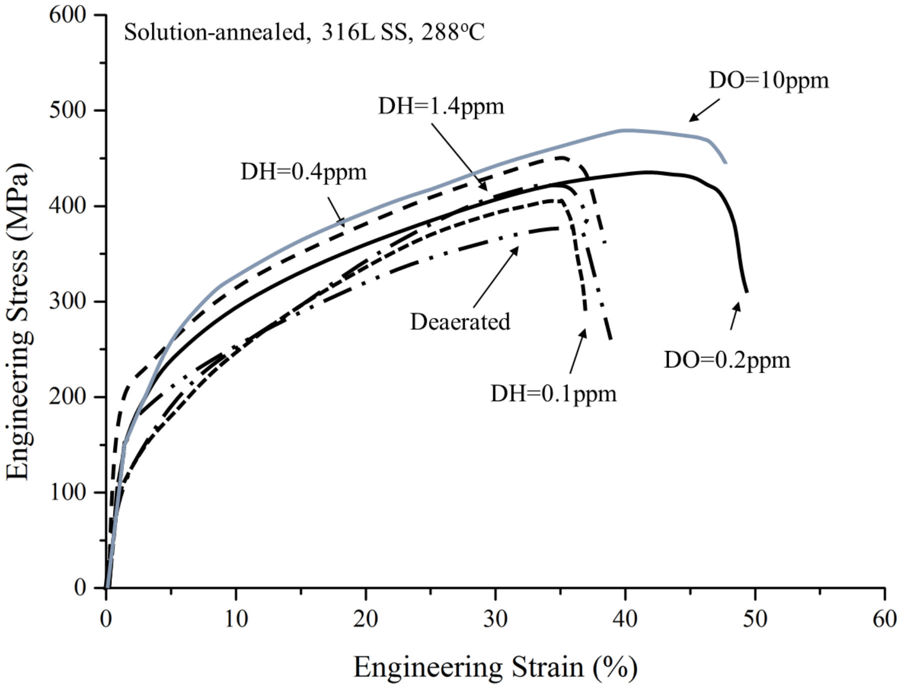

Fig. 4.3 Stress-strain curves of solution-annealed (SA) 316L SS tested at 288°C with various water condition.

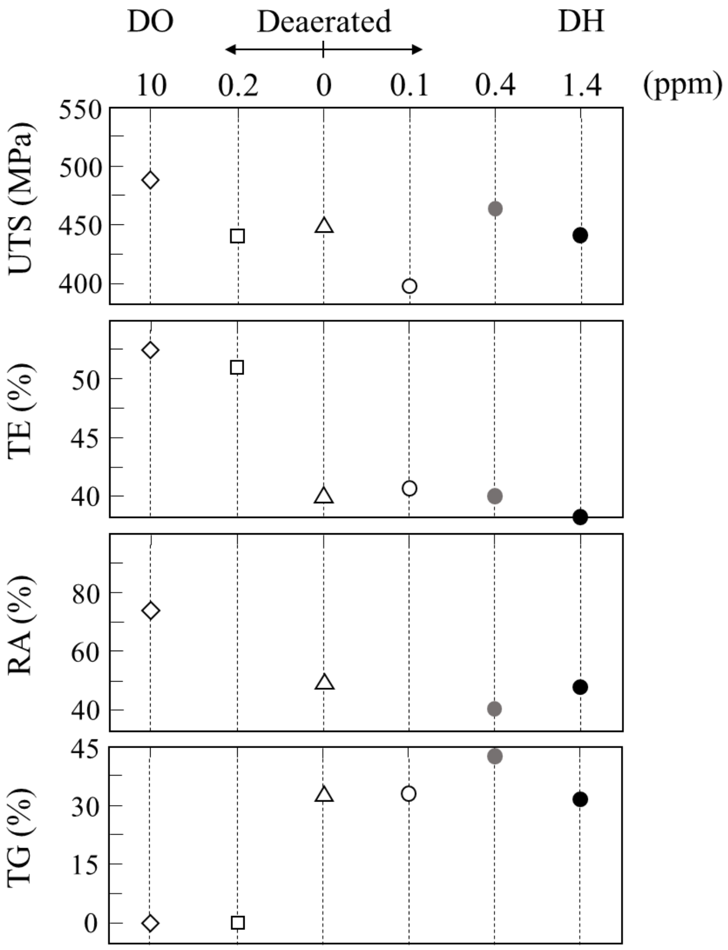

Fig. 4.4 Mechanical properties of SA 316L SS: UTS (ultimate tensile strength), TE (total elongation), RA (reduction in area), TG% (area % of transgranular cracking to fractured surface) tested at 288°C. ●: DH=1.4ppm, ●: DH=0.4ppm, ○: DH=0.1ppm, △: deaerated, □: DO=0.2ppm and ◇: DO=10ppm

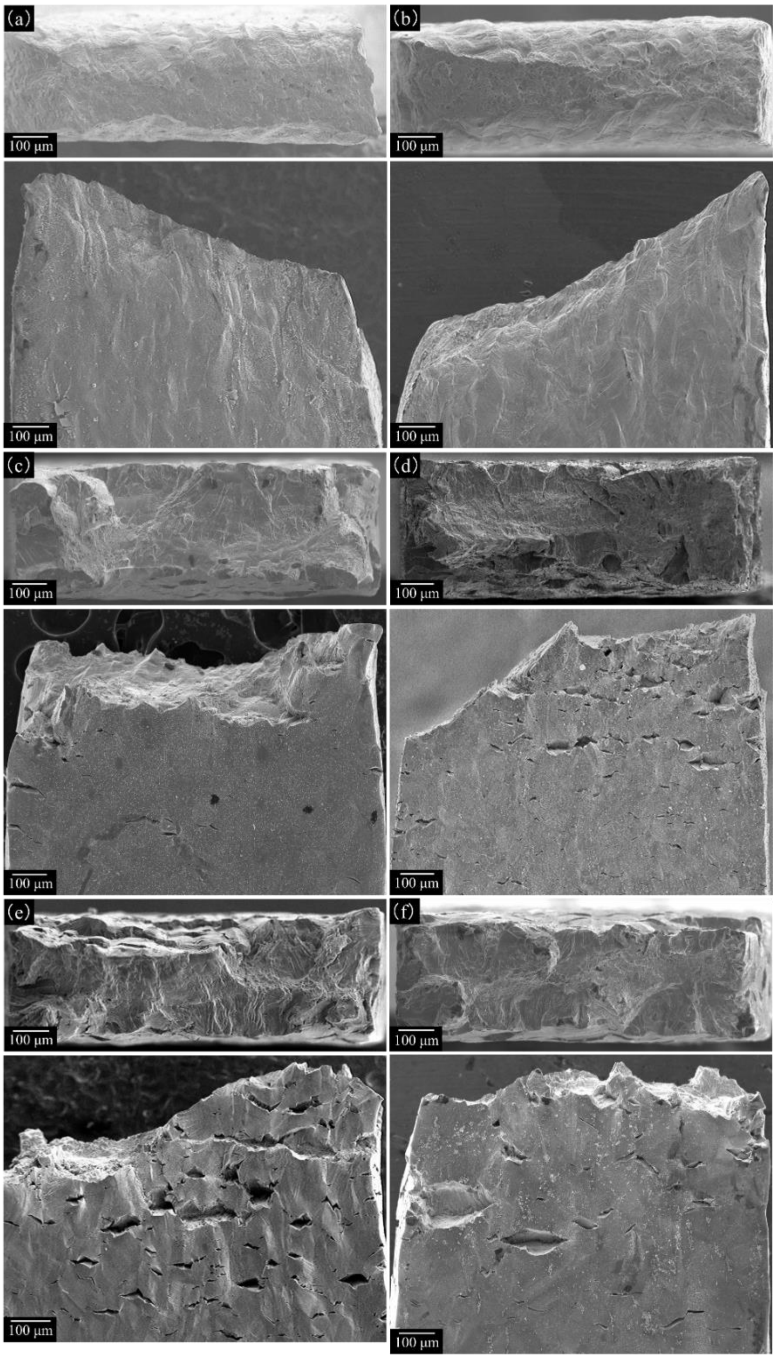

Fig. 4.5 SEM photos of solution-annealed 316L tested at 288°C hot water with (a) DO=10ppm, (b) DO=0.2ppm, (C) Deaerated, (d) DH=0.1ppm, (e) DH=0.4ppm and (f) DH=1.4ppm water condition. In each column, top represents fractured surface, down represents side surface near necking area.

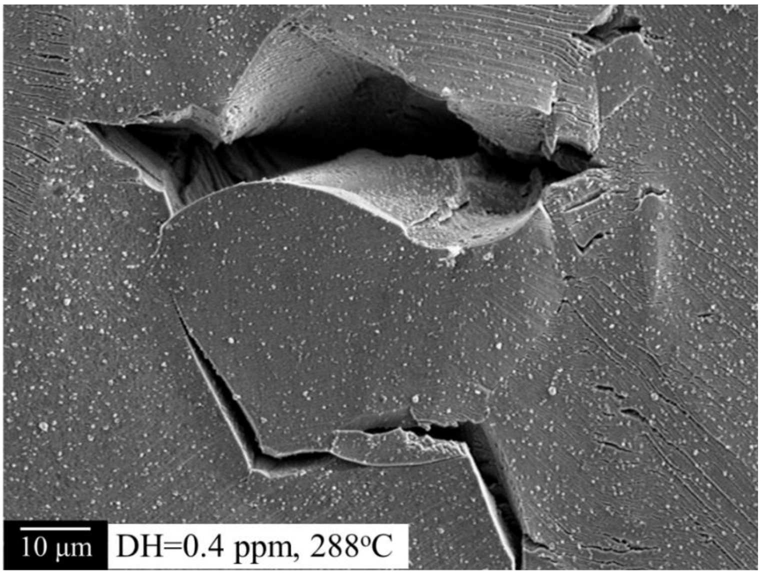

Fig. 4.6 SEM photo of IG fractured grain on side surface of specimen tested at 288°C hot water with DH=0.4ppm water condition.

4.3.2 Temperature effect

SSRTs were conducted at RT, 150°C, 220°C and 288°C. The stress strain curves of the test results in water with DH=0.4 ppm and DH=1.4ppm are shown in Fig. 4.7(a) and (b), respectively. Mechanical properties were summarized in Table 4.2 and plotted in Fig. 4.8, in which for both two testing conditions, reduction in area was decreased as temperature increased, and TG area percentage was increased as temperature increased. The trends of temperature dependence of UTS and TE were slightly different. In DH=1.4 ppm condition, the UTS and TE were monotonically decreased as temperature increased from RT to 288°C. However, a minimum TE was found on the specimen tested in water with DH=0.4ppm at 220°C.

The fractured surface and side surface observed after SSRT at each temperature are shown in Fig. 4.9 (DH=0.4ppm) and Fig. 4.10 (DH=1.4ppm). For both water chemistry conditions, specimens tested at lower temperatures were relatively ductile. TGSCC was found on specimen tested at 220 °C in water with DH=1.4 ppm and at 288 °C in water with DH=0.4 ppm and 1.4 ppm. A small number of side surface cracks were also found on specimen tested at 288 °C, DH=0.1ppm.

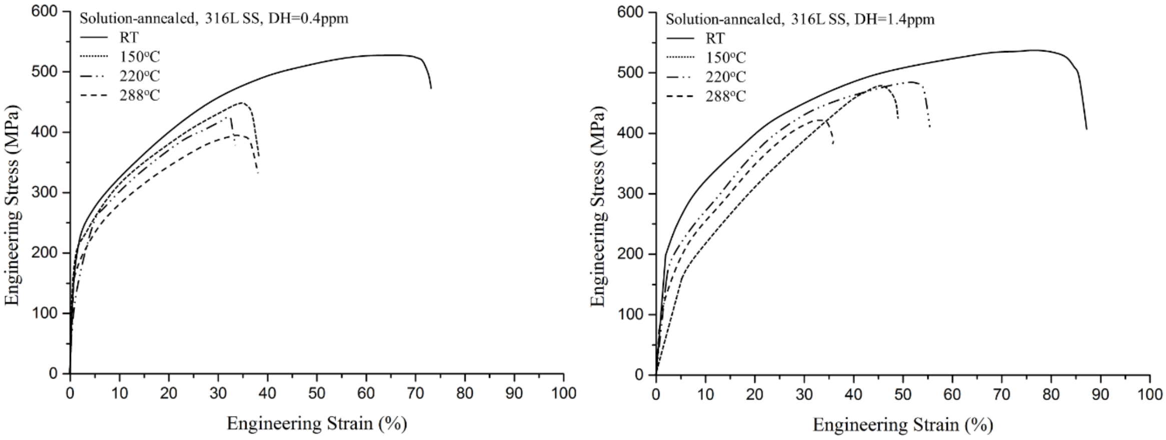

Fig. 4.7 Stress-strain curves of solution-annealed 316L SS tested at temperature ranging from room temperature (RT) to 288^{o}C with DH=1.4 ppm water condition. Solid line: RT / Dotted line: 150 ^{o}C / Dash-dot-dotted line: 220 ^{o}C / Dashed line: 288 ^{o}C

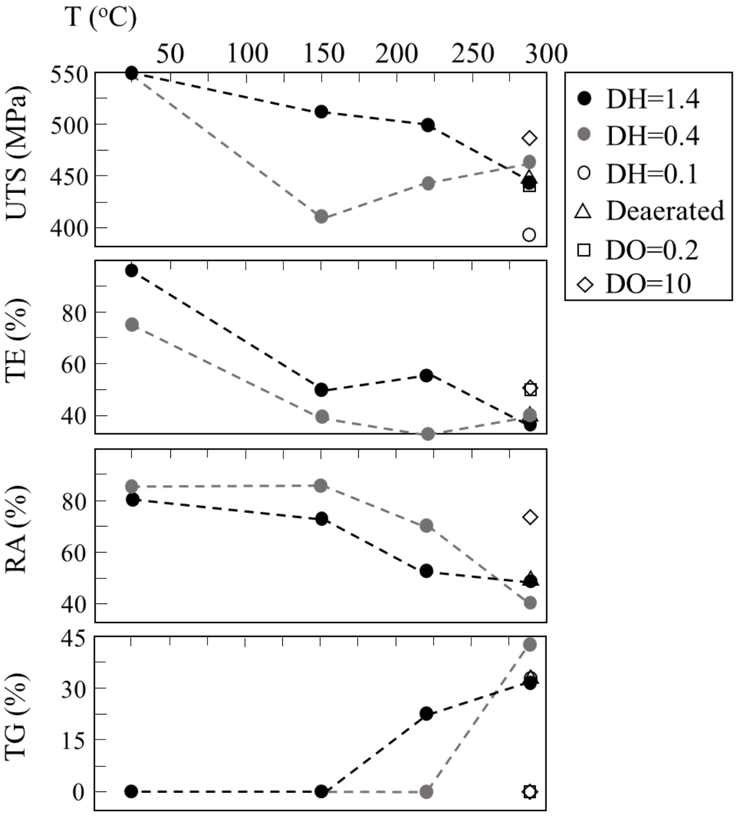

Fig. 4.8 Mechanical properties of SA 316L SS: UTS (Ultimate Tensile Strength), TE (Total Elongation), RA (Reduction of Area), TG% (Area of transgranular cracking to area of fractured surface) tested from RT to 288^{o}C. ●: DH=1.4ppm, ●: DH=0.4ppm, ○: DH=0.1ppm, △: deaerated, □: DO=0.2ppm. ◇: DO=10ppm

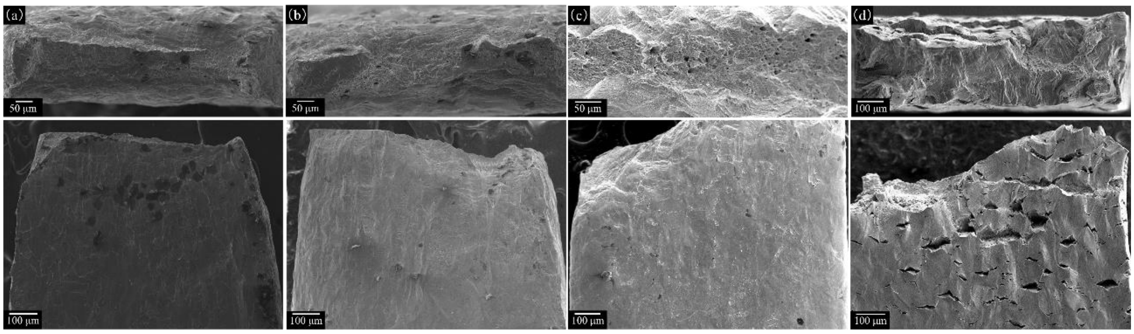

Fig. 4.9 SEM photos of solution-annealed 316L in (a) room temperature water and (b) 150°C, (c) 220°C and (d) 288°C hot water with DH=0.4 ppm water condition. In each column, top represents fractured surface, down represents side surface near necking area.

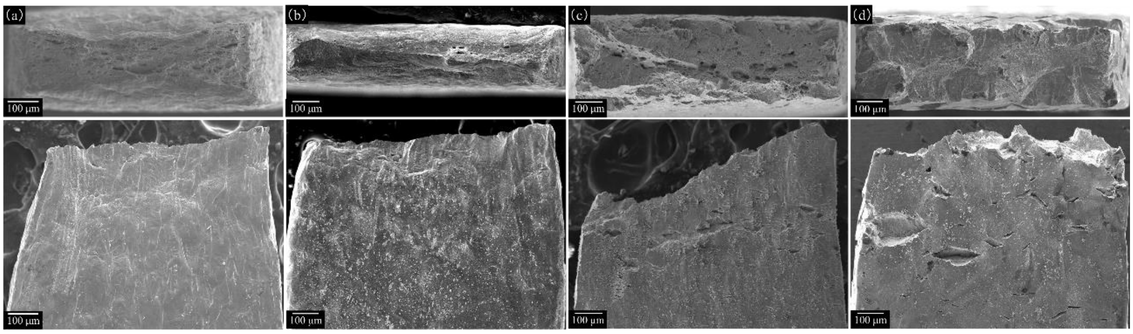

Fig. 4.10 SEM photos of solution-annealed 316L in (a) room temperature water and (b) 150°C, (c) 220°C and (d) 288°C hot water with DH=1.4 ppm water condition. In each column, top represents fractured surface, down represents side surface near necking area.

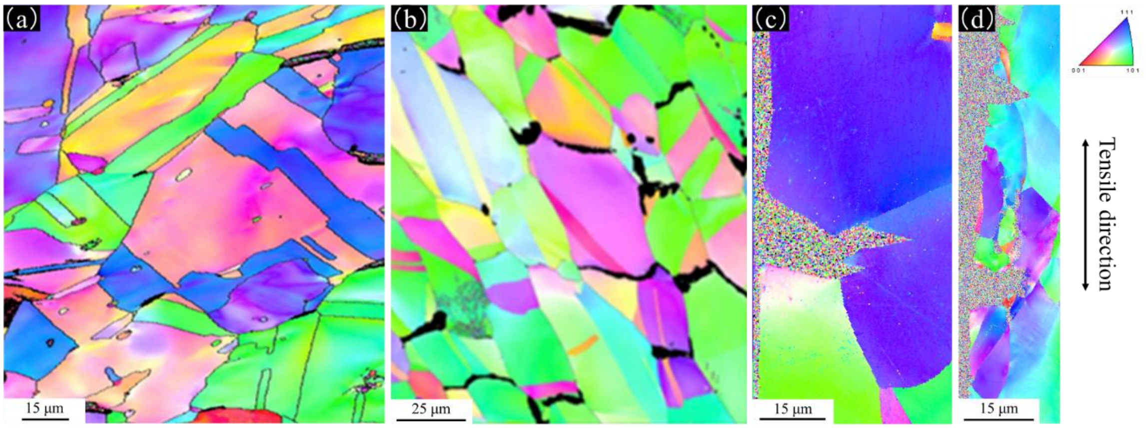

Fig. 4.11 The crack initiation mode of solution-annealed 316L SS at 288°C hot water with (a) DH=0.1 ppm, (b) DH=0.4 ppm (c) DH=1.4 ppm water condition and at (d) 220 °C hot water with DH=1.4 ppm water condition. IG crack was found on first three testing conditions while TG crack was found the last testing condition.

Fig. 4.11 shows the results of EBSD analysis carried out on specimens tested in water with (a) DH=0.1ppm, (b) DH=0.4ppm and (c) DH 1.4 ppm at 288 ^{o}C, and (d) DH 1.4 ppm at 220 ^{o}C. Fig. 11(a) and (b) are top view of the specimen side surface, and (c) and (d) are cross sectional view of one. In all the cases, the perpendicular direction was parallel to the tensile direction. All the specimens tested at 288 ^{o}C appear to exhibit IG crack initiation and penetrate into inside as TG cracks. On the contrary, at 220 ^{o}C, only TG crack initiation followed by TG crack propagation was observed.

Fig. 4.12 shows the oxide film thickness of specimens tested at various water conditions and temperatures. In DO water condition, film thickness was over 1 μm. In deaerated water condition, thickness was down to 150 nm. A minimum thickness was at DH=0.1ppm condition. Thickness was around 200 nm at relative high hydrogen content. On the other hand, as testing temperature increases from RT to 288^{o}C, film thickness increases.

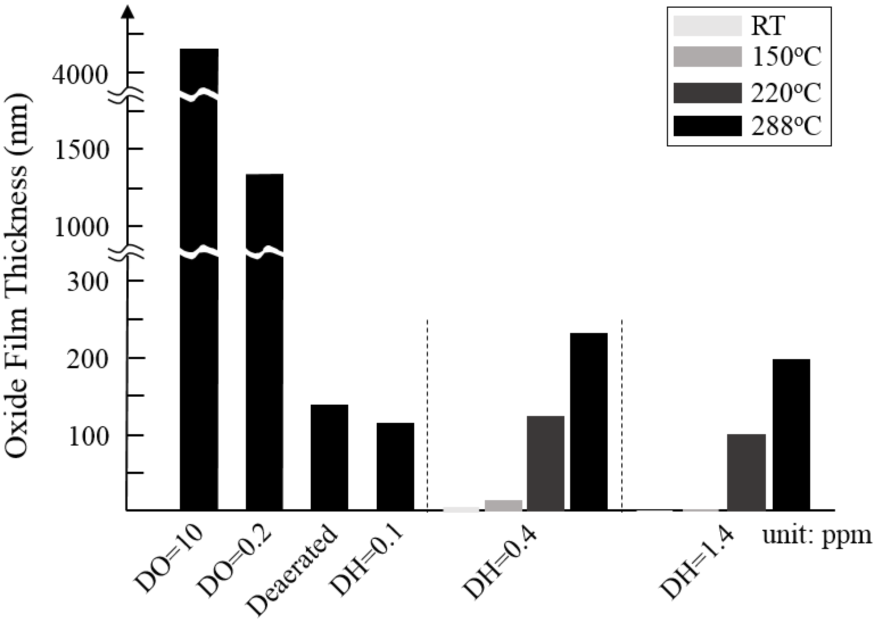

Fig. 4.12 Oxide film of specimens tested at various water conditions and temperatures

4.4 Discussion

4.4.1 TGSCC in hydrogenated water

Solution-annealed 316L SS never broke in a brittle manner in SSRT in hot water dissolved with oxygen (DO) up to 10 ppm, and the fracture mode was completely ductile. However, at a low potential conditions of deaerated water and dissolved with hydrogen DH= 0.1, 0.4 and 1.4 ppm, the fracture mode of solution-annealed 316L SS changed from ductile to brittle fracture showing TGSCC as shown in Fig. 4.6. Although the RA and TG(%) are not remarkably changed by DH content, the crack length or crack growth rate and crack opening distance appear to increase with DH content. It should be noted that at 288 °C the SCC initiates as an IGSCC at very near surface and the fracture mode changed to TGSCC inside.

In the previous study by Nono et al. [14], we reported TGSCC of solution-annealed 316L SS in a hot water with DH=0.4ppm at 288 ^{o}C, and showed that cold work enhanced TGSCC. This suggests that the TGSCC observed in SSRT in hydrogenated water is related with deformation structure such as dislocation bands or dislocation cell structure. Arioka et al. [3] reported an intergranular crack initiation and transgranular crack propagation in water with 30 cc/kg of hydrogen at 320 ^{o}C, which is resemble with the result observed in this study although the test temperature is different.

4.4.2 Mechanism of SCC in hydrogenated water

Although most of the brittle fracture is TGSCC on fractured surfaces in solution-annealed 316L SS, the detailed observation of specimen side surface revealed that the nucleation happened along grain boundaries (IGSCC), as shown in Fig. 4.7. It was considered that once IGSCC started at the surface during necking in the late stage of deformation, the IGSCC changed to TGSCC with progressing of the necking. As mentioned before, Arioka et al. also reported the IGSCC nucleation and TGSCC propagation in 316L SS tested by SSRT in hydrogenated water [3], and the fracture mode change was interpreted in terms of strain rate effect. We also consider a similar interpretation that at the beginning of SCC, an active dissolution of grain boundaries near specimen surfaces happens because of no stable thick oxide film formed in hydrogenated water. Since the active dissolution region of grain boundaries are so limited to the near surface area, and at a higher strain rate during the necking, the IGSCC susceptibility is reduced, no further IGSCC growth happens, but TGSCC substitutes with it probably because only the deformation bands formed by severe deformation is now susceptible to TGSCC at rather high strain rate. Zhong et al. studied the effects of dissolved hydrogen and surface condition on the IGSCC initiation and short crack growth behavior of non-sensitized 316 SS [11], and the SCC was affected by surface condition reflecting that cold work enhanced SCC susceptibility in hydrogenated water in PWR condition. It can be said that in the late stage of SSRT the specimen is cold-worked and enhances SCC susceptibility. Choi et al. investigated crack growth behavior of warm-rolled 316L SS in high-temperature hydrogenated water [13], and showed that the crack growth rate of warm-rolled 316L stainless steel was higher than that of as-received ones in hydrogenated water. They also pointed out that slip band and sensitized GB, which were formed during warm-rolling process and played a role as paths for more active corrosion and SCC, are relatively more effective to CGR than dissolved hydrogen. They also concluded that the dissolved hydrogen decreases the stability of the protective oxide layer and accelerates the corrosion rate.

Since brittle facture is due to the reduction of bond strength between lattice atoms or atoms across the grain boundary, atom dissolution or other potential mechanisms should play a role to cause the reduction of atomic bond strength and consequently cracking. It is known that hydrogen often reduces atomic bond or cohesive force of lattice [19]. For a micro-cell within a crack, an active dissolution reaction happens as an anodic reaction and hydrogen production through the decomposition of water happens as a cathodic reaction. The hydrogen produced in the local region of cathodic reaction may be trapped at the grain boundaries and/or dislocations. In the case that an enough hydrogen to cause cracking is provided on grain boundaries by the cathodic reaction and/or from hydrogenated water, IGSCC may happen and penetrates into bulk as TGSCC along deformation bands. Thus, the active dissolution of atoms is necessary to accompany the cathodic reaction at the surface without thick oxide film, as mentioned by Choi et al. [13]. Hydrogen is also necessary to reduce the cohesive force between atoms to cause brittle fracture. Finally, we think the SCC observed in this study is hydrogen-assisted SCC (HASCC), which explains the temperature dependence of the occurrence of SCC in hydrogenated water.

4.4.3 Test temperature dependence

There two issues to be discussed: one is corrosion rate and the other is hydrogen behavior. As for corrosion rate, the thickness of corrosion layer was increased with temperature, as shown in Fig. 4.12. Since it can be thought that the anodic reaction in a corrosion is accompanied by hydrogen production through cathodic reaction, the amount of hydrogen produced by corrosion reaction increases with temperature. It has been also known that temperature is a key factor that affects hydrogen behaviors such as solubility, diffusion rate, permeability and trapping at defects within the bulk material. At low temperature, hydrogen trapping efficiency is very high but hydrogen cannot move long distance because of low diffusivity of hydrogen. At elevated temperatures, however, although hydrogen diffusivity is now large enough for hydrogen to aggregate to trapping sites, an excess hydrogen within matrix tends to diffuse outward to the material surfaces because of the contribution of binding energy to trap hydrogen is reduced at high temperatures. Therefore, the residual hydrogen is incapable of inducing cracking if below a critical value. These are regarded the reasons why the susceptibility to HIC peaks at intermediate temperature and why HIC is less likely to occur at high temperatures above RT. Nevertheless, the temperature range of HASCC in this work belongs to the elevated temperature region according to HE behavior. This is because corrosion is a necessary condition to cause HASCC, while the reduction cohesive force by hydrogen atoms is an enough condition to cause it.

Hydrogen diffusion distance in metal can be described as following formulas based on Fick's second law and Arrhenius law:

$$X_H = \sqrt{(2D_H t)} \tag{1}$$

$$D_H = D_0 \exp(-E_d/kT) \tag{2}$$

where X_H is hydrogen diffusion distance, D_H is diffusion coefficient, t is testing time, D_0 is intrinsic diffusion coefficient, E_d is activation energy, k is Boltzmann factor and T is absolute temperature. In presumed condition, the hydrogen diffusivity in pure γ-iron at 288 °C is as follows: $D_0 = 1.0 \times 10^{-6}$ [m^2/s], $Q = 47300$ [eV/mol], k=1.38x10^{-23}[J/K], T=561[K], D_H = 3.97 x 10^{-11}[m^2/s]. The diffusivity of practical steel is one-fifth of this value due to existence of defects. For solution-annealed and defect-bearing steel tested at each temperature for 820,000 s that is general testing time, the hydrogen diffusion distance is estimated to be XH = 1.61, 0.75, 0.32, 0.03 mm at 288, 220, 150 and RT, respectively. The distance at 288^{o}C and 220^{o}C are greater than the thickness of test specimens used in this work (0.5 mm).

4.4.4 Effect of DH concentration

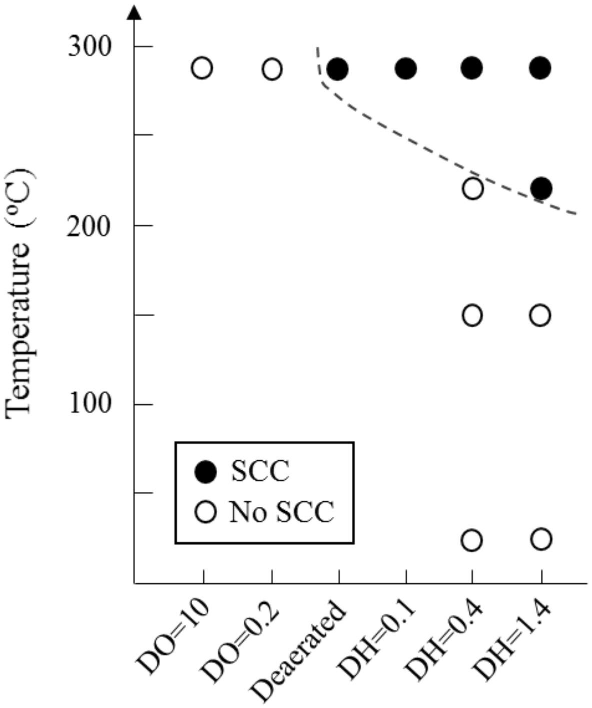

Fig. 4.13 Temperature-SCC map

The relationship between SCC occurrence and testing conditions is mapped in Fig. 4.13. At DH=0.4ppm or below, SCC was found only at 288 °C. On the other hand, under DH=1.4 ppm, SCC was found at relatively lower temperature region. In addition, the main fracture mode of specimens tested at 220°C, DH 1.4ppm are TGSCC. However, the fracture mode of specimens tested at 288°C in deaerated to DH=1.4 ppm are IGSCC at surface (nucleation) and TGSCC in bulk (growth). One can notice a SCC boundary line falls between 220°C and 288°C under DH=0.4ppm and gradually drops below 150 °C under DH=1.4 ppm. Obviously, both temperature and DH affects SCC susceptibility, the higher the temperature or dissolved-hydrogen, the higher the susceptibility to SCC. Nonetheless, temperature strongly affects hydrogen behavior.

As mentioned in session 4.1, prior the onset of HASCC, a critical amount of hydrogen is required at a potential crack-inducing defect site. The hydrogen amount at trapped site, C_H^T, is expressed by the following equation:

$$C_H^T = C_L \exp({}^{E_b}/_{kT}) \qquad (3)$$

where C_L is hydrogen solubility in material, E_b is defect-hydrogen binding energy. This equation indicates that hydrogen trapping ability becomes less with temperature. Integrating the two factors, which are hydrogen diffusivity and hydrogen trapping ability, one can derive a hydrogen gathering rate at trapping sites. It can be said that if the velocity is high, the sooner the HIC will occur; and vice versa, if small, the slower the HIC happens. This temperature dependent factors are named "HASCC indicator" in this work, and we assumed that the solute hydrogen concentration in material, CL, is proportional to the sum of DH in water and hydrogen produced through corrosion reaction, DH'. Therefore, we introduce a proportional constant, α, and CL equals (DH+DH') * α. Then equation (4) is obtained.

$$C_H^T = \alpha(DH + DH')\exp({}^{E_b}/_{kT}) \qquad (4)$$

which indicates that the critical amount of hydrogen to cause HASCC becomes achievable at higher DH, and DH' increases but hydrogen trapping ability decreases with temperature.

Therefore, it is considered that in the test temperature range below 288 ^{o}C, both the oxidation rate and diffusion rate of hydrogen are rate controlling processes of the occurrence of SCC, and the SCC susceptibility increases with temperature. As for the hydrogen binding ability, this temperature range can be low enough to trap hydrogen at crack initiation site such as grain boundaries near specimen surfaces. Further increase in test temperature may reduce the SCC susceptibility because of the reduction of hydrogen trapping capacity by following the equation (4) where temperature effect increases exponentially.

On the assumption that the SCC observed in this study is HASCC, which is accompanied by work hardening, corrosion and hydrogen absorption, the dependence of the SCC on both the test temperature and dissolved hydrogen content was reasonably explained in terms of corrosion assisted hydrogen production while suppressing the formation of protective oxide film on the specimen surface and hydrogen-induced reduction of cohesive force of lattice of austenitic stainless steel.

4.5 Conclusions

The effect of dissolved-hydrogen and temperature on SCC susceptibility of solution-annealed 316L SS was evaluated by means of SSRT method conducted in a simulated hot water circulation loop. Main results are shown as follows:

(1) SCC was never observed in the specimens tested in water dissolved with oxygen up to 10 ppm at 288°C. In the hydrogenated water, however, SCC occurred in the late stage of deformation accompanied by necking.

(2) Presence of hydrogen affects metal-oxygen reaction and oxide film thickness. At 288°C, a minimum thickness was found at deaerated water condition. Meanwhile, the film thickness increases with temperature up to 288°C.

(3) The SCC susceptibility reduced with test temperature below 288 °C where SCC occurred in the water with DH=0.4 and 1.4 ppm, while at 220 °C the SCC occurred at highest DH condition (DH=1.4ppm) only. This indicates a combing effect of DH and test temperature. Test temperature dependence can be interpreted in terms of anodic reaction rate, hydrogen diffusion rate and hydrogen trapping ability.

(4) Finally, the SCC observed in this study is interpreted in terms of hydrogen-assisted SCC (HASCC) which is accompanied by work hardening, corrosion and hydrogen absorption. The dependence of HASCC on both the test temperature and dissolved hydrogen content was reasonably explained by corrosion assisted hydrogen production while suppressing the formation of protective oxide film on the specimen surface and hydrogen-induced reduction of cohesive force of lattice of austenitic stainless steel.

References

[1] Y. Okamura, A. Sakashita, T. Fukuda, H. Yamashita, T. Futami, Latest SCC issues of core shroud and recirculation piping in Japanese BWRs, 2003.

[2] R.. Horn, G.. Gordon, F.. Ford, R.. Cowan, Experience and assessment of stress corrosion cracking in L-grade stainless steel BWR internals, Nucl. Eng. Des. 174 (1997) 313–325. doi:10.1016/S0029-5493(97)00131-3.

[3] K. Arioka, Influence of Temperature, Hydrogen and Boric Acid Concentration on IGSCC Susceptibility of Unsensitized 316 Stainless Steel, J. Inst. Nucl. Saf. Syst. 9 (2002) 116–123.

[4] T. Terachi, T. Yamada, T. Miyamoto, K. Arioka, SCC growth behaviors of austenitic stainless steels in simulated PWR primary water, J. Nucl. Mater. 426 (2012) 59–70. doi:10.1016/j.jnucmat.2012.03.013.

[5] M.B. Toloczko, P.L. Andresen, S.M. Bruemmer, SCC CRACK GROWTH OF COLD-WORKED TYPE 316 SS IN SIMULATED BWR OXIDIZING AND HYDROGEN WATER CHEMISTRY CONDITIONS, in: 13th Int. Conf. Environ. Degrad. Mater. Nucl. Power Syst., Whistler, British Columbia, n.d.: pp. 1–11.

[6] W. Bilanin, D. Cubicciotti, R.L. Jones, A.J. MacHiels, L. Nelson, C.J. Wood, Hydrogen water chemistry for BWRs, Prog. Nucl. Energy. 20 (1987) 43–70. doi:10.1016/0149-1970(87)90011-4.

[7] P.L. Andresen, M.M. Morra, IGSCC of non-sensitized stainless steels in high temperature water, J. Nucl. Mater. 383 (2008) 97–111. doi:10.1016/j.jnucmat.2008.08.005.

[8] S.M. Bruemmer, L.E. Thomas, COMPARISON OF IGSCC CRACK-TIP CHARACTERISTICS PRODUCED IN BWR OXIDIZING WATER AND BWR HYDROGEN WATER CHEMISTRY CONDITIONS, in: 13th Int. Conf. Environ. Degrad. Mater. Nucl. Power Syst., Whistler, British Columbia, n.d.: pp. 1–10.

[9] T. Yeh, M. Wang, Water Chemistry in the Primary Coolant Circuit of a, (2011) 2079–2089. doi:10.13182/NSE11-85.

[10] P. Andresen, P. Chou, Effects of Hydrogen on SCC Growth Rate of Ni Alloys in BWR Water, in: 15th Int. Conf. Environ. Degrad. Mater. Nucl. Power Syst. - Water React., 2011: pp. 2039–2059.

[11] X. Zhong, S.C. Bali, T. Shoji, Effects of dissolved hydrogen and surface condition on

the intergranular stress corrosion cracking initiation and short crack growth behavior of non-sensitized 316 stainless steel in simulated PWR primary water, Corros. Sci. 118 (2017) 143–157. doi:10.1016/j.corsci.2017.02.003.

[12] T. Fukumura, N. Totsuka, Effect of Dissolved Hydrogen Concentration on PWSCC Crack Growth Rate of Alloy 600 at 290℃, J. Inst. Nucl. Saf. Syst. 17 (2010) 122–129.

[13] K.J. Choi, S.C. Yoo, H.H. Jin, J. Kwon, M.J. Choi, S.S. Hwang, J.H. Kim, Crack growth behavior of warm-rolled 316L austenitic stainless steel in high-temperature hydrogenated water, J. Nucl. Mater. 476 (2016) 243–254. doi:10.1016/j.jnucmat.2016.04.051.

[14] M. Nono, T. Nakajima, M. Iwama, R. Kasada, A. Kimura, SCC behavior of SUS316L in the high temperature pressurized water environment, J. Nucl. Mater. 417 (2011) 878–882. doi:10.1016/j.jnucmat.2010.12.150.

[15] G.R. Caskey, Hydrogen compatibility handbook, 1983. doi:10.2172/5906050.

[16] G. Han, J. He, S. Fukuyama, K. Yokogawa, Effect of strain-induced martensite on hydrogen environment embrittlement of sensitized austenitic stainless steels at low temperatures, Acta Mater. 46 (1998) 4559–4570. doi:10.1016/S1359-6454(98)00136-0.

[17] T.C. Chen, S.T. Chen, L.W. Tsay, The role of induced α′-martensite on the hydrogen-assisted fatigue crack growth of austenitic stainless steels, Int. J. Hydrogen Energy. 39 (2014) 10293–10302. doi:10.1016/j.ijhydene.2014.04.144.

[18] C.L. Lai, L.W. Tsay, C. Chen, Effect of microstructure on hydrogen embrittlement of various stainless steels, Mater. Sci. Eng. A. 584 (2013) 14–20. doi:10.1016/j.msea.2013.07.004.

[19] R. A. ORIANI, A Mechanistic Theory of Hydrogen Embrittlement of Steels, (1972) 848–857.

Chapter 5

Stress Corrosion Cracking Susceptibility of 310S Stainless Steel in Hydrogenated Hot Water

5.1 Introduction

The water-cooled ceramic breeder testing blanket module (TBM) is one of key components of International Thermonuclear Experimental Reactor and beyond towards nuclear fusion energy. In the design of the TBM, a reduced activation ferritic/martensitic steel has been selected as structural material cooled by water similar to the current pressurized water reactors (PWR). Behind the TBM there is a primary heat transfer system that is responsible for heat exchange and tritium recovery where long cooling pipes made of 316L stainless steel (SS) are installed [1–6]. In the blankets, tritium, a fuel of fusion reactor, is produced through nuclear reactions and it could penetrate into cooling water. With the aid of radiation, tritium (T) may react with water and forms tritiated water (such as THO or T_2O) and/or TH, T_2 as dissolved gaseous species in the coolant.

Regarding the effect of dissolved hydrogen on stress corrosion cracking (SCC), current PWRs adopt hydrogen injection to reduce corrosion potential for scavenging corrodants for maintaining structural integrity. The content of dissolved-H_2 (DH) is a key and should be kept within a certain range to maximize efficiency while not degrading materials. In order to investigate the effect of hydrogen on SCC, a number of studies were performed by means of slow strain rate test (SSRT) and compact tension (CT) test with focusing on the measurement of crack growth rate (CGR) of solution annealed and/or cold worked SS in simulated PWR primary loop water.

Arioka et al. conducted SSRT on solution-annealed 316 SS at different temperatures and found a minimum CGR at 15cc H_2/kg H2O in the temperature range of 320-340 ^oC and at around 25 cc H_2/kg H_2O at 310 ^oC [7]. On cold-worked 316L SS, Fukumura et al. [8] reported a monotonic increase from 15 to 45 cc H_2/kg H_2O at 320 ^oC, which is supported by Choi et al. tested at 340 ^oC [9]. However, Meng et al. found a monotonic CGR decrease from 0 to 50 cc

H_2/kg H_2O [10]. Nonetheless, Zhong et al. found a CGR peak at 15 cc H_2/kg H_2O at 325 ^oC [11]. Raquet et al. reported a CGR peak at 30cc H_2/kg H_2O at 360 ^oC on V-shape humped 304L SS [12]. As shown above, although the effect of hydrogen content is not clear, it is considered that hydrogen play two roles in suppression of formation of protective film thickness [13] and in reduction of atomic bond strength of which the balance determines the total effect of hydrogen on SCC.

The fracture mode of SCC in the water dissolved with hydrogen is also different among the researchers; transgranular (TG), intergranular (IG) or mix mode. Meng et al. [10] and Chen et al. [14] revealed IGSCC for a cold-worked 316NG tested in the water with DH 2.5 ppm at 310 ^oC. Nono et al. [15], however, reported TGSCC on solution-annealed 316L SS in the water with DH=0.4 ppm at 288 ^oC. Arioka et al. [7] found that crack initiated in IG mode and transformed into TG mode in the water with 30 cc H_2/kg H_2O at 320 ^oC. As for nickel base alloys, several researchers reported that CGR showed a peak [7,8,11] or increased [10] with hydrogen contentment. These above mentioned experimental results suggests that hydrogen effect also depends on material even for iron based austenitic SS.

Austenitic SS also suffer hydrogen embrittlement in a dry hydrogen gas. Caskey [16] carried out tensile tests at temperature ranging from 77-373K for several iron-based austenitic stainless steels charged with deuterium in a deuterium atmosphere (D_2) at 69 MPa, and he found that the susceptibility to hydrogen embrittlement of 310S SS is much less than 304L SS at around 200K. He also indicated that, in Fe-Cr-Ni ternary alloy system, the susceptibility reduced as Ni content was as high as within 15-25 wt%. Han et al. [17] reported the similar results with him. After the hydrogen or deuterium charging in 1 MPa of H_2 and D_2 gas, Zhang et al. [18] tested several types of 316 SS with various Ni content and showed that the susceptibility was reduced with Ni equivalent content of the austenitic steel.

We consider that 310S SS is more resistant to SCC under HT/T_2-dissolved hot water because 310S SS may behave in a similar manner in tritiated water as in hydrogen gaseous environment. In this research, the SCC susceptibility of solution-annealed 310S SS, which is rather highly resistant to hydrogen embrittlement, was examined by means of SSRT in hot water with dissolved-hydrogen and the results are compared with that of 316L SS. Furthermore, the effects of sensitization treatment on the SCC in hydrogenated water was investigated.

5.2 Experimental

5.2.1 Materials

The materials used in this study were commercial plate type 316L SS and 310S SS. Their chemical compositions were listed in Table 5.1. The geometry of tensile specimens is shown in Fig. 5.1, of which the gage section measures 5 mm in length, 1.2 mm in width and 0.5 mm in thickness. All the specimens were solution-annealed at 1050 ^{o}C for 1 hour, followed by quenching into iced water. A part of these tensile specimens were further heat-treated at 700^{o}C for 100 hour followed by water quench so as to simulate sensitization caused by post-weld heat treatment after welding. Specimen surface was polished from #1200 to #4000 with SiC sand papers then buff-polished to 0.25 μm with diamond pastes. After polishing, the specimens were cleaned in ultrasonic cleaner with demineralized water. The grain microstructure of solution-annealed specimens were shown in Fig. 5.2 after the etching in a solution mixed 10 g oxalic acid with 100 ml demineralized water. The averaged grain sizes were measured by means of intersection method and they were 26 and 59 μm for 310S and 316L SS, respectively.

Table 5.1 Chemical compositions of 316L and 310S SS

wt%	C	Si	P	S	Cr	Ni	Mo	Mn	Co	Fe
310S SS	0.02	0.7	0.022	-	24.76	19.17	-	0.8	0.1	bal.
316L SS	0.01	0.73	0.032	0.004	17.41	12.13	2.05	1.06	-	bal.

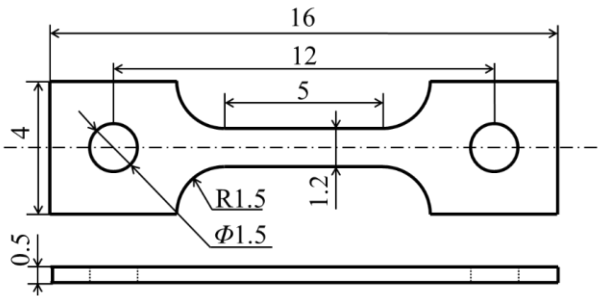

Fig. 5.1 The geometries of miniaturized specimens for SSRT

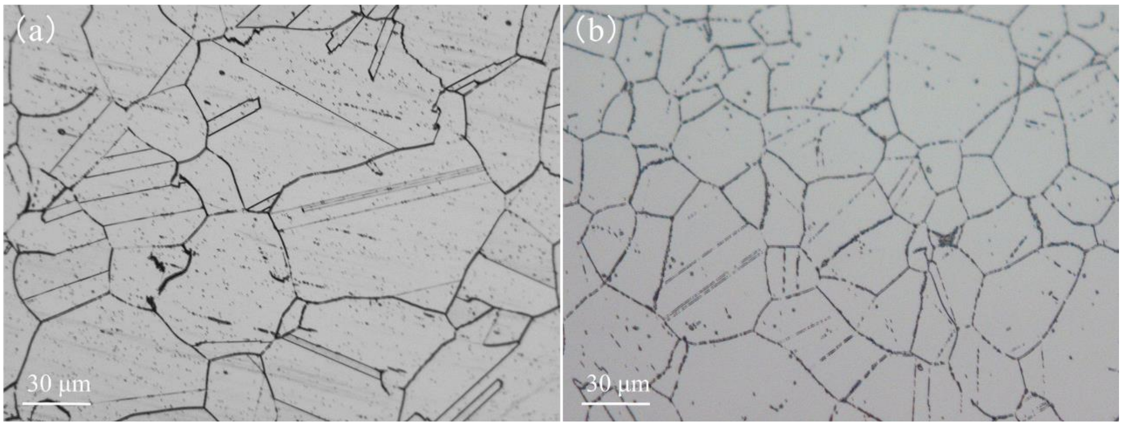

Fig. 5.2 The microstructures of solution-annealed (a) 316L and (b) 310S SS

5.2.2 Hot water loop for SSRT

The hot water circulation loop includes a primary loop and a water chemistry monitoring loop, as shown in Fig. 5.3. The high purity nitrogen and hydrogen were injected into a water tank to control dissolved-oxygen (DO) and dissolved-hydrogen (DH) content. A high pressure pump sent high purity water into a heat exchanger, pre-heater then to the autoclave where a SSRT specimen was set. The hot water is chilled through another heat exchanger and then back to the water tank. SSRT was conducted in the autoclave at a strain rate of 5×10^{-7}/s. Testing temperature and pressure was kept at 288 °C and 7.8 MPa with conductivity kept below 0.1 μS/cm. Two different water conditions were chosen for SSRT: one was of water dissolved with 1.4 ppm of hydrogen (DH=1.4 ppm) and the other was of deaerated condition (both DO and DH < 0.01 ppm).

After SSRT, fracture surface and side surface were observed by a scanning electron microscope (SEM). The fracture mode of crack initiation was examined by electron backscattering diffraction (EBSD) method with the orientation imaging microscopy (OIM) detector equipped in a field-emission type SEM (Ultra-55, Carl Zeiss Co., Ltd.).

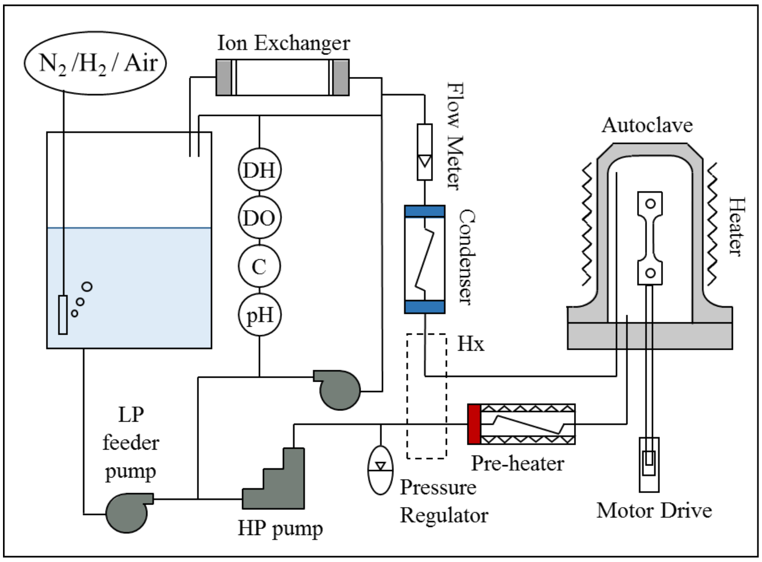

Fig. 5.3 Schematic view of SSRT loop used in this work

5.3 Results

5.3.1 Stress-strain behavior

Fig. 5.4 shows the stress-strain curves of solution-annealed (SA) 316L and 310S SS under deaerated and DH=1.4 ppm hot water condition. Solid lines represent deaerated water condition and dashed lines represent DH=1.4 ppm water condition. The ultimate tensile strength (UTS) and total elongation (TE) of 310S SS are larger than those of 316L SS. Although the difference is not significant, it appears that the total elongation is smaller in the case of DH=1.4 ppm water condition than deaerated water condition. A similar trend was observed for sensitized specimens, as shown in Fig. 5.5, where the stress-strain curves of sensitized (SEN) 316L and 310S SS were shown. The presence of dissolved-hydrogen again reduced the total elongation of 316L and 310S SS. In other words, the dissolved-hydrogen decreases total elongation irrespective of heat treatment conditions. Comparing the total elongations of both steels between SA and SEN, no remarkable difference was observed between two conditions in the water deaerated and DH=1.4 ppm. The stress-strain behavior will be discussed again more in detail after showing fracture behavior.

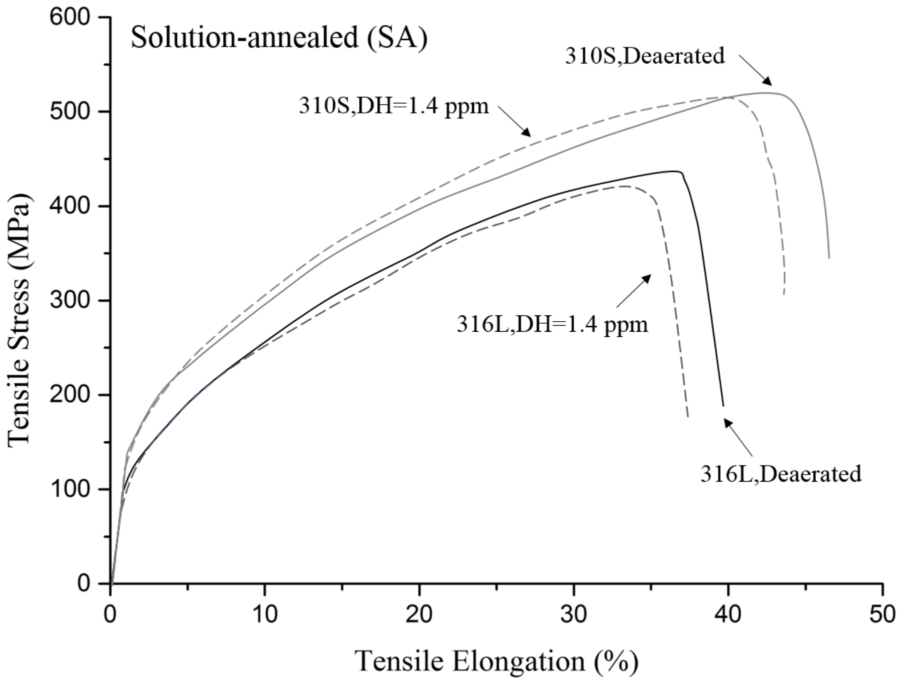

Fig. 5.4 Stress-strain curves of solution-annealed (SA) 316L and 310S SS tested in hot water (288 °C, 7.8 MPa) at deaerated condition (solid line) and with DH=1.4 ppm (dash line) .

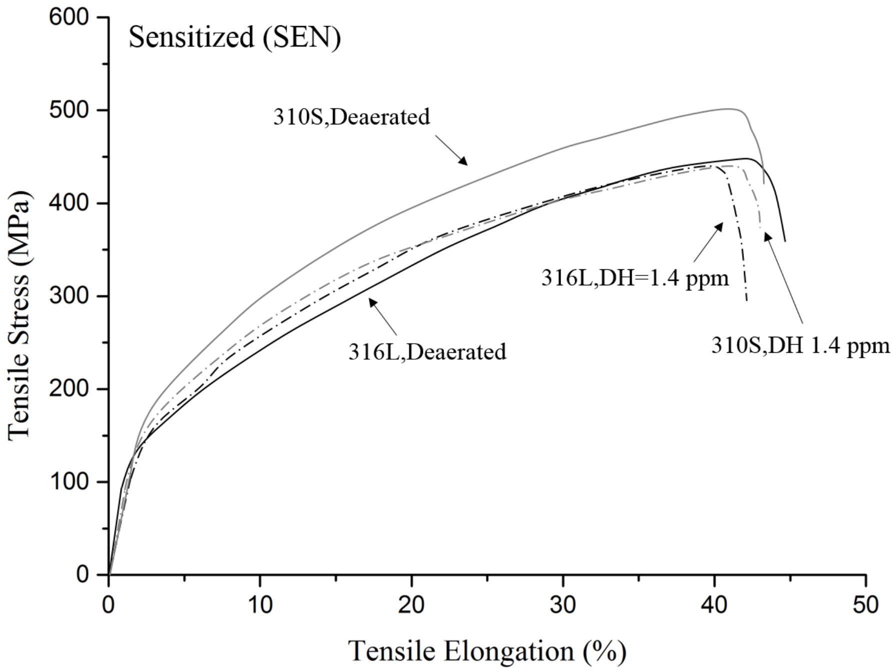

Fig. 5.5 Stress-strain curves of sensitized (SEN) 316L and 310S SS tested in hot water (288 °C, 7.8 MPa) at deaerated condition (solid line) and with DH=1.4 ppm (dash line)

5.3.2 Fracture behavior

The fractography of fractured surface and side surface is summarized in Fig. 5.6 for SA 316L SS/SA 310S SS under (a)/(c) deaerated and (b)/(d) DH 1.4 ppm water condition, respectively. In each column, the top represents the overview of fracture surface; the middle represents the enlarged area squared with white broken line; and the bottom represents side surface near fractured surface. Although the stress-strain behaviors in Fig. 5.5 are almost same among the specimens, the fracture mode is significantly influenced by experimental conditions, such as material and water chemistry. It is obvious that the fracture mode of 310S SS is almost completely ductile, while that of 316L SS is mostly brittle. The brittle fracture mode of 316L SS is mainly transgranular type, exhibiting river patterns, that is, TGSCC. A number of large cracks are also found on the side surfaces of 316L SS, while small cracks appear to be formed on 310S SS. It can be said that 310S SS is more resistant to occurrence of TGSCC than 316L SS. On the enlarged view of fractured surface of 316L SS under deaerated and DH 1.4 ppm (Fig. 5.6(a) and (b)) condition and of 310S SS under deaerated condition (Fig. 5.6(c)), some cracks appear to initiate with IGSCC and propagate as TGSCC with typical river-patterns in 316L SS. But, in 310S SS under DH 1.4 ppm (Fig. 5.6(d)), fine wavy crack patterns are also found. The cross sectional view was observed for the fractured specimens using SEM-EBSD and the results are shown in Fig. 5.7, indicating that the fracture mode of crack initiation of SA 316L and SA 310S SS under DH 1.4 ppm condition is intergranular. However, it is noted that most of crack initiation sites in SEN steels is transgranular type. Accordingly, it is considered that both the solution-annealed steels suffer embrittlement initiating as IGSCC at specimen surface and the cracks mostly penetrate into grains as TGSCC showing river patterns on the fractured surfaces, though the susceptibility to SCC is much lower in 310S SS than 316L SS.

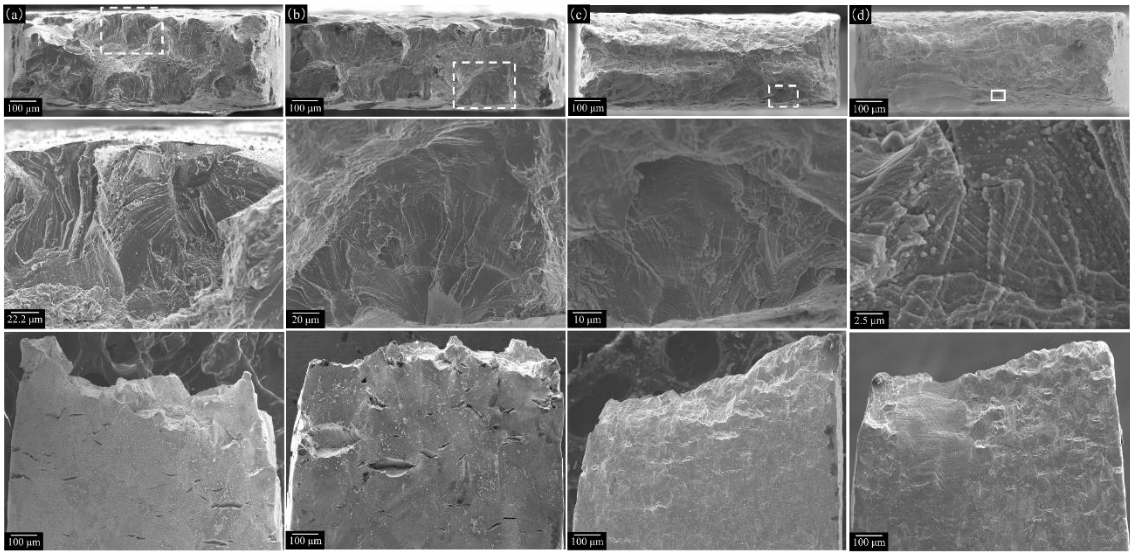

Fig. 5.6 SEM photos of solution-annealed 316L SS under (a) deaerated and (b) DH 1.4 ppm water condition; and 310S SS under (c) deaerated and (d) DH 1.4 ppm water condition. In each column, from top to bottom represents the overview of fracture surface, the enlarged area squared with white line and the side surface near fractured surface

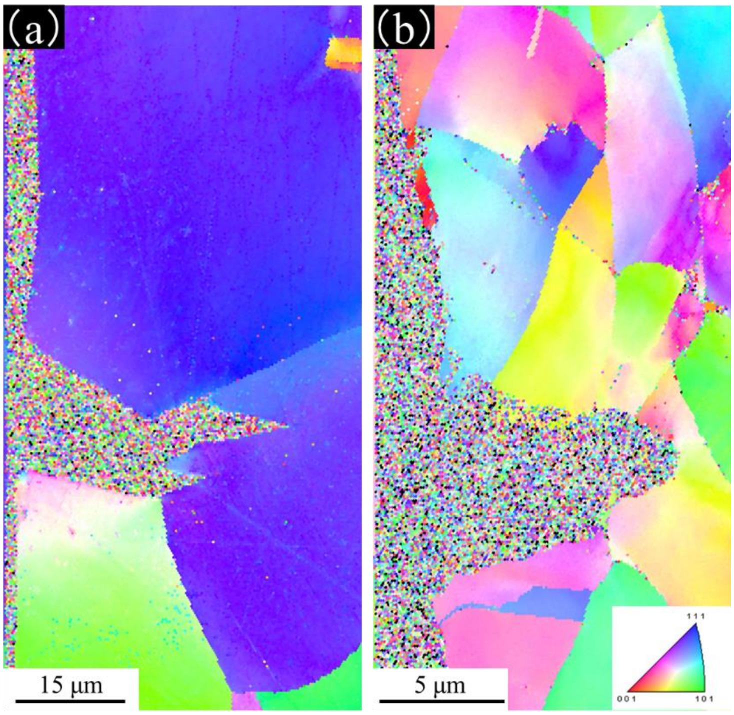

Fig. 5.7 The crack initiation of solution-annealed (a) 316L and (b) 310S SS under DH 1.4 ppm water condition. In both two materials, intergranular crack forms at the surface then propagates into grains as transgranular cracks.

A similar trend but smaller effects were observed for sensitized specimens. The fractography of fractured surface and side surface of SEN 316L SS/SEN 310S SS under (a)/(c) deaerated and (b)/(d) DH 1.4 ppm water condition is summarized in Fig. 5.8. In 316L SS, the brittle fracture ratio (BFR) of DH 1.4 ppm condition is smaller than that of deaerated condition, and in both the conditions cracks initiates and propagates as TGSCC. In 310S SS, the brittle fracture and cracks on side surface are almost unseen under two water conditions. These suggest that the susceptibility to SCC in hydrogenated water is reduced by sensitization treatment in both steels.

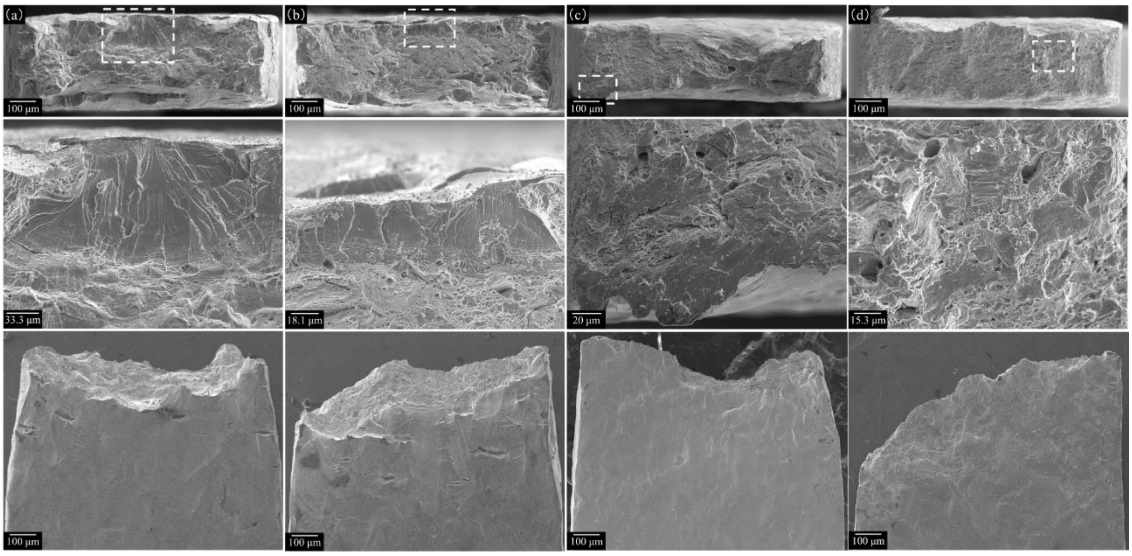

Fig. 5.8 SEM photos of sensitized 316L SS under (a) deaerated and (b) DH 1.4 ppm water condition; and 310S SS under (c) deaerated and (d) DH 1.4 ppm water condition. In each column, from top to bottom represents the overview of fracture surface, the enlarged area squared with white line and the side surface near fractured surface

5.4 Discussion

5.4.1 Experimental conditions

In this research, we examined SCC susceptibility by SSRT method with use of rather small specimens. Compact tension (CT) test with pre-cracked specimens is suitable for crack growth rate measurement under an applied stress intensity factor, while SSRT is a convenient test method to investigate crack initiation process under increasing applied stress. It has been proved by tests with CT specimens that crack growth rates of prior-deformed 304L SS and 316NG SS as well as 316L HAZ and 316NG weld metal in high temperature water decreased significantly after introducing hydrogen gas in to solution [19–22] It was clearly shown that hydrogen suppressed crack growth rate of IGSCC in water with dissolved oxygen. We focused on the investigation of the effect of dissolved hydrogen on the initiation of SCC by means of SSRT method.

As well known, utilization of miniaturized tensile specimens, especially thin specimens, sometime resulted in the change in the fracture mode because of the alternation in stress state. However, in our previous research, the specimen thickness of our miniaturized specimens was thick enough to investigate the trend of crack mode change, IG or TG [23,24] Authors believe that the effect of dissolved hydrogen on SCC susceptibility is significantly affected by material conditions, like sensitized, heat affected or solution-annealed, and it is also considered that the dissolved hydrogen plays different role in SCC between crack nucleation and growth.

5.4.2 SCC in hydrogenated hot water

As reported in the previous works on SCC in hydrogenated water, hydrogen injection into hot water often accelerates the CGR of IGSCC and/or TGSCC depending on the amount of dissolved hydrogen [8,9]. According to the several researches on the effects of amount of dissolved hydrogen on the SCC behavior of austenitic stainless steels, it is considered that there is an appropriate amount of hydrogen to suppress the SCC [7], and the CGR of SCC may show a peak at an amount of dissolved hydrogen [11,12,23,25–28]. With increasing the amount of dissolved hydrogen in hot water, SCC can be accelerated by thickness reduction of protective film but a further increase results in the suppression of SCC caused by reduction of corrosion rate that is accompanied by production of hydrogen at a localized cathodic reaction site.

Although the acceleration mechanism of SCC with increasing dissolved hydrogen is not clear, in the present study, we try to explain the difference in SCC susceptibility between 316L SS and 310S SS in terms of hydrogen-assisted degradation of fracture toughness. It is considered that hydrogen might cause a reduction of fracture stress of stainless steels both at grain boundaries and on slip plane where dislocations in high density exist and may trap an enough amount of hydrogen to cause embrittlement. In this study we consider that the brittle fracture observed in the SSRT in hydrogenated (DH=1.4 ppm) water is due to hydrogen-assisted SCC caused by detrimental effects of hydrogen on the fracture stress of the stainless steels.

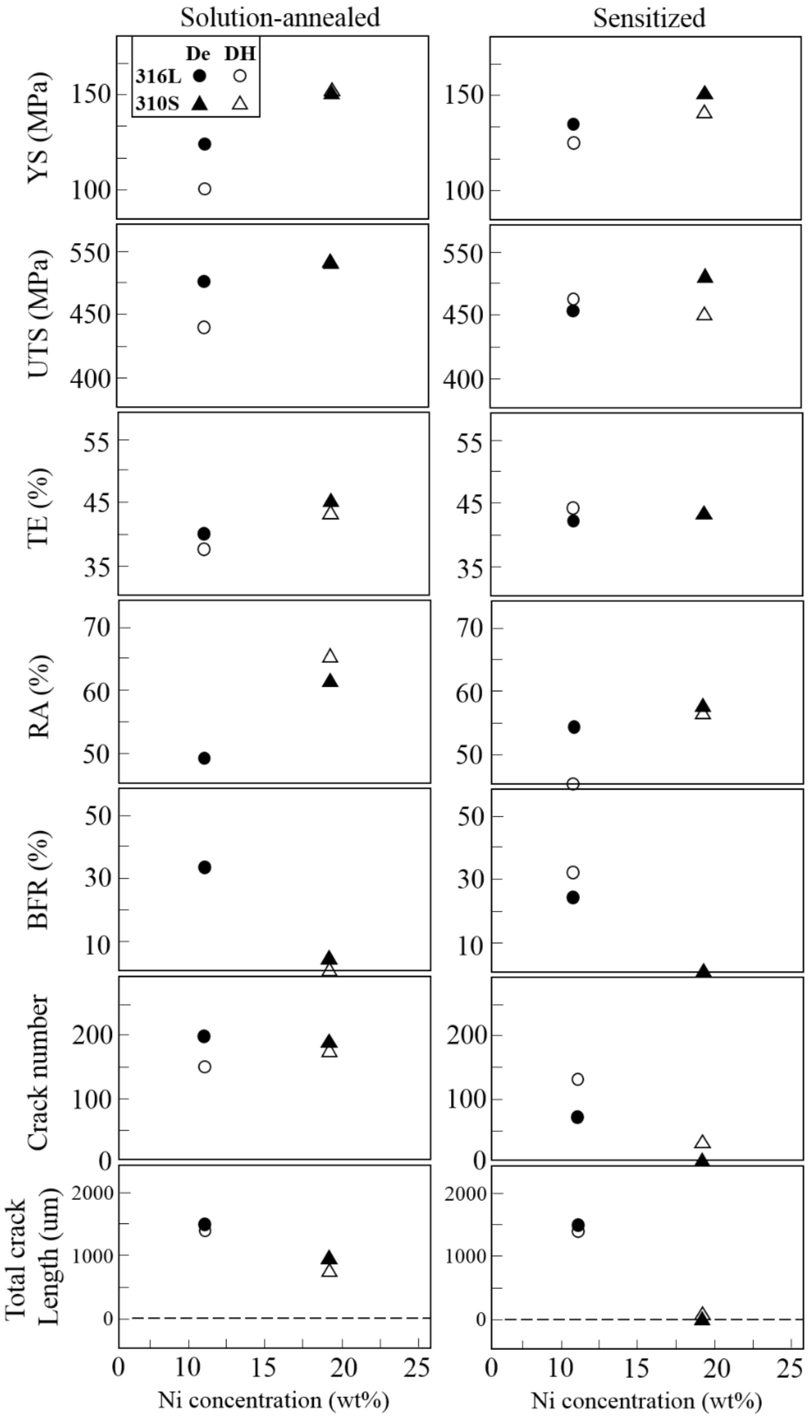

Fig. 5.9 Mechanical properties of 310S SS and 316L SS after solution annealing and sensitization: YS (Yield Stress), UTS (Ultimate Tensile Strength), TE (Total Elongation), RA (Reduction of Area), BFR (Brittle fracture ratio, number of cracks and total crack length) in (left) SA series and (right) SEN series. Circle represents 316L SS while triangle the 310S SS; solid symbol represents deaerated water condition and open symbol the DH 1.4 ppm water condition

5.4.3 Comparison between 310S and 316L SS

The difference in the mechanical properties between 310S and 316L SS is summarized in Fig. 5.9. As mentioned before, the stress-strain behavior, namely, yield stress (YS), ultimate tensile stress (UTS) and total elongation (TE) are almost not influenced by dissolved hydrogen content. However, the fracture relating properties, reduction area (RA), brittle fracture ratio (BFR), the number of cracks and total length of cracks on the side surfaces of specimens indicates remarkable difference between 310S and 316L SS, where RA is defined as the ratio of final-fractured surface area to original cross-section area, and BFR is defined as the ratio of brittle-fracture mode area to final-fractured surface area. It can be said that regardless the existence of hydrogen, in solution-annealed and sensitized steels, the RA of 310S SS is higher than that of 316L SS, and the BFR of 310S SS is lower than that of 316L SS. At solution-annealed condition, the BFR of 316L SS is over 30%, while of 310S SS is less than 5%; and, at sensitized condition, the BFR of 316L SS is over 20%, while 310S SS is almost ductile. Therefore, comparing the results between 316L SS and 310S SS, the susceptibility to SCC is much lower in 310S SS than 316L SS, which is in a good agreement with that of hydrogen embrittlement [16].

The major difference in the chemical compositions between the two steels are chromium (Cr), nickel (Ni) and molybdenum (Mo). Among these elements, Ni is well known as an element increasing stacking fault energy (SFE) in steels. [29–32] Since the higher the SFE is, the smaller the distance between two partial dislocations (shown in Fig. 5.10), in 310S SS with much higher Ni content, moving dislocations easily cross-slip, which increases the number of active slip planes. Hydrogen content per slip plane decreases. Number of slip planes with critical crack-inducing hydrogen content also decreases. As a results, cracking probability reduces, and SCC susceptibility decreases. This mechanism is illustrated in Fig. 5.11.

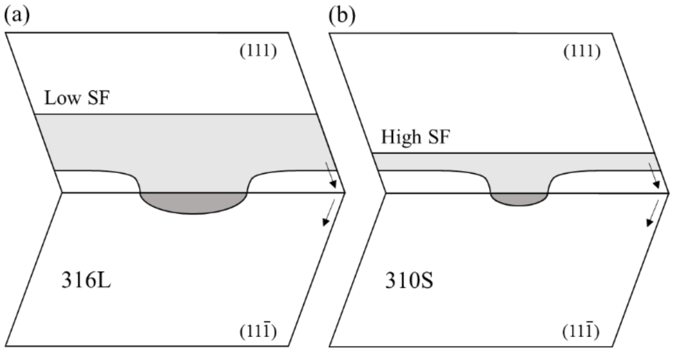

Fig. 5.10 Schematic of effect of Ni addition on stacking fault and cross-slip

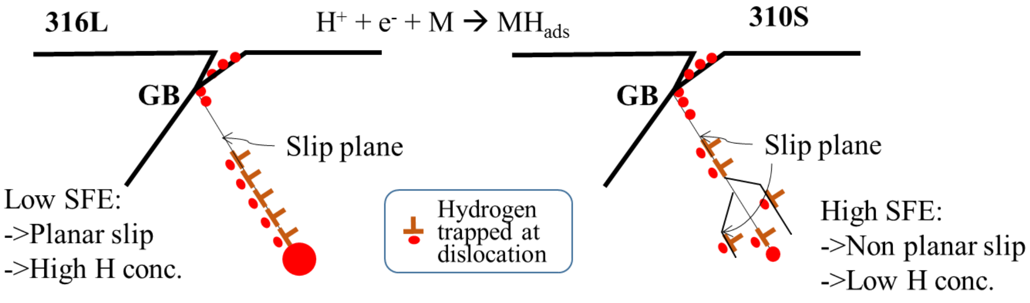

Fig. 5.11 Schematic of effect of Ni addition on reducing SCC susceptibility

Fig. 5.12 shows the examples of typical slip lines on the specimen side surface of SA 316L and SA 310S SS after SSRT in hot water with DH=1.4ppm. The slip lines observed in 316L SS are coarse and straight suggesting that dislocations move on the limited slip planes, while those of 310S SS are fine and wavy that indicates cross-slip occurs frequently and consequently the number of dislocations on a slip plane is small. In Fig. 5.9, the total length of cracks is larger in 316L SS than 310S SS, while the number of cracks is almost same between the two steels. The averaged distance between slip bands of 316L and 310S SS is measured for Fig. 5.12 and estimated to be 2.4 and 1.5 μm, respectively, indicating more frequent cross-slip in 310S SS than 316L SS. When the number of active slip plane increases, the number of dislocations on the unit area of slip plane decreases. Since hydrogen is trapped in the dislocation core, the content of hydrogen on the slip plane is reduced with decreasing dislocation density, and consequently hydrogen effect is reduced. It is considered that at deaerated and DH=1.4 ppm conditions, a lower potential causes suppression of the formation of protective surface oxide film and hydrogen reduces cohesive force of lattice atoms, which results in SCC.

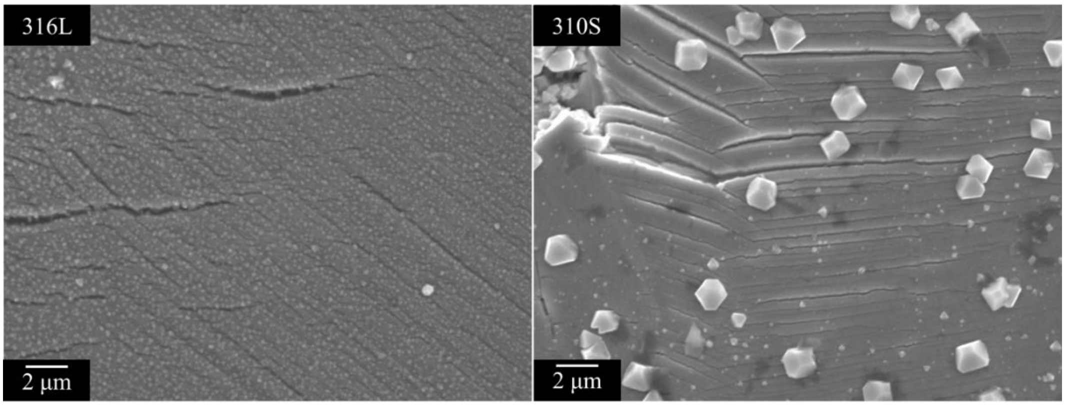

Fig. 5.12 The slip lines morphology on the specimen surface of (left) SA 316L and (right) SA 310S at dissolved-hydrogen 1.4 ppm condition.

5.4.4 Effect of sensitization heat treatment

In general, the IGSCC in hot water with dissolved oxygen is enhanced by so-called sensitization treatment which causes Cr depletion at grain boundaries. In this research, however, the IGSCC was suppressed by sensitization in water with dissolved hydrogen. We are focusing on the interpretation of this behavior by hydrogen trapping in hydrogen assisted SCC.

The microstructure of SEN 316L SS was examined by TEM-EDX line scan, and shown in Fig. 5.13, indicating that small Cr carbide exists both on grain boundaries and in the grains. The Cr is slightly depleted near the grain boundary, creating a Cr-depleted zone. Since carbides are one of effective trapping sites for hydrogen [33], it is considered that hydrogen transport along grain boundaries and through bulk diffusion could be suppressed in the sensitized steels. Both the intergranular and transgranular carbides play a role as a strong hydrogen trapping site, and they prevent hydrogen from concentrating at crack nucleation site as grain boundaries and slip planes in the material, then reduce the susceptibility to SCC at the same amount of dissolved hydrogen. As illustrated in Fig. 5.14. This may explain the difference in cracking mode between SA steels and SEN steels. In SA steels, the brittle fracture initiates as IGSCC and propagate into TGSCC, while in SEN steels, the brittle fracture of 316L SS initiates and propagates as TGSCC, which could be due to suppression of hydrogen transport along grain boundaries caused by hydrogen trapping at grain boundary carbides.

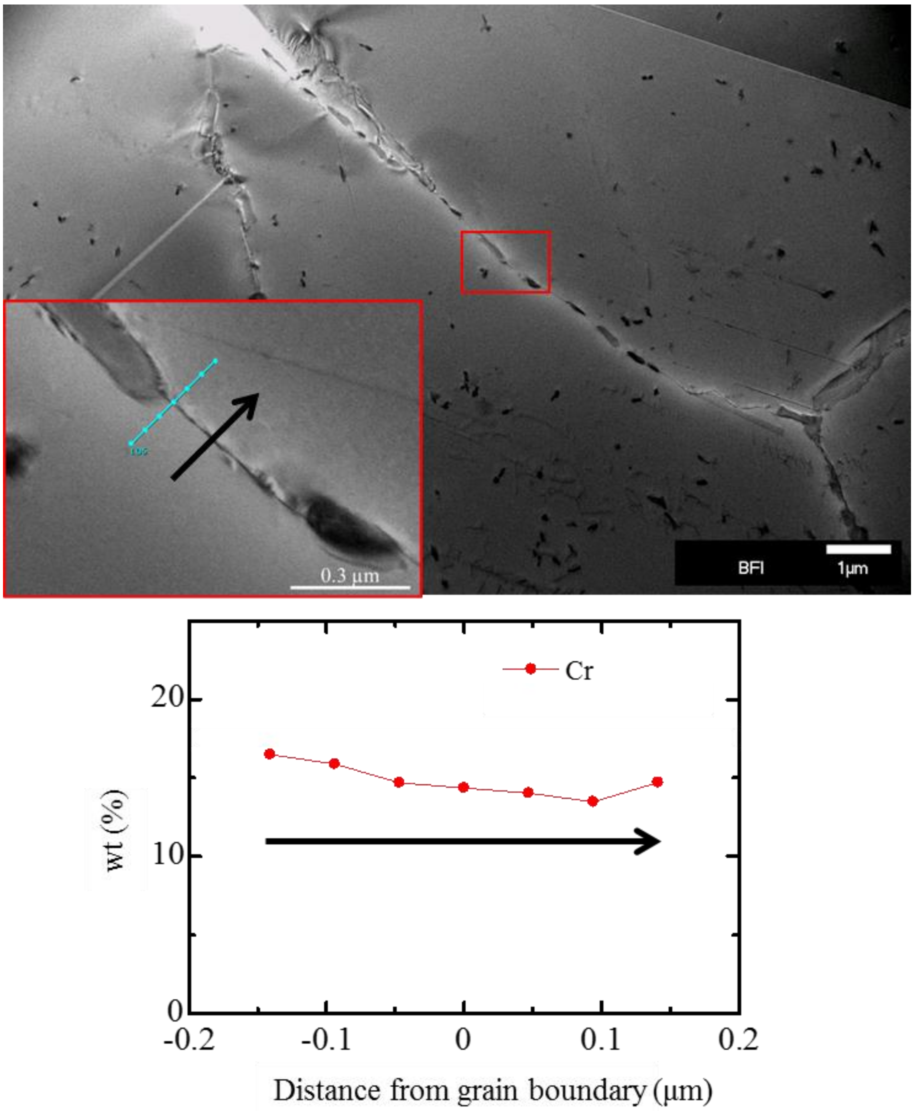

Fig. 5.13 TEM photo and EDX line scan of SEN 316L SS. Cr content is slightly decreased at around grain boundary.

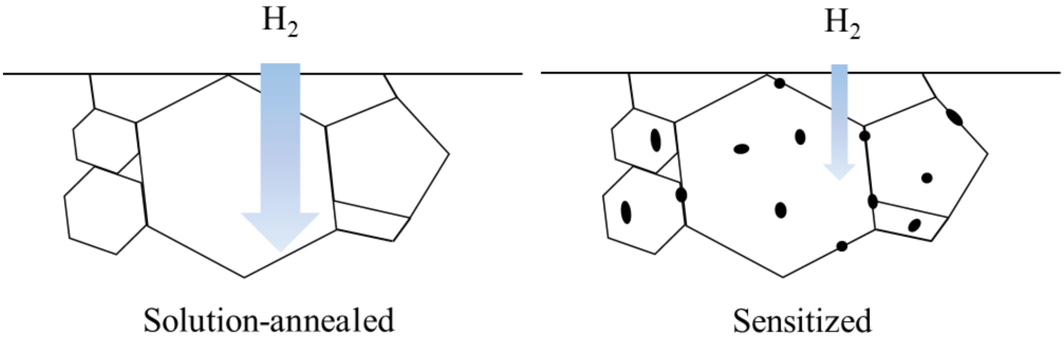

Fig. 5.14 Schematic of effect of carbide on hydrogen trapping and diffusion

5.5 Conclusions

The susceptibility to SCC of 310S and 316L SS in hydrogen-dissolved hot water (both DO and DH < 0.01 ppm and DH=1.4 ppm) at 288 ^{o}C and 7.8 MPa was examined by SSRT at a strain rate of 5 x 10^{-7}/s. The obtained main results are as follows;

(1) The susceptibility to SCC in hydrogenated water was suppressed in SA-310S SS in comparison to SA-316L SS, showing that the BFR of 310S SS is at most 5 %, while that of 316L SS is over 30 %. In both steels the SCC initiated at grain boundaries and transferred to slip planes in grains.

(2) The slip line morphology observation revealed that the slip lines are fine in 310S SS and coarse in 316L SS. The total length of cracks is larger in 316L SS than 310S SS, while the number of cracks is almost same between the two steels. The averaged distance between slip bands of 316L and 310S SS is estimated to be 2.4 and 1.5 μm, respectively, indicating more frequent cross-slip in 310S SS than 316L SS.

(3) Comparing the results between 310S SS and 316L SS, the susceptibility to SCC is in a good agreement with that of hydrogen embrittlement.

(4) Sensitization heat treatment lowers SCC susceptibility of the steels in water with dissolved hydrogen. It is suggested that carbide provides additional hydrogen-trapping site and lowering hydrogen diffusivity, which results in suppression of reaching critical hydrogen content to cause SCC

References

[1] A.A.F. Tavassoli, Assessment of austenitic stainless steels, Fusion Eng. Des. 29 (1995) 371–390. doi:http://dx.doi.org/10.1016/0920-3796(95)80044-X.

[2] P. Lorenzetto, P. Gierszewski, G. Simbolotti, A European proposal for an ITER water-cooled solid breeder blanket, Fusion Eng. Des. 27 (1995) 423–429. doi:10.1016/0920-3796(95)90154-X.

[3] P. Lorenzetto, M. Helie, A. Molander, Stress corrosion cracking of AISI 316LN stainless steel in ITER, J. Nucl. Mater. 233–237 (1996) 1387–1392.

[4] V. Belous, G. Kalinin, P. Lorenzetto, S. Velikopolskiy, Assessment of the corrosion behaviour of structural materials in the water coolant of ITER, J. Nucl. Mater. 258–263 (1998) 351–356. doi:10.1016/S0022-3115(98)00272-4.

[5] D. Tsuru, H. Tanigawa, T. Hirose, K. Mohri, Y. Seki, M. Enoeda, K. Ezato, S. Suzuki, H. Nishi, M. Akiba, Achievements in the development of the Water Cooled Solid Breeder Test Blanket Module of Japan to the milestones for installation in ITER, Nucl. Fusion. 49 (2009) 65024. doi:10.1088/0029-5515/49/6/065024.

[6] Y. Kawamura, H. Tanigawa, T. Hirose, M. Enoeda, S. Sato, K. Ochiai, C. Konno, Y. Edao, T. Hayashi, T. Hoshino, M. Nakamichi, H. Tanigawa, H. Nishi, S. Suzuki, K. Ezato, Y. Seki, T. Yamanishi, Progress of R&D on water cooled ceramic breeder for ITER test blanket system and DEMO, Fusion Eng. Des. 109 (2016) 1637–1643. doi:https://doi.org/10.1016/j.fusengdes.2015.11.002.

[7] K. Arioka, Influence of Temperature, Hydrogen and Boric Acid Concentration on IGSCC Susceptibility of Unsensitized 316 Stainless Steel, J. Inst. Nucl. Saf. Syst. 9 (2002) 116–123.

[8] T. Fukumura, T. Terachi, K. Arioka, Influence of Temperature and Water Chemistry on IGSCC Susceptibility of SUS316 in High-Temperature Water, J. Inst. Nucl. Saf. Syst. 11 (2004) 143–152.

[9] K.J. Choi, S.C. Yoo, H.H. Jin, J. Kwon, M.J. Choi, S.S. Hwang, J.H. Kim, Crack growth behavior of warm-rolled 316L austenitic stainless steel in high-temperature hydrogenated water, J. Nucl. Mater. 476 (2016) 243–254. doi:10.1016/j.jnucmat.2016.04.051.

[10] F. Meng, Z. Lu, T. Shoji, J. Wang, E. hou Han, W. Ke, Stress corrosion cracking of uni-directionally cold worked 316NG stainless steel in simulated PWR primary water

with various dissolved hydrogen concentrations, Corros. Sci. 53 (2011) 2558–2565. doi:10.1016/j.corsci.2011.04.013.

[11] X. Zhong, S.C. Bali, T. Shoji, Effects of dissolved hydrogen and surface condition on the intergranular stress corrosion cracking initiation and short crack growth behavior of non-sensitized 316 stainless steel in simulated PWR primary water, Corros. Sci. 118 (2017) 143–157. doi:10.1016/j.corsci.2017.02.003.

[12] O. Raquet, E. Herms, F. Vaillant, T. Couvant, J. Boursier, Scc of Cold-Worked Austenitic Stainless Steels in Pwr Conditions, 12th Int. Conf. Environ. Degrad. Mater. Nucl. Power Syst. (2005) 1049–1059.

[13] T. Nakagawa, N. Totsuka, T. Terachi, N. Nakajima, Influence of Dissolved Hydrogen on Oxide Film and PWSCC of Alloy 600 in PWR Primary Water, J. Nucl. Sci. Technol. 8 (2001) 111–117. doi:10.1080/18811248.2003.9715330.

[14] J. Chen, Z. Lu, Q. Xiao, X. Ru, G. Han, Z. Chen, B. Zhou, T. Shoji, The effects of cold rolling orientation and water chemistry on stress corrosion cracking behavior of 316L stainless steel in simulated PWR water environments, J. Nucl. Mater. 472 (2016) 1–12. doi:10.1016/j.jnucmat.2016.01.018.

[15] M. Nono, T. Nakajima, M. Iwama, R. Kasada, A. Kimura, SCC behavior of SUS316L in the high temperature pressurized water environment, J. Nucl. Mater. 417 (2011) 878–882. doi:10.1016/j.jnucmat.2010.12.150.

[16] G.R. Caskey, Hydrogen compatibility handbook, 1983. doi:10.2172/5906050.

[17] G. Han, J. He, S. Fukuyama, K. Yokogawa, Effect of strain-induced martensite on hydrogen environment embrittlement of sensitized austenitic stainless steels at low temperatures, Acta Mater. 46 (1998) 4559–4570. doi:10.1016/S1359-6454(98)00136-0.

[18] L. Zhang, M. Wen, M. Imade, S. Fukuyama, K. Yokogawa, Effect of nickel equivalent on hydrogen gas embrittlement of austenitic stainless steels based on type 316 at low temperatures, Acta Mater. 56 (2008) 3414–3421. doi:10.1016/j.actamat.2008.03.022.

[19] Z. Lu, T. Shoji, Y. Takeda, Y. Ito, A. Kai, N. Tsuchiya, Effects of loading mode and water chemistry on stress corrosion crack growth behavior of 316L HAZ and weld metal materials in high temperature pure water, Corros. Sci. 50 (2008) 625–638. doi:10.1016/j.corsci.2007.08.021.

[20] Z. Lu, T. Shoji, T. Dan, Y. Qiu, T. Yonezawa, The effect of roll-processing orientation on stress corrosion cracking of warm-rolled 304L stainless steel in oxygenated and deoxygenated high temperature pure water, Corros. Sci. 52 (2010) 2547–2555.

doi:10.1016/J.CORSCI.2010.03.027.

[21] Z. Lu, T. Shoji, F. Meng, Y. Qiu, T. Dan, H. Xue, Effects of water chemistry and loading conditions on stress corrosion cracking of cold-rolled 316NG stainless steel in high temperature water, Corros. Sci. 53 (2011) 247–262. doi:10.1016/j.corsci.2010.09.018.

[22] Z.P. Lu, T. Shoji, Y. Takeda, Effects of water chemistry on stress corrosion cracking of 316NG weld metals in high temperature water, Corros. Eng. Sci. Technol. 50 (2015) 41–48. doi:10.1179/1743278214Y.0000000186.

[23] P. Andresen, P. Chou, Effects of Hydrogen on SCC Growth Rate of Ni Alloys in BWR Water, in: 15th Int. Conf. Environ. Degrad. Mater. Nucl. Power Syst. - Water React., 2011: pp. 2039–2059.

[24] K. Nakagawa, M. Nono, A. Kimura, Effect of Dissolved Hydrogen on the SCC Susceptibility of SUS316L Stainless Steel, in: Mater. Sci. Forum, PRICM7, 2010: pp. 2887–2890. doi:10.4028/www.scientific.net/MSF.654-656.2887.

[25] S.M. Bruemmer, J.S. Vetrano, M.B. Toloczko, Microstructure and SCC Crack Growth of Nickel-Base Alloy 182 Weld Metal in Simulated PWR Primary Water, in: 13th Int. Conf. Environ. Degrad. Mater. Nucl. Power Syst., Whistler, British Columbia, 2007: pp. 1–11.

[26] N. Totsuka, Y. Nishikawa, N. Nakajima, Influence of Dissolved Hydrogen and Temperature on Primary Water Stress Corrosion Cracking of Mill Annealed Alloy 600, Corros. 2002. (2002) 1–11.

[27] M. Labousse, D. Déforge, F. Gressier, S. Taunier, M.L.C. Edf, OPTIMIZATION OF THE DISSOLVED HYDROGEN LEVEL IN PWR TO MITIGATE STRESS CORROSION CRACKING OF NICKEL ALLOYS . BIBLIOGRAPHIC REVIEW , MODELLING AND RECOMMANDATIONS . Review of experimental results regarding DH effect on initiation and propagation of SCC on, in: Int. Coop. Gr. Environ. Assist. Crack. 2012, 2012.

[28] T. Yamada, M. Aoki, T. Miyamoto, K. Arioka, SCC growth behavior of cold worked alloy 690 in high-temperature water－Dependence of test temperature, dissolved hydrogen in water, grain boundary carbide and chemical composition－, J. Inst. Nucl. Saf. Syst. 21 (2014) 133–143.

[29] L. Vitos, J.O. Nilsson, B. Johansson, Alloying effects on the stacking fault energy in austenitic stainless steels from first-principles theory, Acta Mater. 54 (2006) 3821–

3826. doi:10.1016/j.actamat.2006.04.013.

[30] R.E. Schramm, R.P. Reed, Stacking fault energies of seven commercial austenitic stainless steels, Metall. Trans. A. 6 (1975) 1345–1351. doi:10.1007/BF02641927.

[31] S. Lu, Q.M. Hu, B. Johansson, L. Vitos, Stacking fault energies of Mn, Co and Nb alloyed austenitic stainless steels, Acta Mater. 59 (2011) 5728–5734. doi:10.1016/j.actamat.2011.05.049.

[32] C.G. Rhodes, A.W. Thompson, The composition dependence of stacking fault energy in austenitic stainless steels, Metall. Trans. A. 8 (1977) 1901–1906. doi:10.1007/BF02646563.

[33] A. Kimura, H. Kimura, Effect of Carbon on the Hydrogen Induced Grain-Boundary Fracture in Iron, J. Jpn. Inst. Met. 47 (1983) 807–813. http://gateway.webofknowledge.com/gateway/Gateway.cgi?GWVersion=2&SrcAuth=mekentosj&SrcApp=Papers&DestLinkType=FullRecord&DestApp=WOS&KeyUT=A1983RV92300001%5Cnpapers3://publication/uuid/010B6DE8-0D77-48CB-930B-15D5FCEB533B.

Chapter 6

Stress Corrosion Cracking Behavior of 316L and 310S stainless steels in Fusion Relevant Environments

6.1 Introduction

316L stainless steel (SS) has been considered as one of candidate structural materials for fusion reactors [1–8]. The steel will be mainly used in heat transfer system, delivering cooling water into plasma-facing components and bringing heat away. The system adopts double-loop design and operating condition of primary loop of ITER is similar to that of current pressurized light water reactors. Other proposals suggested using supercritical water as a coolant [9,10]. In the fusion blankets, radiation-generated tritium may penetrate into cooling water. Tritium may react with water and form tritiated water and/or TH, T_2 tiny gaseous bubbles. Behaviors of these species resemble that of dissolved-hydrogen (DH) in water, which may enhance stress corrosion cracking (SCC) of 316L SS and degrade the integrity of piping system of the blankets.

The effect of DH in cooling water has been investigated in past decades. Hydrogen has been proved being able to harvest corrodants such as dissolved oxygen and hydrogen peroxides [11] and consequently retarding crack growth rate (CGR) [12,13]. In pressurized water reactors, hydrogen is also responsible for controlling pH value. Since hydrogen concentration is critical for controlling cooling water, it should be kept within a certain value range while not degrading materials [13–15]. Several studies reported that DH affected CGR in SCC on Ni-based alloys [14,16–18] and stainless steels [19–23] in simulated pressurized water environments.

Recently, we studied the SCC susceptibility of solution-annealed 310S SS by means of slow strain rate test (SSRT) in hot water (288 ^{o}C) with DH, and found that almost no SCC was observed in 310S SS, while a remarkable SCC was found in 316L SS showing a brittle fracture surfaces and cracks on specimen side surfaces [24]. As for the effect of DH in the water on the SCC of 316L SS, several researches were performed and the results varied among them. In the solution annealed steel, the minimum CGR was observed at 15 cc/kg at a temperature between 320 and 340 ^{o}C [25], while in cold-worked 316L SS, the maximum CGR was observed at 320 ^{o}C [22]. Fracture mode also varies among researchers, which might be due to test temperature difference, TGSCC at 288 ^{o}C [27] and IGSCC at 320 ^{o}C [25]. These above results indicates that SCC susceptibility depends on both temperature and DH in hot water.

Similar effects of hydrogen-assisted degradation can also be found in hydrogen gaseous environment. Han et al. [26] tested susceptibility to hydrogen-induced cracking (HIC) of several austenitic steels in 1 MPa H2 and D2 gaseous environment. He reported that at around 200K, 310S SS was least susceptible, 316 SS was next, and 304 SS was most susceptible to HIC. Caskey [27] also came up similar results from the tensile tests conducted in 69 MPa D_2 gas, indicating that the susceptibility decreased as Ni content increased between 15 to 25 wt%. Han [26], Chen [28]and Lai [29] attributed the susceptibility differences between austenitic SSs to the preference of martensite formation. Martensite allowed hydrogen to diffuse faster in materials, resulting in higher hydrogen concentration at crack-tip and accelerating crack growth. On the other hand, stabilized austenitic SS can prevent martensite formation hence reduces susceptibility to HIC. The relationship between HIC susceptibility and Ni content in steel was systematically examined by Zhang and his co-worker [30] in a series of specially alloyed 316L SS with different Ni equivalents. They tested these samples at temperatures ranging from 80 K to 300 K. Results revealed that the susceptibility decreased as Ni equivalent content increased from 24% to 33%.

Since hydrogen behavior in materials, such as diffusion, solubility and binding (trapping) behavior as well as corrosion reactions, is remarkably affected by temperature, it is considered that the SCC in hydrogenated water strongly depends on temperature and probably amount of hydrogen. Especially for application to fusion DEMO reactor, the temperature range of water is expected to be above 300 ^{o}C and possibly in supercritical water. In this work, we investigated the effects of temperature above 288 ^{o}C and DH up to 1.4 ppm on the SCC of 316L SS, which is a candidate structural material for coolant pipes of fusion reactors, and the SCC susceptibility of the 316L SS will be compared with that of 310S SS which is well known to be highly resistant to hydrogen embrittlement [28].

6.2 Experimental

6.2.1 Testing materials

The materials used in this study are commercial rod shaped 316L SS and 310S SS provided by Nilaco Co. The chemical compositions are listed in Table 6.1. Remarkable difference in the chemical compositions between two steels are Cr, Ni and Mo. The steel rods were machined into round-bar type tensile specimens of which the geometries are shown in Fig. 6.1. The gage section of the specimen was 10 mm long and 2 mm in diameter. The specimen was screwed into the connection parts of the tensile machine. Prior the test, specimens were solution-annealed at 1050 ^{o}C for 1 hour, followed by quenching into iced water. Specimen surfaces were polished by SiC sand papers from #800 to #4000 then cleansed in an ultrasonic cleaner.

Table 6.1 Chemical compositions of 316L and 310S SS

wt%	Fe	Cr	Ni	C	Mo	Mn	Si	Co	P	S
316L	bal.	17.41	12.13	0.01	2.05	1.06	0.73	-	0.032	0.004
310S	bal.	24.76	19.17	0.02	-	0.8	0.7	0.1	0.022	-

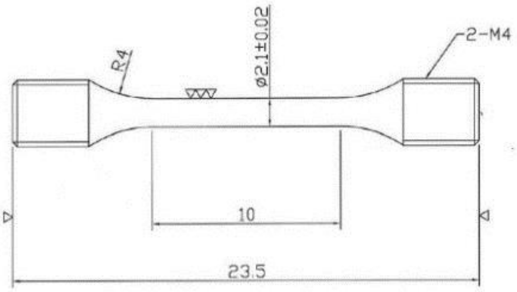

Fig. 6.1 The geometries of tensile specimen for SSRT

6.2.2 Slow-strain rate test (SSRT)

Fig. 6.2 is the schematic view of testing loop, which consists of a primary loop and a water chemistry monitoring loop. The primary loop was capable of providing pressurized water environment (15.5 MPa, 288-340 ^{o}C) and supercritical water (25 MPa, 500 ^{o}C) environment by manipulating a pressure relief valve. A high pressure pump drove water into a pre-heater, two autoclaves, heat-exchanger, and ion-exchanger and back to a water tank. A condenser dumped residual heat to an external chiller. High purity hydrogen and nitrogen were injected into the water tank to control dissolved-oxygen and DH. Deaerated water condition (both the dissolved oxygen and hydrogen are lower than 10 ppb) and the other three DH contents (0.014 ppm, 0.4 ppm and 1.4 ppm) were chosen to simulate different operating conditions. Strain rate was set at 5 x 10^{-7}/s. After SSRT, fractured surface and side surface were examined by scanning electron microscope (SEM)

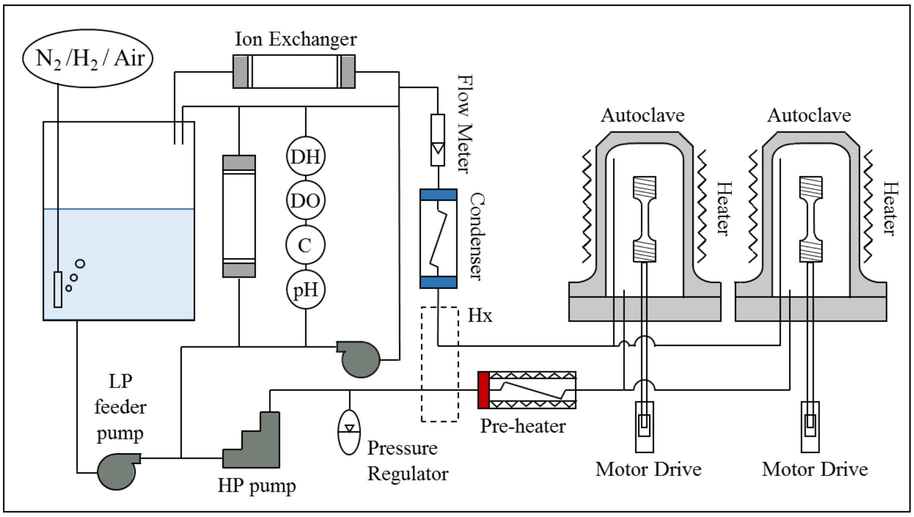

Fig. 6.2 Schematic view of pressurized/supercritical water circulation loop

6.3 Results

6.3.1 Deformation behavior

The stress-strain curves of solution-annealed 316L SS tested at 288 °C in pressurized water at deaerated and various DH content conditions are shown in Fig. 6.3, indicating that there is no remarkable change among the curves obtained for each water condition, although the DH content is different. However, the fracture behavior is affected by DH content significantly, and the detailed discussion will be given latter after showing fractured surface observation results.

The stress-strain curves in pressurized water at 340 °C and supercritical water at 500 °C at deaerated and various DH content conditions are shown in Fig. 6.4. Solid line represents deaerated water condition; dot line the DH=0.014 ppm; dash-dot-dot line the DH=0.4 ppm and dash line the DH=1.4 ppm. Mechanical properties such as ultimate tensile strength (UTS) and total elongation (TE) were summarized in Table 6.2. Comparing the curves among three testing temperatures, no trend nor remarkable difference was found between hydrogen-free and DH=1.4 ppm in 288 °C and 500 °C. On the contrary, a clear DH dependence existed in the tensile properties at 340 ^{o}C. Both UTS and TE decreased as DH content increased from 0 to 1.4 ppm. The UTS reduced from 430 MPa to 390 MPa; and TE reduced from 44% to 35%.

Stress-strain curves of solution-annealed 310S SS tested at pressurized water (288/340 ^{o}C) and supercritical water (500 ^{o}C) with deaerated and DH=1.4 ppm water condition were shown in Fig. 6.5. Mechanical properties were also summarized in Table 6.2. All the properties were not influenced by DH at all the test temperatures.

Table 6.2 Summary of mechanical properties: YS (Yield Stress), UTS (Ultimate Tensile Strength), TE (Total Elongation), RA (Reduction of Area), TG% (Area of transgranular cracking to area of fractured surface), IG% (Area of intergranular cracking to area of fractured surface) and BFR (Brittle fracture ratio, defined as summation of TG and IG) of solution-annealed 316L and 310S SS tested at pressurized water (288/340 ^{o}C) and supercritical water (500 ^{o}C) environment with different DH content. Deaerated water condition is denoted as DH=0 ppm.

Temperature (^{o}C)	Material	DH (ppm)	YS (MPa)	UTS (MPa)	TE (%)	RA%	TG%	IG%	BFR%
288	316L	0	124	421	41.9	40.3	51.4	0.0	51.4
		0.014	90	411	45.1	52.2	31.8	0.7	32.5
		0.4	121	438	39.4	40.3	51.8	0.0	51.8
		1.4	122	470	42.9	36.7	35.4	0.0	35.4
	310S	0	109	448	53.1	66.7	0.0	0.0	0.0
		1.4	151	474	50.4	64.5	4.9	0.0	4.9
340	316L	0	101	433	44.4	37.3	25.3	0.0	25.3
		0.014	104	431	42.2	41.7	39.5	6.8	46.3
		0.4	122	390	34.2	31.8	22.0	17.3	39.3
		1.4	125	393	35.0	38.2	9.4	26.3	35.8
	310S	0	147	486	53.6	63.1	0.0	0.0	0.0
		1.4	136	471	49.2	52.1	16.5	0.0	16.5
500	316L	0	88	444	48.5	57.6	6.0	0.0	6.0
		1.4	161	465	40.2	63.6	0.0	0.0	0.0
	310S	0	143	478	53.1	57.8	15.3	0.0	15.3
		1.4	137	470	50.7	59.1	4.4	0.0	4.4

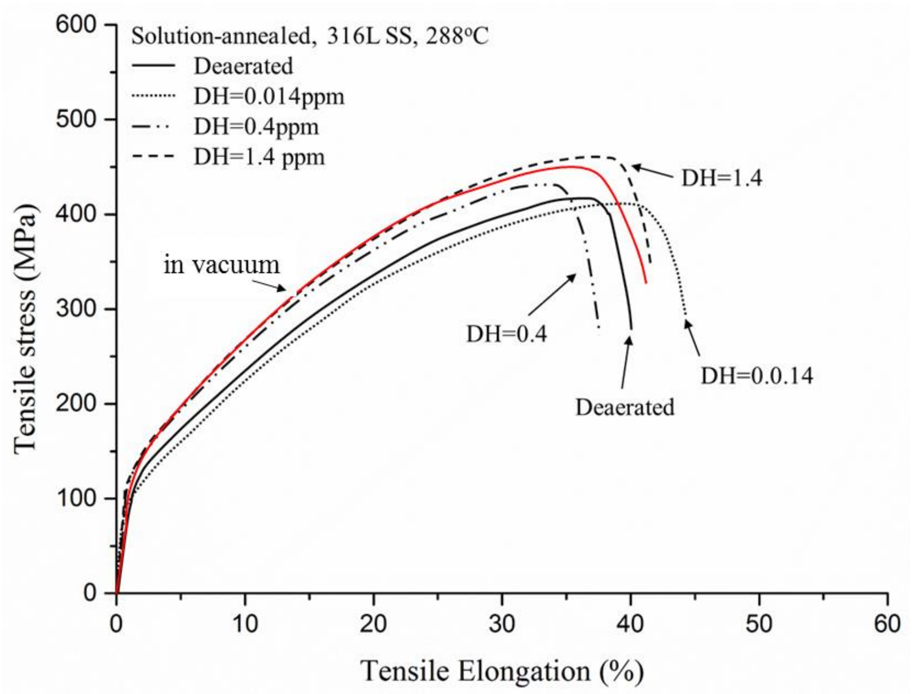

Fig. 6.3 Stress-strain curves of solution-annealed 316L SS tested at 288 ºC in pressurized water at deaerated condition (solid line) and with dissolved-hydrogen (DH) 0.014 ppm (dot line), 0.4 ppm (dash-dot-dot line) and 1.4 ppm (dash line). The stress strain curve of 316L SS tested in a vacuum at a strain rate of 1 x 10^{-6}/s is also shown.

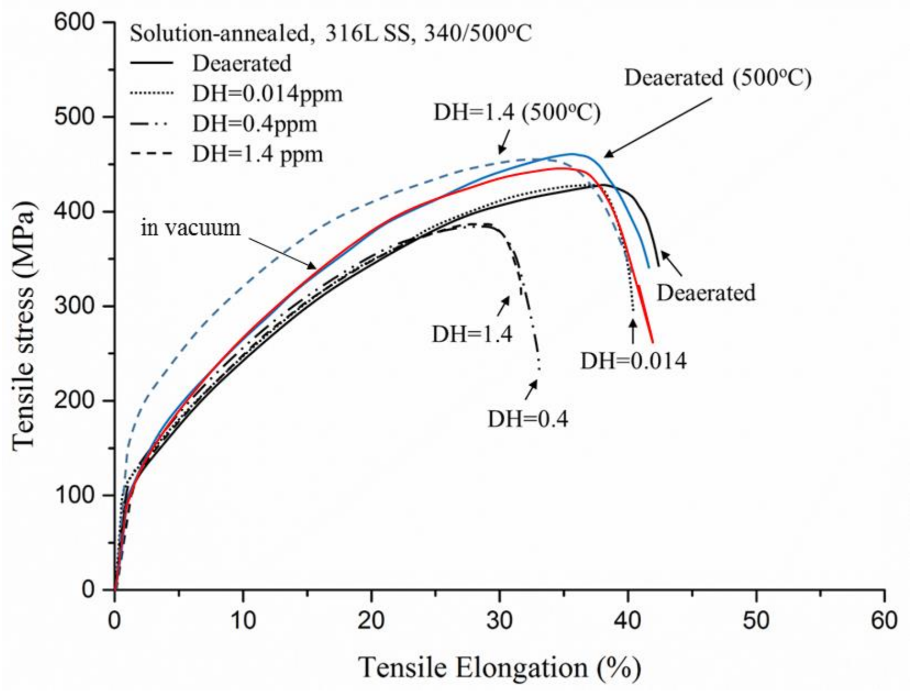

Fig. 6.4 Stress-strain curves of solution-annealed (SA) 316L SS tested in 340oC pressurized water (black line) and 500 ºC supercritical water (blue line) at deaerated condition (solid line); and with DH (DH) 0.014 ppm (dot line), 0.4 ppm (dash-dot-dot line) and 1.4 ppm (dash line).The stress strain curve of 316L SS tested in a vacuum at a strain rate of 1 x 10^{-6}/s is also shown.

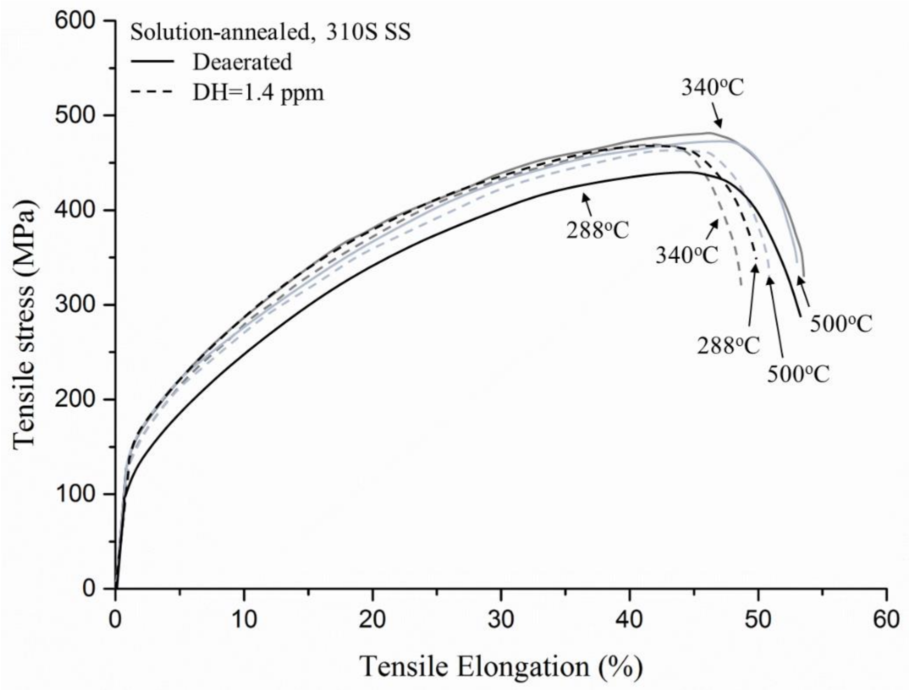

Fig. 6.5 Stress-strain curves of solution-annealed (SA) 310S SS tested in pressurized water (288 ^oC/340 ^oC, black/gray line) and supercritical water (500 ^oC, light lines) at deaerated condition (solid line) and with DH 1.4 ppm (dash line).

6.3.2 Fracture mode examination

Fractured surfaces and side surfaces near necking region of solution-annealed 316L SS tested at 288, 340 and 500 ^oC at deaerated and DH=1.4ppm water condition are shown in Fig. 6.6. In each column, photos in left hand side represented fractured surface and photos in right hand side represented the side surface near necking region. Irrespective of water condition, it is clearly shown that the fracture mode depends on test temperature: a brittle fracture was only observed in the peripheral of the fractured surfaces at 288 and 340 ^oC, while almost complete ductile fracture mode was observed at 500 ^oC. The observation of side surface cracks revealed that crack opening and propagation were more significant at 340 ^oC. In order to clear the DH dependence of fracture mode, the fracture behavior was investigated for tested specimens in hydrogenated water with DH=0.014 and 0.4 ppm, as shown in Fig. 6.7, indicating similar results with Fig. 6.6. The reduction in area (RA) and the percentage of TG and IG area were summarized in Table 6.2 and Fig. 6.11, where brittle fracture ratio (BFR) is defined as a summation of TG and IG area ratio. Although the stress-strain behavior of solution-annealed 316L SS at 288 ^oC is not significantly affected by DH condition, fracture mode varies among the specimens tested in the different conditions. It was recognized that the most of fractured mode was TGSCC with typical river patterns on the fractured surface in which the percentage of TGSCC ranged from 30% to 45%, although there was no systematic DH dependence of the brittle fracture mode. As shown in Fig. 6.4, however, the total elongation was decreased with increasing DH content in hot water at 340 °C, in which the fracture mode changed from TGSCC to a mixed mode of IGSCC initiation with propagation in TGSCC mode. The fraction of IGSCC increased with increasing DH content, while the total brittle fracture ratio appeared to decrease a bit. Fig. 6.8 shows SEM photos of IGSCC/TGSCC transition region on the fractured surface of solution-annealed 316L SS tested at 340 °C in pressurized water with (a) deaerated, (b) DH=0.014ppm, (c) DH=0.4 ppm and (d) DH=1.4 ppm condition. The distance from surface to IG/TG intersection increases as DH content increases, indicating that IGSCC is enhanced by increasing DH at this temperature. At 500 °C, however, fracture behavior was not affected by DH, as shown in Fig. 6.6 and Fig. 6.9.

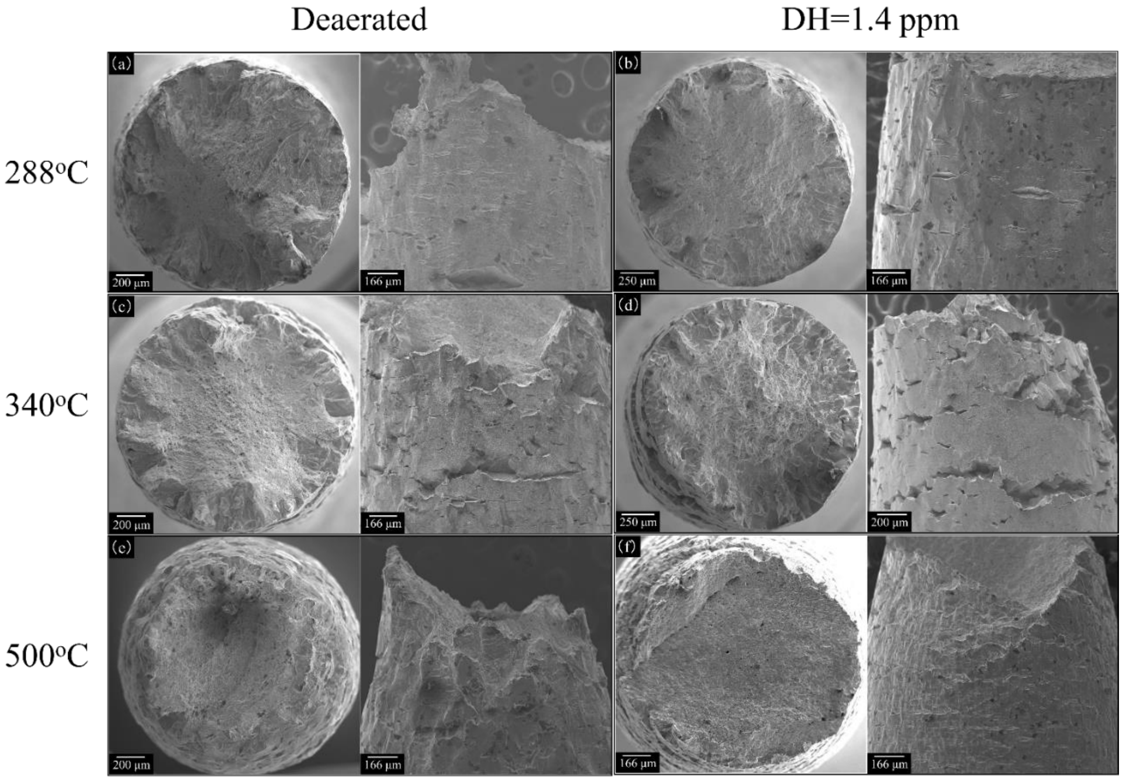

Fig. 6.6 SEM photos of solution-annealed 316L SS tested in pressurized water at (a)(b) 288 °C, (c)(d) 340 °C and in supercritical water at (e)(f) 500 °C with (a)(c)(e) deaerated condition and with (b)(d)(f) DH=1.4 ppm. In each column, photo in right hand side is side surface near necking region; in left hand side is fractured surface

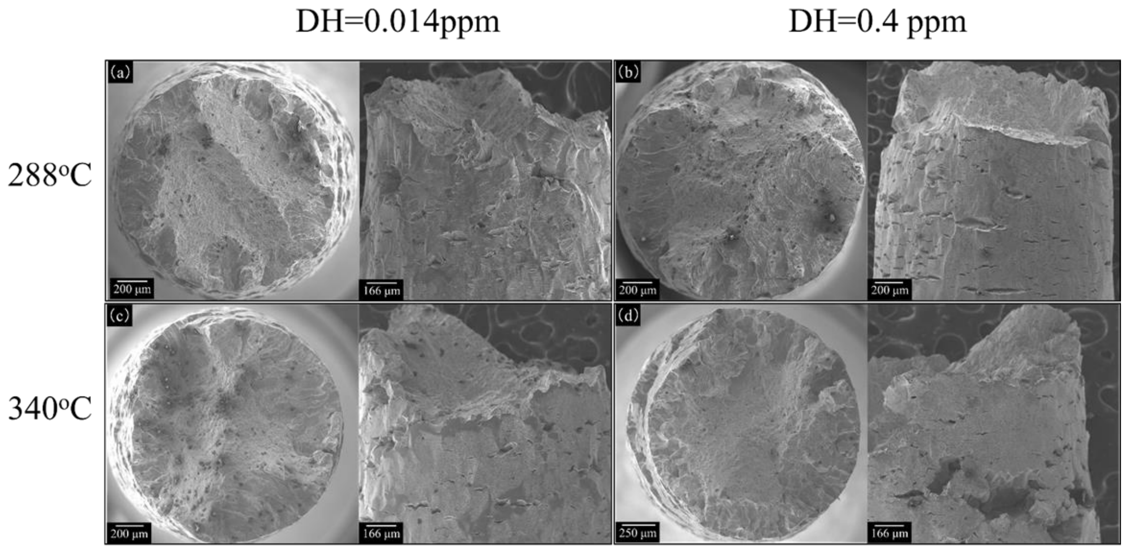

Fig. 6.7 SEM photos of solution-annealed 316L SS tested in pressurized water at (a)(b) 288 °C, (c)(d) 340 °C with (a)(c) DH=0.014ppm and (b)(d) 0.4 ppm. In each column, photo in right hand side is side surface near necking region; in left hand side is fractured surface

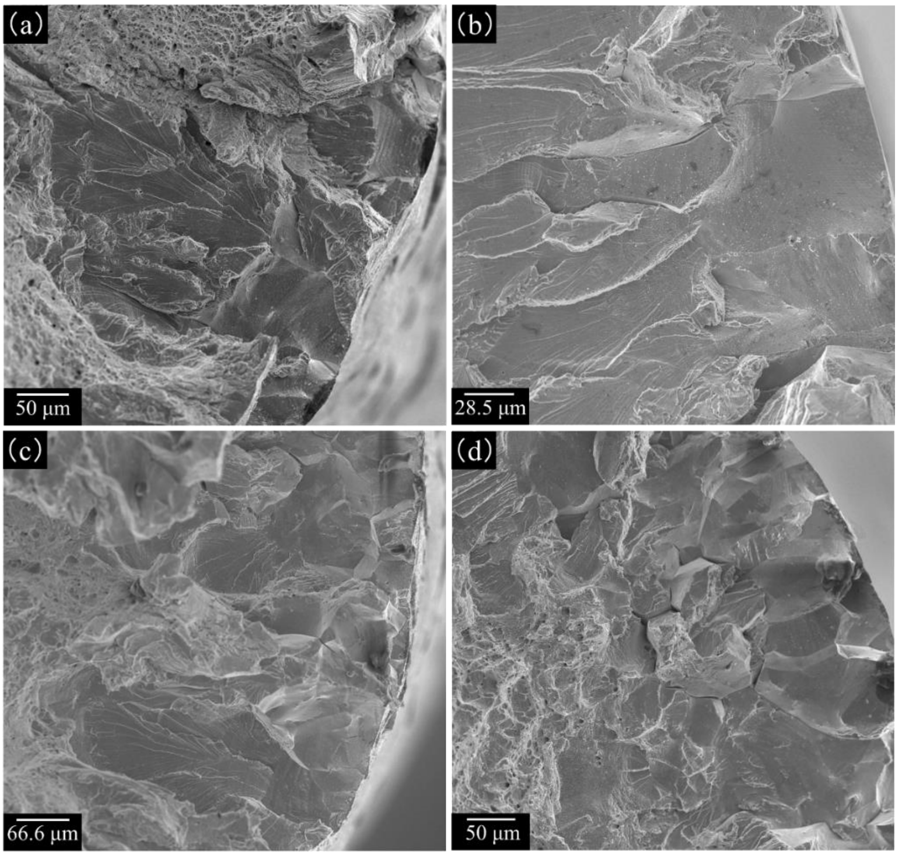

Fig. 6.8 SEM photos of intergranular/transgranular (IG-TG) transition region on fractured surface of solution-annealed 316L SS tested in 340 °C pressurized water with (a) deaerated, (b) DH=0.014ppm, (c) DH=0.4 ppm and (d) DH=1.4 ppm condition. The distance from surface to IG-TG crack intersection increases as DH content increases.

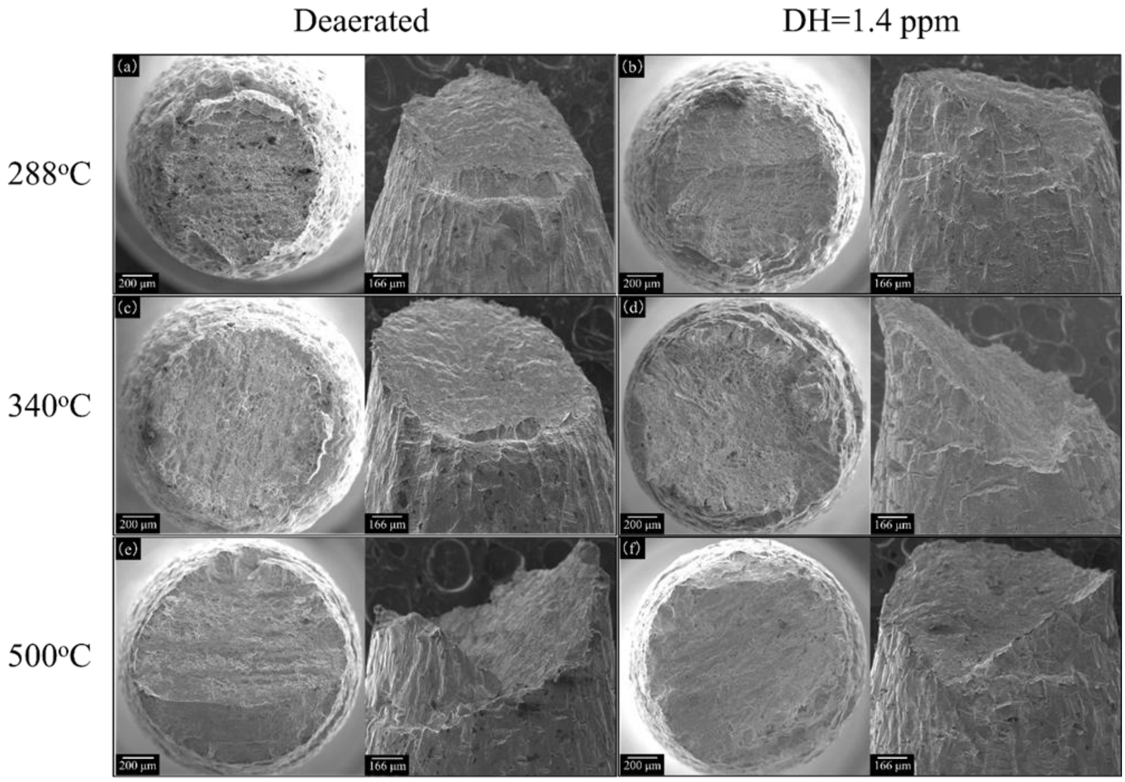

Fig. 6.9 SEM photos of solution-annealed 310S SS tested in pressurized water at (a)(b) 288 ^{o}C, (c)(d) 340 ^{o}C and in supercritical water at (e)(f) 500 ^{o}C with (a)(c)(e) deaerated condition and with (b)(d)(f) DH=1.4 ppm. In each column, photo in right hand side is side surface near necking region; in left hand side is fractured surface

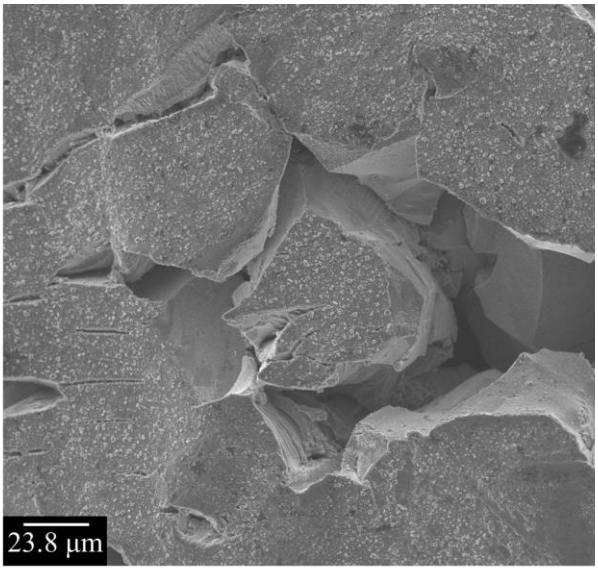

Fig. 6.10 SEM photo of fractured grain on side surface close to necking region of solution-annealed 316L SS tested at 340 ^{o}C pressurized water with DH=1.4 ppm. The grain suffered intergranular fracture more than transgranular fracture.

As for 310S SS, the SCC susceptibility in hydrogenated water is much lower than 316L SS at 288/340 °C, as clearly shown in Fig. 6.11 and Table 6.2. The TG area ratio of specimens tested at 288/340 °C with DH=1.4ppm water condition appears to be higher than that with deaerated water condition. It is in agreement with the small reduction of TE. However, at 500 °C, the TG area ratio of 310S SS appears to be larger than 316L SS, which is reverse trend of those at 288/340 °C.

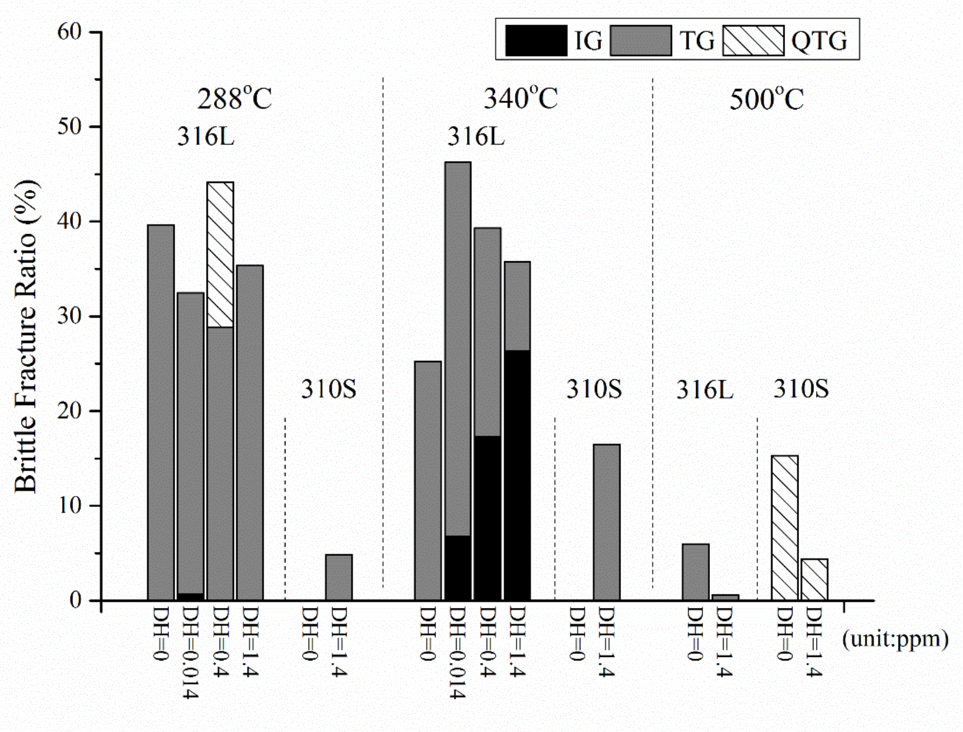

Fig. 6.11 Bar chart of brittle fracture ratio (BFR) of solution-annealed 316L and 310S SS tested in pressurized and supercritical water with deaerated and various dissolve-hydrogen water condition. Deaerated water condition is denoted as “DH=0.” Black color represents intergranular (IG) crack, gray color represents transganular (TG) crack and slash bar represents quasi-cleavage TG (QTG). Almost ductile behavior was found on following test conditions: 316L SS in 500 °C, DH=1.4ppm and 310S SS in 288 °C/340 °C, DH=0.

6.4 Discussion

6.4.1 SCC susceptibility at different temperatures

The above experimental results on 316L SS showed that the SCC susceptibility rather depended on both test temperature and DH content. In this study, the highest SCC susceptibility was observed at 340 °C which is the targeted coolant temperature of current design of fusion DEMO reactors. The most noticeable behavior is the change in the fracture mode from TGSCC to IGSCC with increasing test temperature from 288 to 340 °C and DH content from almost zero (deaerated) to DH=1.4 ppm. At 288 ^{o}C, almost no IGSCC was observed on the fractured surface, although a very limited IGSCC initiation was recognized[22]. Many previous researchers pointed out the contribution of hydrogen to the enhancement of SCC of solution annealed stainless steels in hydrogenated water as mentioned in the introduction. At supercritical water regime, the dielectric constant is smaller than that of ordinary water, as shown in Fig. 2.2. It is considered being a reason of smaller SCC susceptibility in supercritical water.

In this study, we could conclude that the SCC susceptibility of SA 316L SS in hydrogenated water becomes highest at around 340 ^{o}C but reduces at 500 ^{o}C. This test temperature dependence has been also observed for hydrogen-induced cracking (HIC) of the steel, in which a critical amount of hydrogen is necessary to cause HIC, although the peak temperature is below room temperature in the case of HIC. This temperature dependence was interpreted in terms of hydrogen diffusion and trapping as follows. With increasing temperature the diffusivity of hydrogen becomes large but hydrogen trapping efficiency becomes small, consequently showing a peak temperature to maximize the amount of hydrogen at a trapping site. The increase in the ratio of IGSCC with increasing DH indicates the IGSCC requires more hydrogen than TGSCC. Fig. 6.10 shows an IG fractured grains close to the specimen side surface of 316L SS tested at 340 ^{o}C at DH=1.4 ppm water condition.

6.4.2 Comparison between 316L and 310S SS

Fig. 6.11 clearly shows that solution-annealed 310S SS is much more resistant to the SCC in hydrogenated water than 316L SS at 288 and 340 ^{o}C, that is, RA and TE of 310S SS were larger than that of 316L SS; and BFR of 310S SS was smaller than 316L SS at 288 and 340^{o}C. At 500 ^{o}C, the susceptibility of 310S SS appeared to be more affected by the amount of DH than 316L SS. The lower SCC susceptibility in 310S SS at 288/340 ^{o}C can be explained by higher Ni content in 310S SS, as discussed in our previous paper [24], while those observed at 500 ^{o}C needs more detailed works.

6.5 Conclusions

The susceptibility to SCC of solution-annealed 316L SS and 310S SS in pressurized water (288/340 ^{o}C) and supercritical water (500 ^{o}C) at deaerated condition and with DH ranging from 0.014 to 1.4 ppm were examined by means of SSRT at a strain rate of 5 x 10^{-7}/s. The obtained main results are as follows:

(1) SCC susceptibility of 316L SS depends on test temperature and DH content. The SCC susceptibility a bit increased with increasing test temperature from 288 to 340 ^{o}C, while it became much smaller in super critical water at 500 ^{o}C.

(2) At 340 ^{o}C, the fracture ratio of IGSCC increased with increasing DH content in the pressurized water, although almost no IGSCC was observed at 288 ^{o}C at any DH conditions. The IGSCC initiated at near specimen surface and transferred to TGSCC inside the specimen.

(3) The SCC susceptibility of 310S SS is significantly lower than that of 316L SS in the hydrogenated water at 288 and 340 ^{o}C, while the trend appears to be reverse at 500 ^{o}C.

(4) It is suggested that the DH content on specimen surface affects cracking behavior. Higher DH content was needed to trigger IGSCC at 340 ^{o}C

References

[1] Y. Gohar, C.C. Baker, H. Attaya, M. Billone, R.C. Clemmer, P.A. Finn, A. Hassanein, C.E. Johnson, S. Majumdar, R.F. Mattas, D.L. Smith, H. Stevens, D.K. Sze, L.R. Turner, Fusion Technol. 15 (1989) 864–870.

[2] A. Kimura, S. Matsubara, T. Misawa, Mater. Trans. 34 (1993) 1097–1105.

[3] A.A.F. Tavassoli, Fusion Eng. Des. 29 (1995) 371–390.

[4] P. Lorenzetto, P. Gierszewski, G. Simbolotti, Fusion Eng. Des. 27 (1995) 423–429.

[5] P. Lorenzetto, M. Helie, A. Molander, J. Nucl. Mater. 233–237 (1996) 1387–1392.

[6] V. Belous, G. Kalinin, P. Lorenzetto, S. Velikopolskiy, J. Nucl. Mater. 258–263 (1998) 351–356.

[7] D. Tsuru, H. Tanigawa, T. Hirose, K. Mohri, Y. Seki, M. Enoeda, K. Ezato, S. Suzuki, H. Nishi, M. Akiba, Nucl. Fusion. 49 (2009) 65024.

[8] Y. Kawamura, H. Tanigawa, T. Hirose, M. Enoeda, S. Sato, K. Ochiai, C. Konno, Y. Edao, T. Hayashi, T. Hoshino, M. Nakamichi, H. Tanigawa, H. Nishi, S. Suzuki, K. Ezato, Y. Seki, T. Yamanishi, Fusion Eng. Des. 109 (2016) 1637–1643.

[9] M. Enoeda, Y. Kosaku, T. Hatano, T. Kuroda, N. Miki, T. Honma, M. Akiba, Nucl. Fusion. 43 (2003) 1837–1844.

[10] M. Akiba, M. Enoeda, D. Tsuru, H. Tanigawa, T. Hirose, K. Mohri, Y. Seki, K. Ezato, S. Suzuki, H. Nishi, S. Mori, Fusion Eng. Des. 84 (2009) 329–332.

[11] W. Bilanin, D. Cubicciotti, R.L. Jones, A.J. MacHiels, L. Nelson, C.J. Wood, Prog. Nucl. Energy. 20 (1987) 43–70.

[12] P.L. Andresen, M.M. Morra, J. Nucl. Mater. 383 (2008) 97–111.

[13] P. Andresen, P. Chou: Proc. 15th Int. Conf. Environ. Degrad. Mater. Nucl. Power Syst. - Water React., 2011: pp. 2039–2059.

[14] M. Labousse, D. Déforge, F. Gressier, S. Taunier, M.L. Calvar, E. Lemaire, T. Couvant, F. Vailant: Proc. Int. Coop. Gr. Environ. Assist. Crack, 2012.

[15] P.L. Andresen, A. Ahluwalia, J. Wilson, J. Hickling: VGB NPC 08 Water Chem. Conf., 2008.

[16] T.S. Bulischeck, D. Van Rooyen, Corros. 37 (1981) 597–607.

[17] N. Totsuka, T. Terachi, K. Takakura: Proc. 15th Int. Conf. Environ. Degrad. Mater. Nucl. Power Syst. - Water React., 2011: pp. 1667–1682.

[18] N. Totsuka, Y. Nishikawa, N. Nakajima, Corros./2002. (2002) 1–11.

[19] K.J. Choi, S.C. Yoo, H.H. Jin, J. Kwon, M.J. Choi, S.S. Hwang, J.H. Kim, J. Nucl. Mater. 476 (2016) 243–254.

[20] Z. Lu, T. Shoji, F. Meng, Y. Qiu, T. Dan, H. Xue, Corros. Sci. 53 (2011) 247–262.

[21] F. Meng, Z. Lu, T. Shoji, J. Wang, E. hou Han, W. Ke, Corros. Sci. 53 (2011) 2558–2565.

[22] X. Zhong, S.C. Bali, T. Shoji, Corros. Sci. 118 (2017) 143–157.

[23] X. Zhong, S.C. Bali, T. Shoji, Corros. Sci. 115 (2017) 106–117.

[24] Y.-J. Huang, K. Kawakita, A. Kimura: Proc. 18th Int. Conf. Fusion React. Mater., 2018

[25] K. Arioka, J. Inst. Nucl. Saf. Syst. 9 (2002) 116–123.

[26] G. Han, J. He, S. Fukuyama, K. Yokogawa, Acta Mater. 46 (1998) 4559–4570.

[27] G.R. Caskey: Hydrogen compatibility handbook for stainless steels, (DP-1643), 1983.

[28] T.C. Chen, S.T. Chen, L.W. Tsay, Int. J. Hydrogen Energy. 39 (2014) 10293–10302.

[29] C.L. Lai, L.W. Tsay, C. Chen, Mater. Sci. Eng. A. 584 (2013) 14–20.

[30] L. Zhang, M. Wen, M. Imade, S. Fukuyama, K. Yokogawa, Acta Mater. 56 (2008) 3414–3421.

Chapter 7

Summary

Stress corrosion cracking (SCC) is one of major degradation issue in current light water reactors. It is a potential issue of future water-cooled nuclear energy systems as well. Several works pointed out that SCC occurred on Ni-based alloys under hydrogen-dissolved hot water and primary water of pressurized water reactors. However, available information for austenitic Fe-based stainless steels is limited.

In this research, SCC behavior of solution-annealed 316L and 310S stainless steel was examined via slow-strain rate test (SSRT) in hot water, pressurized water and supercritical water with dissolved-hydrogen ranging from 0.014 to 1.4 ppm. The effects of testing temperature and sensitization heat treatment were also examined. This dissertation comprises seven chapters.

Chapter 1 introduces the importance of nuclear energy and briefly states its development and status in Japan. In current in-service light water reactors and future nuclear energy systems, the widely applied 316L steel potentially faces integrity degradation issue under hydrogenated water environments. The objectives of this research are to elucidate degradation mechanism and examine the performance of 310S steel, which is considered being a next candidate material for water-cooled energy systems.

Chapter 2 reviews SCC inducing factors and major mechanisms. Two major degradation mechanisms, metal dissolution and hydrogen embrittlement, were discussed. Available research works of Fe-based stainless steels and Ni-based alloys under hydrogenated high temperature water environment are gathered and discussed.

Chapter 3 summarizes chemical compositions of testing materials; schematics of water circulating loops for SSRT and information of analysis equipment used in the following chapters. The methodology for the evaluation of SCC susceptibility was discussed for SSRT and compact tension test.

Chapter 4 examined the stress corrosion cracking susceptibility and initiation behavior of 316L SS in hot water below 288 ^{o}C at deaerated condition and with dissolved-hydrogen (DH) =1.4 ppm. SSRT was carried out at a strain rate of 5 x $10^{-7}s^{-1}$. Results show that the susceptibility of 316L SS depends on both DH content and temperature. Transgranular (TG) crack occurred on specimens tested at 288 ^{o}C with deaerated and DH content ranging from 0.1 to 1.4 ppm. Intergranular crack was also observed on specimen tested at DH=0.4 ppm. Further, the appearance of TG crack was found at 220 ^{o}C with DH=1.4 ppm, implying higher hydrogen content is able to affect fracture mode of specimens. A map delineated the boundary of effects of combinations of temperature and DH content.

Chapter 5 examined the SCC susceptibility of solution-annealed 310S stainless steel, which is more resistant to hydrogen embrittlement, by means of SSRT in hot water (288 ^{o}C) with DH, and the results were compared with those of 316L SS. Almost no SCC was observed in 310S SS, while remarkable SCC was found in 316L SS showing a brittle fracture surfaces and cracks on specimen side surfaces, although no significant change was observed on stress-strain behavior. The SCC started as IGSCC while necking and transferred to TGSCC. It was also shown that sensitization resulted in the suppression of IGSCC. It is considered that carbides provide additional trapping sites for hydrogen and suppress accumulation of hydrogen on the slip plane. The TGSCC can be interpreted in terms of decohesion of slip plane where hydrogen is accumulated at the core of dislocations in high density. It is suggested that a higher nickel content increases stacking fault energy and facilitates cross slip of dislocations, which resulted in the reduction of hydrogen concentration on a unit area of slip plane.

Chapter 6 examined the SCC susceptibility of 316L and 310S SS in pressurized water (288/340 ^{o}C) and supercritical water (500 ^{o}C) at deaerated condition and with DH ranging from 0.014 to 1.4 ppm were examined by means of SSRT method at a strain rate of $5 \times 10^{-7}s^{-1}$. SCC susceptibility of 316L SS depends on test temperature and DH content. The SCC susceptibility, which was evaluated as a brittle fracture ratio, a bit increased with increasing test temperature from 288 to 340 ^{o}C, while it became much smaller in supercritical water at 500 ^{o}C. At 340 ^{o}C, the fracture ratio of IGSCC increased with increasing DH content in the pressurized water, although almost no IGSCC was observed at 288 ^{o}C at any DH conditions. The IGSCC initiated at near specimen surface and transferred to TGSCC inside the specimen. The SCC susceptibility of 310S SS is significantly lower than that of 316L SS in the hydrogenated water at 288 and 340 ^{o}C, while almost no difference was observed at 500 ^{o}C. It is suggested that hydrogen content on specimen surface affects cracking behavior. Higher content was needed to trigger IG cracking.

Chapter 7 is the summary of this dissertation. Throughout the works from chapter 4 to chapter 6, SCC map was drawn to show the susceptibility boundary of 316L SS at various dissolved-oxygen, dissolved-hydrogen and temperature. The “hot zone” covers almost all DH content with temperature bounded between 220 °C and 340 °C. Sensitization induced carbides provide additional hydrogen trapping sites and suppress accumulation of hydrogen on the slip plane. It is considered that hydrogen suppresses the formation of protective oxide film on the specimen surface, which enhance progress of cracking at the crack tip where hydrogen may reduce the cohesive force between Fe atoms, leading to TGSCC along deformation bands and to IGSCC at grain boundaries.

Contrary to 316L steel, 310S steel has better resistance to SCC in hydrogenated water condition. The beneficial effects of nickel addition, along with effects of additional trapping site provided by carbides, are in a good agreement with resistance to hydrogen embrittlement in hydrogen gaseous environment.

List of publications and presentations

1. Publications:

- Y.-J. Huang, K. Kawakita, A. Kimura, “Stress Corrosion Cracking Susceptibility of SUS310S in Hydrogenated Hot Water Environments” [Re-submitted to Nuclear Materials and Energy on Feb., 2018]
- Y.-J. Huang, T. Yamaguchi, H. Murai, H. Sugino, T. Nakajima, M. Nono, K. Kawakita, A. Kimura, “SCC initiation of 316L SS in hydrogenated hot water below 288°C” [Submitted to Corrosion Science]
- Y.-J. Huang, A. Kimura, “SCC Susceptibility of 316L and 310S stainless steel in Fusion Relevant Environments” [Submitted to Trans. of JIM]

2. Presentations:

International Conferences:

- Y.-J. Huang, K. Kawakita, A. Kimura, “SCC Behavior of SUS316L and SUS310S in Fusion Relevant Environments,” The 18th International Conference on Fusion Reactor Materials (ICFRM-18), Nov. 5-10, 2017, Aomori, Japan,
- Y.-J. Huang, K. Kawakita, H. Je, A. Kimura, “SCC Behavior of SUS316L and SUS310S in Fusion Relevant Environments,” 1st IAEA workshop on “Challenges for coolants in fast spectrum system: Chemistry and materials”, July 5-7, 2017, Vienna, Austria
- Y.-J. Huang, A. Kimura, “SCC Mapping of SUS316L in Hot Water Dissolved with Hydrogen and/or Oxygen,” 1st IAEA workshop on “Challenges for coolants in fast spectrum system: Chemistry and materials,” July 5-7, 2017, Vienna, Austria
- Y.-J. Huang, K. Kawakita, A. Kimura, “Stress Corrosion Cracking of SUS310S in Hydrogen Dissolved Hot Water,” The Nuclear Materials Conference (NuMat 2016), Nov. 7-10, 2016, Le Corum, Montpellier, France
- Y.-J. Huang, H. Je, A. Kimura, “SCC Behaviors on Candidate Materials in Hydrogenated Supercritical Pressurized Water,” 9th Pacific Rim International Conference on Advanced Materials and Processing (PRICM9), Aug. 2016, Kyoto, Japan,

- Y.-J. Huang, K. Kawakita, H. Je, A. Kimura, "Corrosion Behavior of Candidate Stainless-steels for In-core Structure Applications," 4th IAM-KIT/IAE-KU Seminar on Advanced Energy Materials and Chemistry, Jan. 2016, Karlsruhe Institute of Technology, Germany

Domestic Conferences:

- Y.-J. Huang, K. Kawakita, A. Kimura, "SCC mapping of SUS316L and SUS310S in hydrogenated hot water environments," 2017 Annual Fall meeting (161th) of JIMS, Sept. 2017, Hokkaido, Japan
- Y.-J. Huang, K. Kawakita, A. Kimura, "SCC behavior of SUS316L and SUS310S in ITER operating environments," 2017 Annual Spring meeting (160th) of JIMS, Mar. 2017, Tokyo, Japan
- Y.-J. Huang, K. Kawakita, A. Kimura, "SCC behavior of austenitic stainless steels in hot water with dissolved hydrogen," Symposium of Zero-Emission Energy, Oct. 2016, Kyoto University, Japan
- Y.-J. Huang, K. Kawakita, A. Kimura, "SCC susceptibility of SUS310S in high temperature environments," 2016 Annual Fall meeting (159th) of The Japan Institute of Metals and Materials (JIMS), Sept. 2016, Osaka, Japan
- Y.-J. Huang, K. Kawakita, H. Je, A. Kimura, "Corrosion Behaviors of Candidate Structure Materials in Hydrogen-dissolved High Temperature Water," the 11th Fusion Energy Forum Meeting, July 2016, Kyushu Univ., Japan

Acknowledgement

First of all, with all my hearts, I thank my parents and my younger brother. Without their everlasting support and encouragement, I cannot walk far and reach this goal.

Second, I thank my venerable advisor, Prof. Akihiko Kimura for his insightful opinions, suggestions and financial support. His enthusiasm, patience and generosity deeply impress me. I also thank Assoc. Prof. Yabuuchi for his professional tech supports in many aspects; and kind secretary Ms. Wada for her great assistance in administrative procedures.

Third, I'd like to thank Assoc. Prof. Kondo at DuET, Kyoto University; Prof. Matsukawa and Assoc. Prof. Kasada in Tohoku University for skillful assistance and time-spending on discussion. Prof. Jia-Horng Huang, Prof. Ge-Ping Yu in NTHU, Taiwan, for their insightful, fruitful discussions and suggestions. Thank Dr. Kuan-Che Lan in UNLV, Dr. An-ni Wang in Technische Universität Ilmenau for their professional opinions and selfless experience sharing. Thank consultant Leo Hung, from PTT, Taiwan, for his constant and encouraging mental support.

My thanks also go to lab mates: Daniel Morrall, Eva Hasenhuetl, Peng Song, Zhe-xian Zhang, Gin Gao, Kousuke Kawakita who make my academic life more colorful. Besides, I sincerely appreciate all assistance from supporting staff, Mr. Hayashi, Mr. Omura, Mr. Hashitoyo in Kyoto University; and all the foundations laid and efforts made from previous master students. Thank Prof. Tsung-Kuang Yeh and Dr. Mei-Ya Wang for instructions.

Last but not least, I thank my best friends: Ting-Shuo Jhang, Hsiang-Yu Hsieh and Che-Wei Kuo. Thank Hsiao-Han Huang for her 15-year in life journey. All of yours' optimistic minds, passions and love have delighted my life.